A study of the Impact of Triggered Star Formation

By

Michael Willcock

Supervisor: Dr James Urquhart

School of Physical Sciences

University of Kent

December 2020

Abstract

This thesis presents a statistical study of the impact of triggered star formation at the boundary of HII regions. HII regions are bubbles of ionised gas created by high energy radiation feedback from a host massive star. HII regions expand into their surrounding molecular gas due to the extreme temperature difference between the hot ionised gas of the HII region and the cool molecular gas of its natal clump. This results in the gas being swept up and compressed by ionising radiation. This compressed gas can then fragment and collapse to form stars. This is known as triggered star formation and is known to occur through mechanisms such as "The collect and collapse method" and "Radiative Driven Implosion".

We visually analysed 5410 sources from the ATLASGAL survey, with the help of the GLIMPSE survey, to categorize them into "triggered" and "non-triggered" sources by visually inspecting the source for signs of triggered star formation and using the ATLASGAL contours to distinguish between finer details of the sources. We then compared the physical properties of these sources to see if we could find a difference between the sources that we had deemed triggered and those that were not. We also looked for a peak in source counts at the rim of their host bubbles in an attempt to replicate the results from Thompson et al. (2012) and S. Kendrew et al. (2012). Finally we try and set a lower limit of star formation taking place in the inner Galaxy that occurs through a triggering mechanism.

We found statistically significant differences between the temperature, luminosity and luminosity to mass ratio when looking between triggered and non-triggered sources and found no significant differences between the radius and mass of the two different source categories. We find a peak in source counts at a distance of 1 bubble radius, this result being in line with the results of Thompson et al. (2012) and S. Kendrew et al. (2012).

With this difference in physical properties, it is likely that there is a significant difference in star formation occurring between our triggered and non-triggered sources, likely as a result of their parental HII regions impact on the surrounding molecular gas which points towards triggering.

Finally with our catalogue providing a reasonable statistical representation of star formation in the inner Galaxy, we set a lower limit of ~ 12 % for triggered star formation that occurs in the inner Galaxy, once contaminating sources are excluded.

Acknowledgements

I would like to thank my supervisor, Dr James Urquhart for his support, guidance and patience throughout the completion of this thesis. Thank you for all the work you have put in, in assisting me with the research and writing up of this work. I would also like to express my thanks to Dr Sam Billington for his sharing of expertise and assistance in the use of Linux, MySQL and Python for the coding aspect of this thesis.

The ATLASGAL project is a collaboration between the Max-Planck-Gesellschaft, the European Southern Observatory (ESO) and the Universidad de Chile. It includes projects E-181.C-0885, E-078.F-9040(A), M-079.C-9501(A), M-081.C-9501(A) plus Chilean data.

This work is based [in part] on observations made with the Spitzer Space Telescope, which is operated by the Jet Propulsion Laboratory, California Institute of Technology under a contract with NASA.

Contents

Chapter 1

Introduction

1.1 Star Formation

1.1.1 The Interstellar Medium

The interstellar medium (ISM) is very inhomogeneous. Huge clouds of gas and dust exist and are sites of interest amidst the vast emptiness of space. The observable universe is composed mostly of Hydrogen (approximately 70% by mass), which comes in several forms such as molecular hydrogen(H_2), neutral hydrogen (HI) and ionised hydrogen (HII) with helium contributing the majority of the remaining mass and all other matter making up the last few % (collectively referred to in astrophysics as metals).

HI in its ground state does not tend to produce emission lines by electronic transitions and emission, nor is the absorption spectra easy to detect since HI requires photons of UV strength to liberate electrons from their ground state. However, it is possible to detect HI using the 21-cm radio emission that occurs during a process that results in the reversal of the spin of the electron relative to the proton in HI. This emission however, is extremely rare but due to the enormous quantity of HI that exists in the ISM the emission is easily seen.

H_2 also exists in the ISM and is found in molecular clouds. It can exist in these clouds due to an outer barrier of HI gas that shields the H_2 from incoming radiation and prevents it from being ionized into HI. The formation of H_2 in these clouds is made

possible by the presence of dust grains. It has been found that dust grains existing in these molecular clouds can both shield H_2 from UV radiation and enhance H_2 formation. This enhancement occurs for two reasons:

1. A dust grain can provide a site on the surface of the grain where the hydrogen atoms can meet, rather than requiring chance encounters in the ISM

2. The dust provides a sink for the binding energy that must be liberated if a stable molecule is to form. The liberated energy goes into heating the grain and ejecting the H_2 molecule from the formation site. Bradley W. Carroll (2007)

When looking at the production of H_2 within a molecular cloud it is worth noting that the presence of turbulence within such a cloud is thought to accelerate the production of H_2 when compared to the non-turbulent case, Glover and Mac Low (2007). This is a result of the turbulent motions within the cloud bringing in fresh amounts of atomic hydrogen for production. The principle of turbulence in molecular clouds is thought to be crucial to star formation and is discussed in more detail later in this section.

H_2 has no emission or absorption lines in the visible or radio regions of the electromagnetic spectrum associated with the temperatures found in the ISM but excited H_2 can be seen in shocks in the near infra-red (IR). A solution to this is the use of tracers to track the location of H_2. One makes the assumption that a high abundance of the used tracer corresponds to an equally high abundance of H_2. The most commonly used tracer is carbon monoxide, CO, as it has the highest abundance ratio to H_2 of $\sim 6\times10^{-5}$ (Gordon and Burton (1976)), and is around 100 times more abundant than other molecules, Scoville and Solomon (1974). Carbon monoxide is seen when it collides with H_2 and undergoes a rotational transition that is visible at $\sim$ 2.6 mm (Burton (1977)). Other tracers commonly used include CH, OH, CS, C_3H_2, HCO^+ and N_2H^+ Bradley W. Carroll (2007). Other molecules such as ^{13}CO or $C^{18}O$ are also used, these molecules are known as isotopomers.

1.1.2 Molecular Clouds

Molecular Clouds as detailed above are huge clouds of dust and gas that exist in the interstellar medium. They are where the majority of molecular hydrogen can be found and as a result it is still thought that these clouds are where the majority of star formation occurs, Zuckerman and Palmer (1974). Molecular clouds differ from one another based on a few parameters, these parameters are mass, temperature, number density and interstellar extinction and these are used to classify molecular clouds into groups for easier identification.

Table 1.1 shows the 4 main types of molecular cloud along with their ranges of Mass, Temperature, Extinction, Diameter and Number Density. The assigned n/a value to the extinction of a giant molecular cloud does not mean that there is no extinction present, only that due to the size and scale of a giant molecular cloud the range of extinctions present in such a cloud would be too vast to fit in our table.

A small digression here would be to mention the concept of interstellar extinction. The dust that exists in the ISM and in molecular clouds can alter the properties of starlight that reaches us through scattering and absorption processes. This extinction is primarily noted in the changing of the perceived magnitude of starlight that reaches us from distant stars. This is governed by the following equation.

$$m_\lambda = M_\lambda + 5log_{10}d - 5 + A_\lambda \tag{1.1}$$

Equation 1.1 is used to work out the difference in the observed magnitude of a star caused by distance and interstellar extinction. m_λ is the apparent magnitude of the star, M_λ is the absolute magnitude of the star, d is the distance in parsecs and A_λ is the extinction. A_λ can change based on the physical properties of the dust blocking the light. The thicker and denser the dust, the higher the value of A_λ and the more the light is attenuated.

Cloud Type	Mass ($M\odot$)	Temp (K)	Extinction (mag)	Diameter (pc)	Number Density (cm^{-3})
Diffuse Clouds	3 - 10	15 - 50	1 - 5	1 - 3	$5x10^2$ - $5x10^3$
Giant Clouds	10^5-10^6	15	n/a	50	$1x10^2$ - $3x10^2$
Dark Clouds	10^4	10	5	10	$5x10^2$
Dense Cores	10	10	10	0.1	$1x10^4$

Table 1.1: This table shows the different types of molecular clouds that exist in the interstellar medium. Note - there is no extinction value of GMC's due to the variation that occurs across them which results in a very wide range of values.

Turbulence in Molecular Clouds

Before we discuss the conditions needed to be met for gravitational collapse and by extension the star formation process to begin, we must first discuss the phenomena thought to allow these conditions to occur in the first place. It was previously thought that pre-existing gravitational instabilities within molecular clouds led to density fluctuations in the gas that went on to collapse to form stars. This is no longer thought to be the case, instead it is thought that this is the role of a phenomena known as supersonic turbulence, Bruce G. Elmegreen and Scalo (2004).

Bruce G. Elmegreen and Scalo (2004) describe turbulence as "non linear fluid motion, resulting in the excitation of an extreme range of correlated spatial and temporal scales" and McKee and Ostriker (2007) describe a turbulent fluid as "one in which the velocity at any point fluctuates irregularly". Turbulence is, essentially, differences in the velocity of the gas contained within a molecular cloud. These differences are thought to arise from changes in kinetic energy brought on by energy injected into the cloud, Bruce G. Elmegreen and Scalo (2004). This energy is taken from both external and internal sources.

There are several external energy sources however, most are thought to not contribute enough to sustain the level of observed turbulence seen in molecular clouds. Supernova explosions are one such example, providing a huge amount of energy to the ISM however, due to the difficulty of transferring energy from the diffuse ISM into the dense molecular cloud, much of the energy is lost resulting in a minimal amount being contributed. Cloud-cloud collision is also discussed as a potential mechanism however, it is thought that these collisions occur too rarely to be seen as the main input from external sources. Thus, it

is currently thought that the main input of turbulence from external sources is inherited during, and carried on from, the birth of the molecular cloud.

Internal energy injection comes from stellar feedback from forming and newly formed stars. Lower mass stars support local regions against gravitational collapse, but do not produce enough energy to sustain observed levels of turbulence across the whole molecular cloud. More massive stars on the other hand, inject more energy into the cloud via HII regions. These HII regions are capable of producing enough energy to support the turbulence requirements of the molecular cloud and have been observed to dominate the energy injection in certain molecular clouds by as much as an order of magnitude, McKee and Ostriker (2007).

These findings were built upon the work of Bruce G. Elmegreen and Scalo (2004) who reported that sources of this energy are thought to be winds from stellar sources, predominantly massive stars and Wolf-Rayet stars, with supernova also contributing to the figure, and lower mass stars and planetary nebulae contributing a negligible amount.

In addition, whilst HII regions are seen to support their parent molecular clouds by injecting energy to fuel the clouds internal turbulence, thus preventing against cloud wide gravitational collapse, later in their lives they produce so much energy they can begin to destroy the molecular cloud that they are in, photo-evaporating the surrounding material instead of ionising it. These are known as blister HII regions and are thought to be one of the mechanisms by which molecular clouds are destroyed.

Velocity fluctuations brought on by turbulence are thought to be responsible for altering the density structure of the molecular cloud. These alterations are what create the density fluctuations necessary for star formation to take place as they allow material to clump together getting to a point where the gravitational force overcomes the support from turbulence and thermal pressure and begins the collapse process responsible for forming stars.

1.1.3 Star Formation

Before a molecular cloud can collapse to form a star a series of conditions must be fulfilled prior to the star formation process. These conditions were first defined by Sir James Jean in 1902. He used the virial theorem to derive what came to be defined as the Jeans Mass. Equation 1.2 is the first step to the process of deriving the Jeans Mass and represents the condition that must be fulfilled if hydrostatic equilibrium is to be reached between the outwards thermal pressure and the inwards gravitational pressure of a molecular cloud.

$$\frac{dp}{dr} = -\frac{G\rho(r)M_{enc}(r)}{r^2} \tag{1.2}$$

In Equation 1.2, dp/dr is the change in pressure with respect to the radial distance from the protostar, G is Newtons gravitational constant, ρ is the density of material at radius r, M_{enc} is the mass of the material enclosed by a sphere of radius r, and r is the distance from the centre of the clump.

When one applies virial theorem to Equation 1.2 and also applies the condition that in order for a cloud to undergo gravitation collapse, the inwards gravitational pressure must exceed the outwards thermal pressure, it becomes possible to obtain Equation 1.3:

$$M_J = \left(\frac{5kT}{G\mu m_H}\right)^{3/2}\left(\frac{3}{4\pi\rho_0}\right)^{1/2} \tag{1.3}$$

where M_{J} is the Jeans mass, k is the Stefan Boltzmann constant, T is the temperature of the cloud, G is Newtons gravitational constant, μ is the mean molecular weight of the cloud, m_{H} is the mass of hydrogen and ρ_0 is the initial mass density of the cloud.

Equation 1.3 can also be expressed in terms of the radius of the cloud:

$$R_J = \left(\frac{15kT}{4\pi G\mu m_H\rho_0}\right)^{1/2} \tag{1.4}$$

where the variables are as previously stated for Equation 1.2.

Both of these equations represent a minimum condition that must be met in order for gravitational collapse occur in a molecular cloud. If the mass of the cloud is greater than the Jeans mass ($M_{cloud} > M_J$), then the cloud is of sufficient mass to begin gravitational collapse. Similarly with Equation 1.4 if the radius of the cloud is greater than the Jeans length ($R_c > R_J$) then the gravitational collapse process will start.

These equations are idealised in that they assume the cloud is in a vacuum and thus ignores the existence of an external pressure force from the interstellar medium. This led to a third equation being derived, the Bonnor-Ebert mass.

$$M_{BE} = \frac{c_{BE}\nu_T^4}{P_0^{1/2}G^{3/2}} \tag{1.5}$$

where

$$\nu_T = \sqrt{kT/\mu m_H} \tag{1.6}$$

and is referred to as the isothermal sound speed and c_{BE} is a dimensionless constant given by $c_{BE} = 1.18$, Bradley W. Carroll (2007)

If the cloud can be represented by either of the Jeans formula (Equations 1.2 & 1.3) then it is likely the cloud will begin to undergo gravitational collapse and is said to be in free fall. This collapse is isothermal, meaning that it occurs at a constant temperature, and the time taken for the cloud to undergo gravitational collapse, known as the free-fall time, can be calculated from

$$t_{ff} = \left(\frac{3\pi}{32}\frac{1}{G\rho_0}\right)^{3/2} \tag{1.7}$$

The free-fall time is defined as the time taken for the cloud to collapse under self gravity if no other forces are present and it is worth noting from Equation 1.7 that the free-fall timescale does not depend on the radius of the cloud and is solely dependent on its density.

The star formation process

To help in explain how the collapsing molecular cloud process continues to form a main sequence star, we will use an example of a 1 $M\odot$ spherical cloud of solar composition that

has started undergoing gravitational collapse. As stated in the previous paragraph, the initial stages of gravitational collapse of a molecular cloud are isothermal and the cloud will collapse over a timescale given by Equation 1.7. When the density of the material in the centre of the cloud reaches a critical value (for the 1 M$\odot$ example $\rho = 10^{-10}$ kg m^{-3}), the region becomes optically thick and the collapse ceases to be isothermal and starts transitioning to a more adiabatic process, this is where the region ceases to be classified as a cloud and from now on will be referred to as a core. The collapse continues adiabatically, which dramatically increases the pressure of the core, such that it becomes almost equal to the inward gravitational force. This central region is now almost in hydrostatic equilibrium (and for the 1M$\odot$ example is approximately 10AU in diameter, Bradley W. Carroll (2007)). This region is now what is referred to as a protostar.

During this inner process, the outer envelope of the cloud is still in gravitational free-fall, which leads to the falling material collapsing onto the nearly hydrostatic surface of the forming protostar. This results in a supersonic shock wave forming at the surface that transfers most of the falling materials kinetic energy into thermal energy, which in turn begins to heat up the protostar. This change in temperature leads to a change in pressure that starts a second stage gravitational collapse, this is due to the temperature reaching a sufficient value to cause H_2 to dissociate into individual hydrogen atoms. This is an endothermic process that removes energy needed to maintain the pressure. This collapse continues until the core shrinks to such a size that the pressure can once again reach hydrostatic equilibrium with the inwards gravitational force (for the 1M$\odot$ cloud the diameter of the collapsing core is approximately 0.01AU).

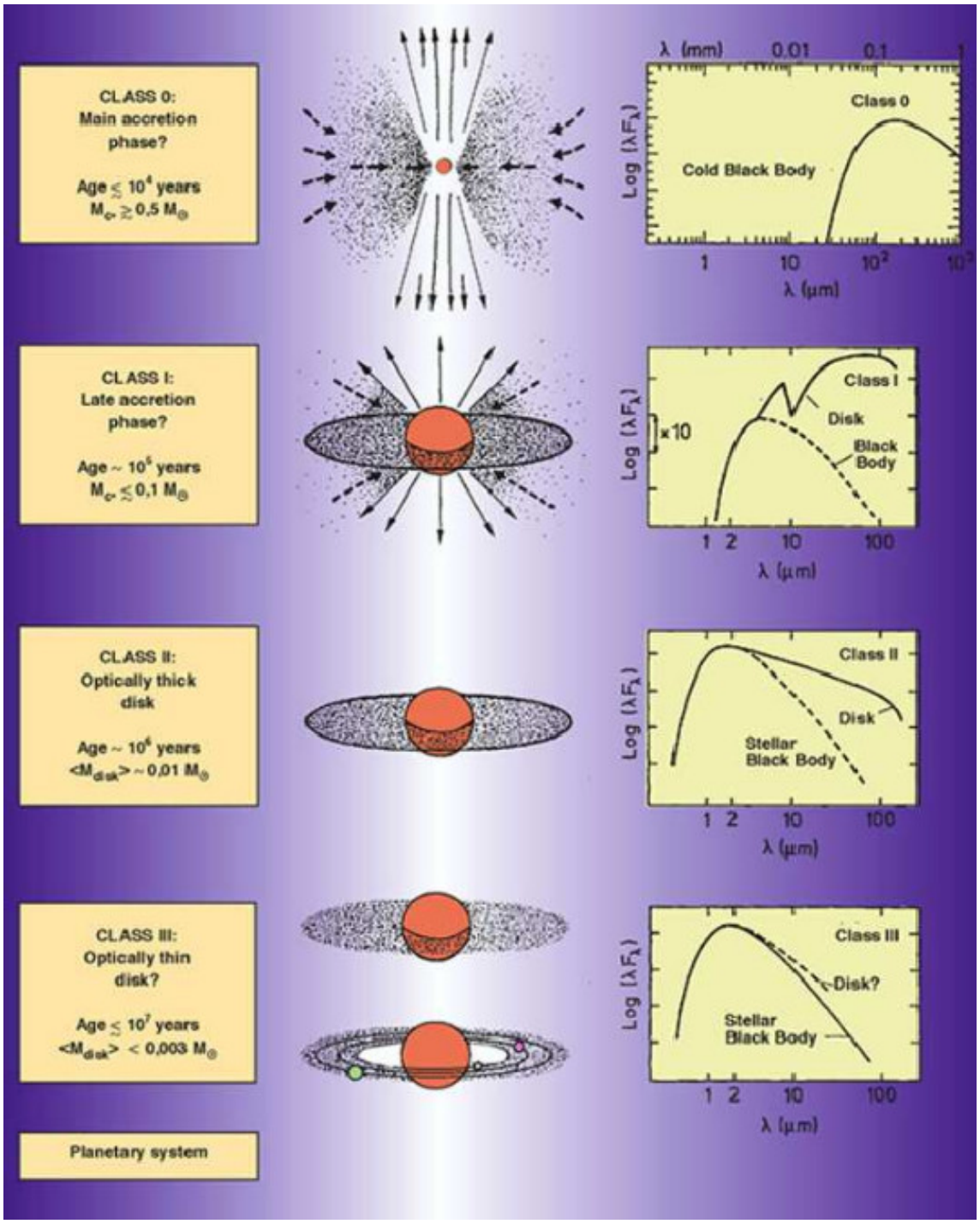

Figure 1.1: Reprinted from Fuente (2001), this figure shows the process of the later stages of low mass star formation.

An accretion disk begins to form around the protostar caused by the increased of rotation of the core due to the conservation of angular momentum, this is the first stage of Figure 1.1, where the accretion disk is not yet fully formed but the equatorial nature of the accretion is shown by the arrows. The angular momentum of the core is increased by the in-falling material. This in turn creates bipolar outflows that helps to dissipate

the (accreted materials) angular momentum by dispersing energy into the ISM.

These outflows are extremely powerful and begin to disperse the molecular cloud surrounding the protostar, stage 1 of Figure 1.1 shows the strength of these outflows, removing material available for accretion from the poles of the protostar before the accretion disk is fully formed. As the star formation process continues, the core temperature continues to rise until it reaches 10^6 K. It is at these temperatures that Deuterium begins to burn. The protostar is now optically visible and having accreted the majority of its mass any further accretion is stopped. The protostar is now considered to be pre main sequence and any remaining material that has not yet been accreted will be eroded away by stellar winds and outwards radiation pressure from the pre main sequence star, this is represented by the final 3 stages of Figure 1.1 where the accretion disk decreases in mass until finally it is fully dispersed with the only remnants of it represented by the planetary system seen in the final stage. Once the Deuterium is exhausted the star begins to move towards the main sequence and will reach it, once the stars energy production is dominated by the burning of Hydrogen located in the core. This is where the star will remain for 90% of its life.

Nuclear Core Reactions

The fusion of Hydrogen to Helium in the core of a star is the process that generates the energy needed for the star to exist. It functions by two separate mechanisms, the Proton-Proton (PP) Chain fusion reaction and the Carbon, Nitrogen and Oxygen (CNO) cycle. Figure 1.2 shows the PP chain reaction, it details the reaction stages by which Hydrogen atoms receive enough thermal energy to overcome the coulomb repulsion force, first fusing into Deuterium, before it then fuses with a single Hydrogen atom to form a Helium Isotope, two of these Helium isotopes will then fuse together to form a normal Helium atom, thereby completing the reaction.

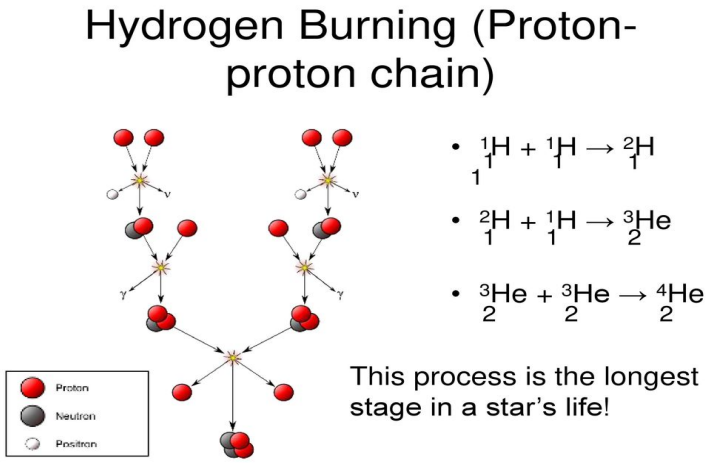

Figure 1.2: This image shows the proton-proton reactions that occur during nuclear fusion in the cores of stars. This reaction is dominant in lower mass stars due to the lower temperature sensitivity needed for it to occur.
https://slideplayer.com/slide/13459265/

The PP Chain reaction seen in Figure 1.2 is the dominant fusion reaction seen in lower mass stars, this is due to the lower temperature sensitivity of the reaction compared to its counterpart, the CNO cycle which makes it more efficient at lower temperatures.

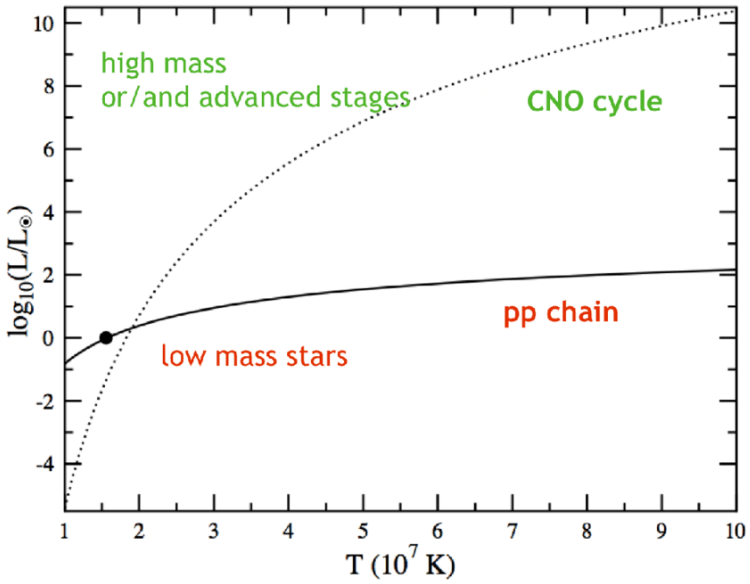

Figure 1.3: This image displays the temperature sensitivity of the proton-proton chain and CNO cycle. It is clear to see that at higher temperatures, such as those found in massive stars, the CNO cycle will become the dominant fusion mechanism.
https://www.researchgate.net/figure/The-respective-weights-of-the-p-p-chain-and-CNO-cycle-in-the-global-stellar-luminosity_fig9_267157073

The temperature dependence of the two reactions can be seen in Figure 1.3, where

the lines on the graph represent the efficiency of the two separate processes. In lower mass stars where the core temperature is $< \sim 2\text{x}10^7$ K, the PP chain is the more efficient reaction hence why, in lower mass stars where the core temperature is lower, the PP chain reaction is favoured. Once the temperature exceeds $\sim 2\text{x}10^7$ K however, the sensitivity of the CNO cycle becomes favourable due to the temperature of the core and becomes the more efficient reaction to produce Helium by, seen after the lines cross in Figure 1.3. The high temperatures needed for the efficiency increase of the CNO cycle is the reason why this reaction is favoured in higher mass stars where the core temperature is substantially hotter compared to lower mass stars. For a star to favour the CNO cycle compared to the PP chain it requires a mass > 1.2 M$\odot$.

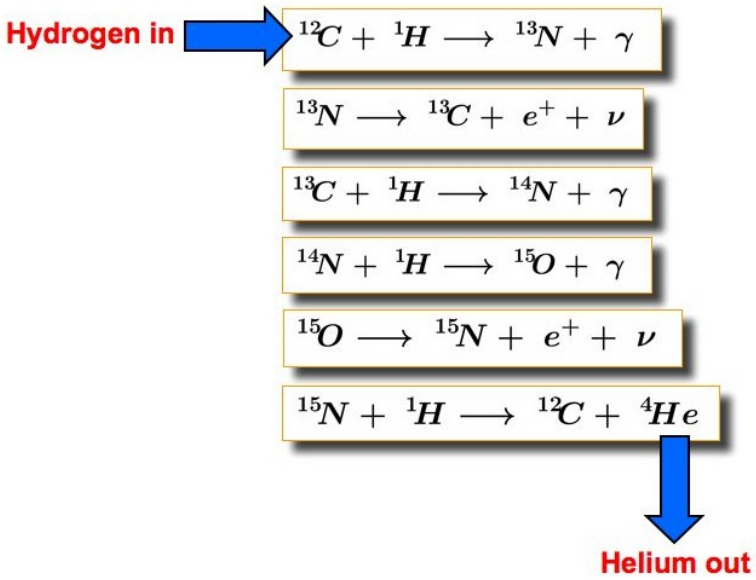

Figure 1.4: This image shows the CNO cycle that occurs during nuclear fusion in the core of stars. Due to this reaction being highly sensitive to temperature it is only found as the dominant fusion mechanism in high mass stars.
Image credit: Swinburne Astronomy Productions
`http://astronomy.swin.edu.au/cosmos/C/CNO+cycle`

Figure 1.4 shows the physical process of the CNO cycle. This process involves the heavier elements of Carbon, Nitrogen and Oxygen catalyzing the reaction of Hydrogen to Helium, it has a significantly higher energy output than the PP chain reaction but due to its temperature sensitivity is only favourable in stars with masses > 1.2 M$\odot$, this mass corresponds to the lines crossing in Figure 1.3.

After the protostar phase the evolution of a stellar object continues and is predicted

by the Hayashi Track, seen in Figure 1.5. This track represents a boundary between the allowed hydrostatic stellar models and those that are forbidden. It was observed by Hayashi (1961) when they plotted mass against temperature and found the link between the two variables. To the right of the track, there is no mechanism that can adequately transport the luminosity out of the star at those low effective temperature; hence no stable stars can exist there. To the left of the track, convection and/or radiation is responsible for the necessary energy transport, Bradley W. Carroll (2007). Furthermore, by definition, there is no fusion possible prior to the MS track seen in Figure 1.5.

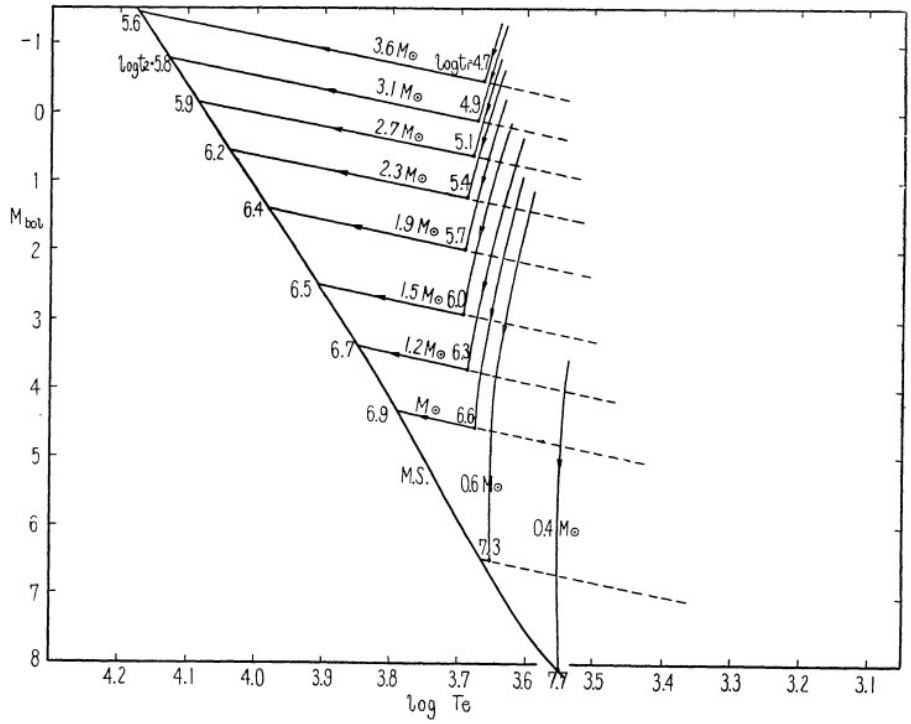

Figure 1.5: This figure displays an example of a Hayashi Track. It is listed as Figure 2 in Hayashi (1961). It shows the evolutionary tracks of stars with their logged temperature on the x-axis and the bolometric magnitude on the y-axis.

1.1.4 High Mass Star Formation

Star formation is governed by two timescales. The first is the free-fall timescale and is described above by Equation 1.7. The second is known as the Kelvin-Helmholtz timescale (t_{KH}) and is described by the following equation:

$$t_{\mathrm{KH}} = \frac{GM^2}{RL} \tag{1.8}$$

The Kelvin-Helmholtz timescale replaces the free-fall timescale when, the rate of evolution of a protostar becomes controlled by the rate at which the star can thermally adjust to the collapse and is significantly larger than the free-fall timescale ($t_{\mathrm{KH}} \gg t_{\mathrm{ff}}$). This translates to the protostars stellar evolution slowing and after the Kelvin-Helmholtz timescale takes over a 1M$\odot$ star will take around 40Myr to fully reach the main sequence.

In certain circumstances the Kelvin-Helmholtz timescale will be less than the free-fall timescale. This occurs in massive star formation where the central temperature is so high it becomes more efficient for the protostellar core to fuse H_1^1 into He_2^4 via the CNO cycle (see Figure 1.4) instead of the PP chain (see Figure 1.2), this increase in efficiency can be seen in Figure 1.3 where after the core temperature exceeds 2x10^7 K, the CNO cycle will produce far higher luminosities than the PP chain. This results in the star forming with significantly higher luminosities and travelling nearly horizontally across the H-R diagram, because of its rapid evolution, instead of following the plots of lower mass, main sequence stars. Due to the rapidness of the star's evolution, it will reach the main sequence whilst still accreting matter and will continue to accrete material until the outward pressure from the star becomes large enough to slow, or even fully stop, the accreting material.

Very little is known about the early stages of high-mass star formation. High-mass protostars are found exclusively in giant molecular clouds and are much less common than lower mass stars, making up only around 1% of total stellar population. They are also found at far greater distances and tend to be more heavily obscured by their natal molecular clump. This makes them far more difficult to observe and, when coupled with their extremely rapid evolution compared to lower mass stars, means that there are significantly fewer observable high-mass protostars at any given time compared to lower mass protostars. Figure 1.6 shows an example of an active star forming region in W43. In this figure examples of regions actively forming stars can be seen highlighted in blue. The main emission from this image is from a cluster of massive stars towards the centre. Other examples of star formation can be seen on the right-hand side of the image where two of the sites in particular appear to be linked by filaments, astronomers have found.

Figure 1.6: This figure displays a false colour image of Westerhout 43 (W43). This is a $7x10^6 M_\odot$ giant molecular cloud in our Galaxy that is currently undergoing both regular and massive star formation. The blue gas represents the regions of active star formation whereas the red and yellow represents the cooler background material that is not associated with star formation. This image was taken by ESA's Herschel space observatory and as such is a combination of 3 different wavelengths of light. 70 microns (blue), 160 microns (green) and 250 microns (red). It spans $\sim 3^o$ on the long side; north is up and east to the left.
`http://www.esa.int/ESA_Multimedia/Images/2017/07/Intense_star_formation_in_the_Westerhout_43_region`

A full comprehensive theory of massive star evolution from birth to death does not yet exist. This is because, especially in the early phases of formation, debates still arise as to how various stages form and evolve. Disagreements also still exist between numerical and computational simulations and observational evidence. Indeed, a review by Frédérique Motte, Bontemps, and Louvet (2018) states that the theoretical upper limit of stellar mass reaches up to 140 $M_\odot$ however, it can be seen from observations that stars can form with masses larger than this such as the largest star observed to date, R136a1.

The star cluster that contains R136a1 is located in the Large Magellanic Cloud and has been known about since the early 1980's with observations being unable to determine individual stellar masses and resulted in a region that appeared to be of ~ 3000 $M_\odot$. Chu, J. P. Cassinelli, and M. G. Wolfire (1984) detailed a number of stars of maximum mass ~ 750 $M_\odot$ however, the subject of the mass of the region was still debated with findings

reporting as much as 2000 $M_{\odot}$ until the mid 1990's when observations started to clear up the puzzle and the individual nature of the clustered stars became more apparent. Its current mass, of $\sim 315\ M_{\odot}$, was detailed in Crowther et al. (2016).

A current issue of massive star formation involves how they initially form from high mass clumps. If high mass stars form from massive protostellar cores or massive dense cores (MDC's) then massive prestellar cores should exist and be readily available to find. High mass prestellar cores however, still remain elusive to find. If they are in fact precursors to massive protostellar cores, then surveys should find between 1-10 more starless MDC's than protostellar MDC's. Whilst starless MDC's are observed as described in Frédérique Motte, Bontemps, and Louvet (2018), they are not found with the frequency expected.

Frédérique Motte, Bontemps, and Louvet (2018) comment on this and mention a few solutions including temperature caused bias in the submm surveys and differences in expected density between protostellar and prestellar MDC's. In fact, the differences in density brings in to question whether prestellar MDC's are even capable of forming massive stars with the likelihood being that they preferentially form clusters of intermediate stars instead. In fact, Svoboda et al. (2016) state that starless MDC's will not form massive stars unless they manage to gain additional mass before progressing to the protostellar phase.

Figure 1.7 displays a mechanism for forming high-mass stars without the need for massive prestellar cores. It was proposed by Tigé et al. (2017) and relies on surrounding material being directed to the surface of a low mass protostar by pre-existing structures in the cloud. As can be seen in stage 1 of Figure 1.7 the structures create gravitational funnels that channel material available for accretion towards these star forming regions. The mechanism is discussed further below in the competitive accretion section.

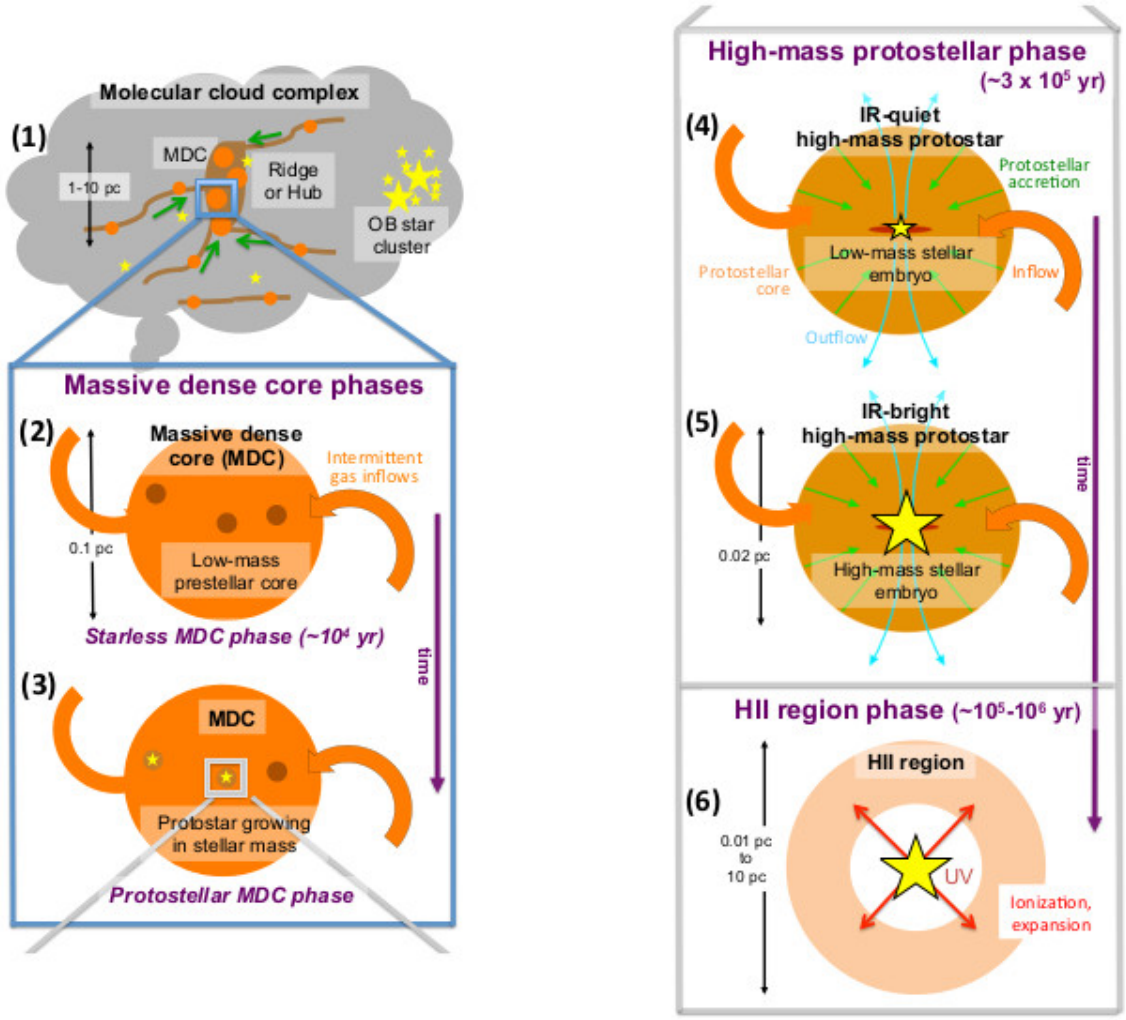

Figure 1.7: This figure is taken from ESO: Tigé et al. (2017). It details a potential formation mechanism for high mass stars by which low mass prestellar cores are transformed into a high mass stellar embryo via channeled accretion of material from preexisting structures that occur within the parental molecular cloud.

Another issue that is associated with massive star formation is how a protostellar core would become massive enough to form a high mass star where some evidence suggests a mechanism by which these cores would fragment due to gravitational instabilities and form clusters of low/intermediate mass stars. Hayashi (1961) and Krumholz (2015) comment on solutions to these mechanisms. The first of which involves a phenomenon called turbulence. The turbulent core model was first proposed by McKee and Tan (2002) and suggests that supersonic microturbulence is responsible for the prevention of fragmentation of a MDC. Hayashi (1961) state an alternative to such high levels of turbulence in the form of strong magnetic fields, which are discussed below.

Radiative Feedback and Magnetic Fields

Krumholz (2015) details two solutions to the fragmentation problem. The first is that of radiative feedback from the protostellar object. This is where the radiation emitted from the forming protostar raises the temperature of the accreting gas, this in turn raises the pressure of the gas which ultimately raises the Jeans Mass. It was found by Krumholz, Richard I. Klein, and McKee (2007), Krumholz, Cunningham, et al. (2010), Krumholz, Richard I. Klein, and McKee (2011), Bate (2009), Bate (2012) and Offner et al. (2009) that when radiative feedback was included as part of the hydrodynamical simulation the effect of fragmentation was reduced.

Peters et al. (2010) reportedly found that even with radiative heating from stellar photons, fragmentation still occurred. However, Krumholz (2015) disregards this saying that the work done by Peters et al. (2010) did not include dust reprocessed radiation fields and was also limited to regions of much lower density than typical massive star forming environments.

The other mechanism at work to reduce fragmentation involves magnetic fields. There are two ways in which magnetic fields are found to reduce fragmentation on massive star formation.

1. The removal of angular momentum from the protostar. It was found that the rapid rotation of the protostellar core causes the magnetic field lines embedded in it to become twisted. This in turn funnels angular momentum from the inner regions to the outer regions of the core. This process is known as magnetic braking.

2. Magnetic fields can also provide extra pressure support that prevents certain regions from collapsing, unless their magnetic flux to mass ratios are below a critical value. This is given by the following equation

$$\left(\frac{\Phi}{M}\right)_{crit} = (4\pi G)^{\frac{1}{2}} \tag{1.9}$$

Regions that contain gas of mass small enough for $\Phi/M < \Phi/M_{\rm crit}$ are said to be

magnetically sub critical. This means that they do not have the mass required to overcome magnetic pressure support and collapse.

It was found by P. Hennebelle et al. (2011) that fragmentation is reduced by a factor ~ 2, when compared to purely hydrodynamical simulations. Commerçon, Patrick Hennebelle, and Henning (2011) and Myers et al. (2013) both found that the strength of these two processes is that they compliment each other. With the removal of angular momentum via magnetic braking, material is channeled more efficiently towards the centre, this in turn raises the rate of accretion, which raises the luminosity and leads to the radiative heating being more effective.

These effects also magnify one another by working principally in two different regions. Radiative heating suppresses fragmentation out to $\sim$ 1000 Au and regions beyond 1000 Au are found to be magnetically sub-critical. The fact that these mechanisms work best where the other is weakest allows the combinations of them to reduce fragmentation much more strongly than one might initially guess.

Another issue to do with massive star formation is finding a theoretical framework so that simulations can support the models. Mathematical calculations associated with upper mass limits on star formation originally showed that the maximum mass a stellar core can form at is no greater than 40 $M_\odot$ (Kahn (1974)), this upper limit has been revised as new data was made available with masses ranging from as low as $\sim 7M_\odot$, found by Mark G. Wolfire and Joseph P. Cassinelli (1987), up to 140 $M_\odot$, found by Frédérique Motte, Bontemps, and Louvet (2018). However, observation show these values are incorrect, with the example of Star R136a1, the most massive star discovered to date, that has an approximate mass of 315 $M_\odot$ (Crowther et al. (2016)), from this observation it is clear that stars are capable of forming with masses far greater than the theoretical limit.

This limit is due to stars forming through accretion. When massive protostellar cores reach a certain mass, they start to emit powerful ionising radiation. This radiation pressure has been thought to slow and then terminate accretion as the material is halted, pushed and then dispersed by the powerful radiation. Before a solution to this problem

was found, several theories were formed as to how the protostellar core would gain enough mass to become classified as a high-mass protostar.

Proposed Models

Coalescence

This is a model whereby two protostars in a star forming cluster will collide during their formation process and merge into one massive star. In order for this to be a viable mechanism the density of the clusters must be at least 10^4 stars pc^{-3}. This method was proposed by Ian A. Bonnell, Bate, and Zinnecker (1998). Observations have shown that whilst some clusters do posses the required density for this to be considered a valid formation mechanism, the vast majority do not.

Spherical Accretion

This process comes from a fundamental alteration to the parent giant molecular cloud such that the gas to dust ratio of the cloud is reduced, this allows for very high accretion rates to occur breaking the upper mass limit but, this reduction in the gas to dust ratio is only present in giant molecular clouds that have been altered by shocks or perhaps a supernova and is unsupported by observation, Mark G. Wolfire and Joseph P. Cassinelli (1987).

Turbulent Core Model

McKee and Tan (2003) suggest a method which they term the "Turbulent Core Model" to form massive stars. This is a simple method where massive star formation is comparable to low mass star formation. The requirement for this is that massive stars would thusly only form from massive clumps. These clumps are supported by internal turbulence from the rest of the molecular cloud which would stop the clump from fragmenting into small clumps that would only go on to form lower mass stars.

Competitive Accretion

This method of massive star formation describes a scenario that would only be present

in stellar clusters, which given that all massive stars are thought to exclusively form in stellar clusters anyway could be advantageous. In this process the most massive clumps fragment creating a reservoir of available gas. This gas is then gravitationally funneled by other forming cores and towards other accreting protostars allowing them to grow in size to become massive protostars. A restriction on this process is that there must be a large available reservoir of gas stemming from an inefficient fragmentation process. A second restriction comes from the fact that the gas must be free to move under the same gravitational acceleration as the stars. This method of massive star formation is supported by observations from F. Motte, Andre, and Neri (1998); Johnstone, Wilson, et al. (2000); Johnstone, Di Francesco, and Kirk (2004); Charles J. Lada and E. A. Lada (2003); Bastian and Goodwin (2006) and I. A. Bonnell (2008)

Tigé et al. (2017) propose a mechanism, very similar to that of competitive accretion which is also detailed and elaborated on in the aforementioned review of massive star formation published by Frédérique Motte, Bontemps, and Louvet (2018). This mechanism can be seen in Figure 1.7 and displays a very similar process to competitive accretion whereby ridges and hubs funnel material toward a low mass protostars (Seen globally in stage 1) allowing it to accrete additional material until it becomes a massive protostar (seen in stages 2-5).

Accepted Models

Non-Spherical/Equatorial Accretion

The first method that was found that allowed massive stars to overcome this mass limit is that of non-spherical/equatorial accretion. This process arises from the assumption that the majority of the radiation pressure exerted by a protostar is not emitted uniformly but instead forms two powerful jets that are emitted from the polar regions of the protostar. These jets will disperse accreting material around the poles but due to their direction will not have an affect on the material being accreted near the equator of the protostar. This allows the protostar to continue accreting material far beyond the original mass limit posed back in 1987. This mechanism has been popular over the past decade with

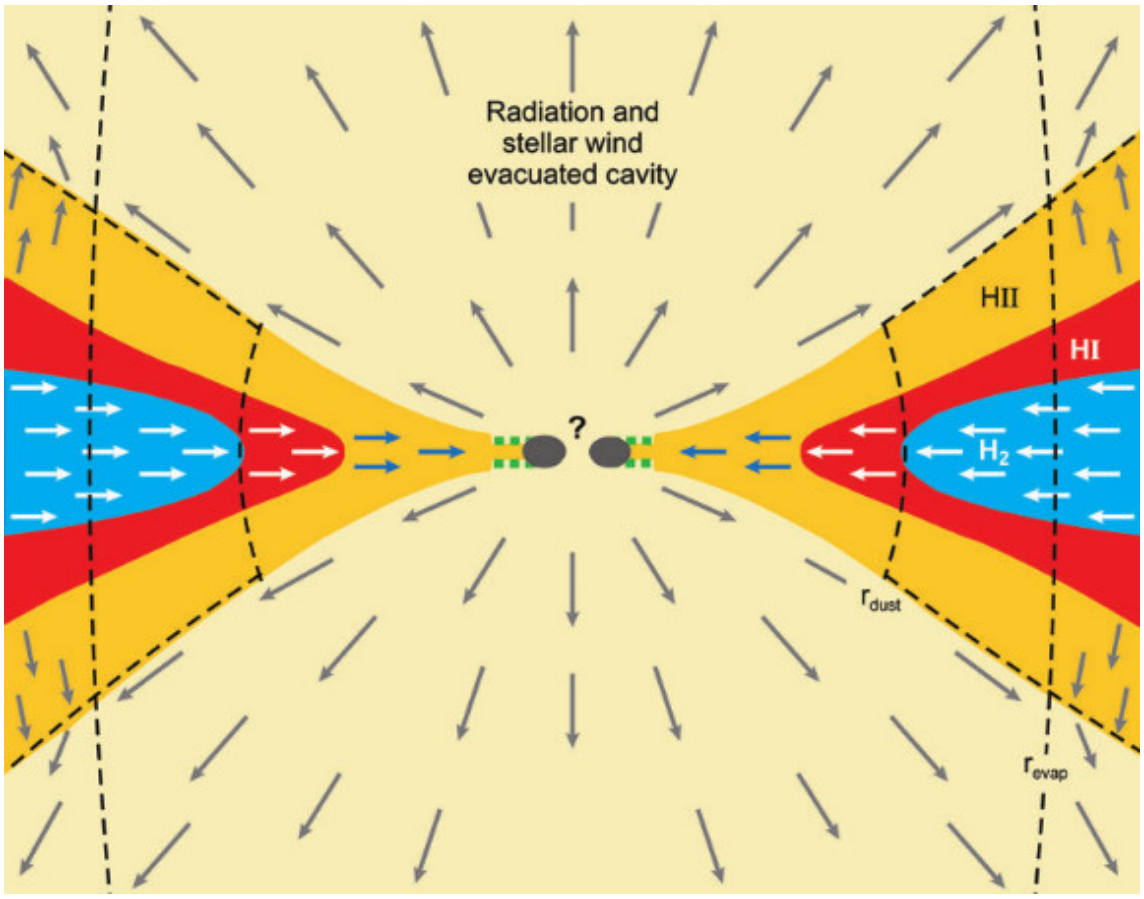

Figure 1.8: This figure displays an example of a binary protostellar system undergoing the process of equatorial accretion. In this particular example the material at the equator of the system is also self-shielded from the polar outflows and additional radiation pressure. This figure was taken from Zinnecker and Yorke (2007)

.

R. Kuiper et al. (2011), Ian A. Bonnell and Bate (2006) and Keto (2007) all investigating this mechanism.

Cesaroni et al. (2007) commented on evidence of disks existing around massive stars and observational evidence for them, concluding that, it seems plausible that massive stars form through disk accretion similar to low mass ($< 8\ M_{\odot}$). However, Cesaroni et al. (2007) do comment that they found no evidence of disks present around early O type stars and so state that in the case that there are no disks possible for such stars, alternative formation mechanisms must be proposed. Furthermore they state that a possible reason for the lack of disks could be due to the sensitivity of instruments used and that new, higher resolution surveys, such as ALMA are likely to be key of key importance in solving this problem.

Figure 1.8 taken from Zinnecker and Yorke (2007) shows how material at the equatorial regions of a pair of massive binary protostars. In this example the accreting material (shown as blue H_2 is self-shielded from the outward radiation pressure (shown as yellow HII and red HI) and combined with its position around the equator allows the binary system to continue its accretion process despite the powerful outflows from the binary pair (shown by the outward radial arrows).

Protostellar expansion

The other method occurs when the protostar swells up due to accreted material. As the radius of the protostar increases its surface temperature decreases. When one looks at a black body emission graph of a stars surface temperature compared to its radiation output, it can be seen that this causes the protostars maximum emitted radiation wavelength to decrease. This lessens the power of the radiation pressure, slowing the dispersion of the surrounding material, which enables the possibility of further accretion past the point of the theoretical mass limits.

1.2 Massive Stars and HII regions

HII regions form when the corresponding surface temperature of massive stars becomes high enough that their peak radiation energy reaches an intensity of 13.6 eV. Radiation at this energy level or higher has enough energy to completely ionise molecular hydrogen. Because massive stars reach this point whilst still embedded in their natal clump, they begin to ionise their surrounding molecular gas.

This causes a bubble of ionised hydrogen to form around the host star (or stars as HII regions can be created by binary systems), it is this bubble that is then classified as a HII region. As the aforementioned 13.6 eV radiation intensity threshold is required to create these ionised bubbles, only stars of high masses can maintain this energy output. On the traditional stellar classification system (O, B, A, F, G, K, M) it is found that O type and B type stars are able to form HII regions. They are referred to as OB stars by astronomers. An example of a HII region can be seen in Figure 1.9, which shows the HII

region S305 which has been created by a pair of O type massive stars.

The temperature of the ionized Hydrogen that makes up the HII region is very high (>10000K) whereas, the temperature of the molecular Hydrogen may be as low as 10 K. This temperature difference results in a pressure difference that causes the HII region to expand. The massive star at the centre of the HII region aids this process as the stellar winds it emits creates a supersonic ionisation front at the boundary of the HII region that travels radially outwards into the surrounding material causing a rapid expansion of the HII region. The expansion will cease once the ionized gas reaches a pressure equilibrium with the surrounding material however, except in regions of very dense surrounding material, this will not occur before the death of the host star, Deharveng, Schuller, et al. (2010).

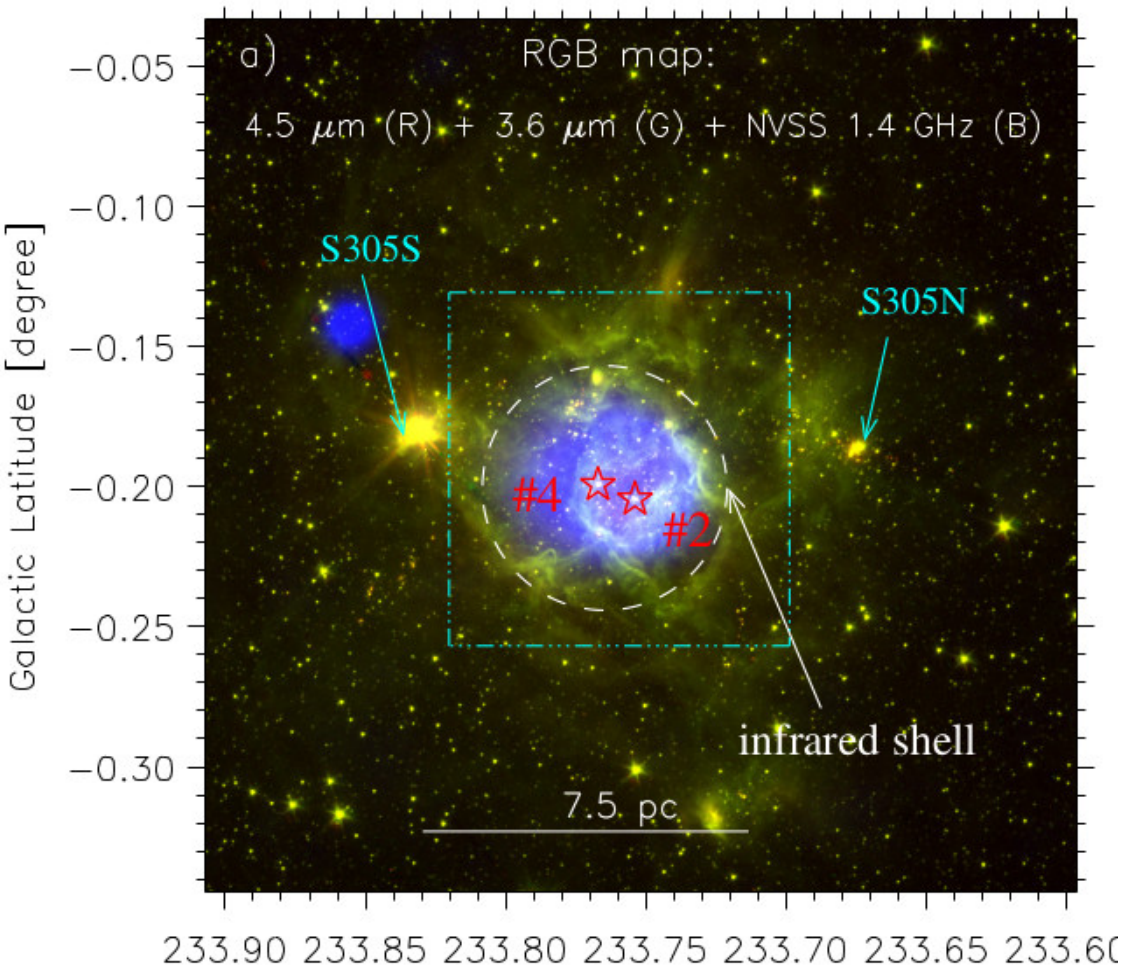

Figure 1.9: This image shows the HII region S305. This HII region was created by two O type stars. The three colour image corresponds to red, Spitzer 4.5 μm: green, Spitzer 3.6 μm: blue, NVSS 1.4 GHz. The shell of the HII region is highlighted by the dashed circle. This image was taken from Dewangan et al. (2020)

.

The high energy radiation emitted by the massive star drives the expansion of the HII region and leads to the formation of an ionisation front at the border of the HII region, this can be seen in Figure 1.9 where the outer shell of the HII region S305 is highlighted by the broken white circle, note that this circle is not uniform as the border of the HII region will expand at different rates due to in-homogeneity's in the density of the surrounding material. This causes the molecular hydrogen of the stars natal clump to be swept up by the ionisation front, which causes the material in contact with the ionisation front to move faster than the material in other parts of the cloud. This compresses the material and forms a boundary at the edge of the HII region. At this boundary a number of processes can occur, some of which, can lead to a phenomenon known as triggered star formation.

Details of HII regions can be found in textbooks such as Spitzer (1978) - Physical processes in the interstellar medium. Whilst revisions to the HII region formation mechanism have been made by others such as, Franco, Tenorio-Tagle, and Bodenheimer (1990) and Keto (2002) to include more detailed mechanisms.

1.3 Triggered Star Formation

Stars can form in a number of different ways. One type of star formation is called spontaneous star formation. This corresponds to stars that appear to form without any particular mechanism or trigger initiating the formation process. There may be a mechanism causing the stars to form but that is yet to be observed for this particular type of formation classification.

Another process by which stars can form is through a process known as triggering. This is where some mechanism kick starts the process of star formation instead of it occurring spontaneously, Dale, T. J. Haworth, and Bressert (2015). There are 3 subcategories of triggering that were presented by Dale, T. J. Haworth, and Bressert (2015) to try and state a formal definition of triggered star formation. These are:

1. Type I triggering: a temporary or long-term increase in the star formation rate.

2. Type II triggering: an increase in the final star formation efficiency.

3. Type III triggering: an increase in the total final number of stars formed, Dale, T. J. Haworth, and Bressert (2015).

However, for this project as we are looking at triggering as a whole. We shall be examining all of these subcategories under the parental banner of triggering.

This process has been studied as far back as 1977 when Elmegreen and Lada published a paper on what became known as the "collect and collapse" method (B. G. Elmegreen and C. J. Lada (1977)), a method which is discussed later in this section. The other method of triggered star formation that is discussed is known as Radiative Driven Implosion (RDI) and is first mentioned by Sandford, Whitaker, and R. I. Klein (1982). These

two processes are described in detail below as they have been observed to contribute directly to triggered star formation at the boundaries of HII regions. Triggered star formation has mostly been studied as a result of ionisation feedback from massive stars and HII regions (Dale, T. J. Haworth, and Bressert (2015)), however, other mechanisms exist including a process by which molecular clouds collide, known as cloud-cloud collisions (Loren (1976)), and the possibility of star formation being triggered by supernova explosions. As this project specifically involves HII regions we will not be discussing these other mechanisms in any further detail.

Radiative Driven Implosion

RDI is the method by which molecular material on the edge of a HII region is compressed by the ionising radiation from the massive star at the centre of the HII region. The ionising radiation forms a D-type shock (composed of denser (D), slower moving gas than its counterpart, an R (rarefied) - type shock) that impacts the molecular material (Urquhart, Morgan, and Thompson (2009)), forming an ionisation front that can be seen in the first panel of Figure 1.10. The radiation then erodes the less dense molecular material until it reaches the dense clumps, this allows an observer to now classify the environment as a bright rimmed cloud (BRC), this process in part can be seen in panels 2 & 3 of Figure 1.10 where the initially wide span of material has been compressed and eroded down into a much narrower and denser clump. A bright rimmed cloud is so named because it will appear as an extremely bright region on the edge of the HII region compared to darker globules at the boundary, Sugitani et al. (1989). These dense clumps now protrude into the HII region and are compressed on all sides by the ionising radiation. As explained in detail below, the ionising radiation will propagate through the cloud, this causes the cloud to be compressed further, which can lead to the formation of dense cores inside the cloud. These cores then collapse, which begins the process of star formation.

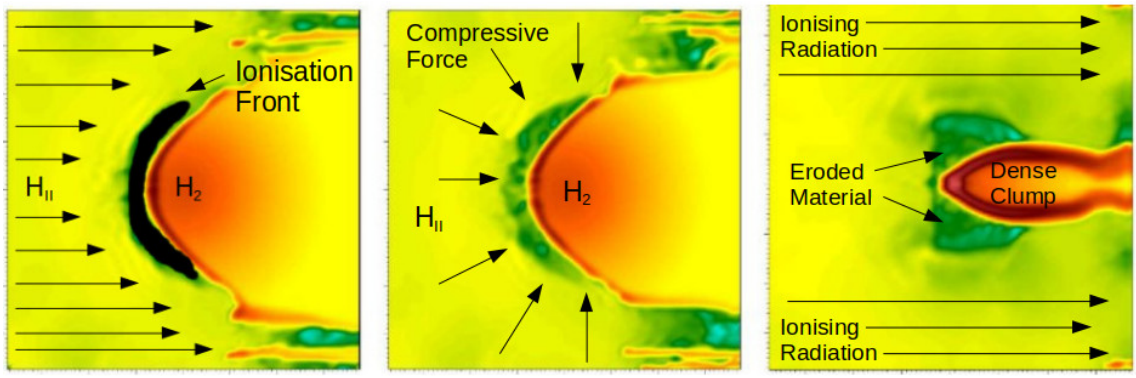

Figure 1.10: This figure shows a numerical simulation from Thomas J. Haworth, Harries, and Acreman (2012) where ionising radiation in a HII region is approaching a dense clump of molecular hydrogen. In the first panel it can be seen where the incoming radiation forms an ionisation front where the dense H_2 is resisting erosion. The second panel shows how the ionising radiation will surround the H_2 and begin to compress it. The third panel shows how much of the original clump of H_2 has been eroded or compressed into a much denser clump/core of H_2. This material could collapse, either spontaneously or thanks to further ionisation pressure from the HII region and form a star.

The pressure balance between the external, hot ionised gas and the cooler molecular gas within the cloud has emerged as a key diagnostic that can be used to evaluate the impact the arrival an ionisation front has on the dynamics and future evolution of the cloud ,Urquhart, Morgan, and Thompson (2009). The following options are presented in Urquhart, Morgan, and Thompson (2009) as predictions from numerical models of processes that occur when a molecular cloud is exposed to strong far-UV radiation from a nearby HII region.

1. The intensity of the ionising radiation is too low and/or its pressure is too little to compress the material and the clump is unaffected by the radiation.

2. The intensity of the ionising radiation is too strong and/or the density of the molecular material is too small. This allows the ionisation front to travel supersonically through the cloud which results in an almost immediate photoionisation of the cloud. This second process has two names either an ionisation flash by Lefloch and Lazareff (1994) or cloud zapping by Bertoldi (1989).

3. The final option in an almost Goldilocks like scenario involving the ionising radiation

being of sufficient intensity and/or the cloud being of the correct density. This allows the ionisation front to dominate the whole evolution of the cloud and also drives an isothermal shock into the cloud, Urquhart, Morgan, and Thompson (2009). This compresses the gas which can fragment and collapse to form a new generation of stars.

Urquhart, Morgan, and Thompson (2009) states that the numerical models mentioned previously show that the third option is the most common for a wide range of possible input parameters as well as being the most interesting in determining which clouds are likely to host triggered star formation. If the ionisation front described in the third option is of a high enough pressure to overcome the nebula and the molecular gas within the bright rimmed cloud, it starts to form a layer around the molecular gas composed of ionised material known as an ionisation boundary layer (IBL). However, a large amount of the ionising UV radiation will make it through the IBL and will start to ionise the gas forming a Photon Dominated Region (PDR).

The extreme pressure differences between the hot ionised layers of the cloud and the cooler molecular layers causes more isothermal shocks to be driven into the cloud. These shocks compress the material until dense cores can begin to form. The subsequent shocks then cause these cores to collapse, which will begin star formation. These shocks will also cause the collapse of cores that already formed before the arrival of the ionisation front potentially enhancing star formation at that location within the cloud. Sugitani et al. (1989) details three globules near HII regions: IC 434, IC 1396, and SI45 associated with bright rims. The results achieved from ^{13}CO observations matched recent hydrodynamical simulations meaning that stars formed in proximity to their parental HII regions had a strong chance of being triggered though the RDI mechanism. Urquhart, Morgan, and Thompson (2009) list a selection of 24 BRC sources that are associated with PDR's or IBL's in Table 4b, in their publication, and are good candidates for triggered star formation. They also state in their conclusion that only 50 percent of the BRC's they identified as currently undergoing RDI are in the process of forming stars. The other 50 percent are said to be in very early stages of gravitational collapse, Urquhart, Morgan,

and Thompson (2009).

Collect and Collapse Method

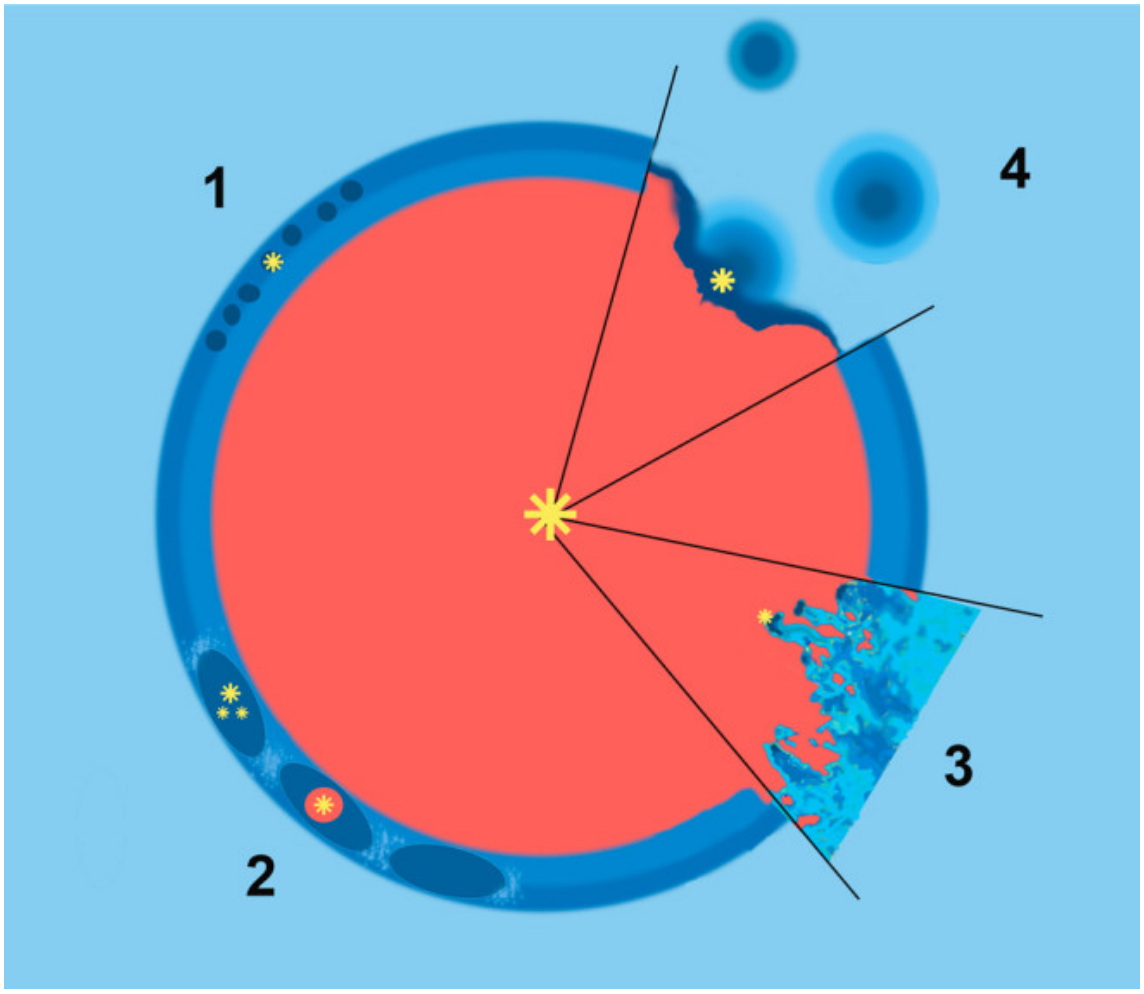

Figure 1.11: This figure shows a graphic of an expanding HII region. 1&2 show examples of small and large gravitational instabilities at the boundary of the HII region caused by its expansion. Such instabilities as these are likely caused by the collect and collapse process as they are regularly spaced around the border of the HII region. This figure is taken from Deharveng, Schuller, et al. (2010).

In the collect and collapse method the HII region expands into the surrounding molecular clump. Due to the pressure difference at the boundary of the HII region caused by the temperature difference between the hot ionised material of the HII region and cooler molecular material of the surrounding gas, the molecular material is swept up by the expanding HII bubble. This forms an inhomogeneous shell of compressed molecular material that ends up being evenly distributed around the HII region and can be imagined

as a preliminary stage to points 1 & 2 of Figure 1.11.

As the HII region expands, driven by the ionising radiation, this shell will build up over millions of years, eventually gaining enough mass to become gravitationally unstable as proposed by B. G. Elmegreen and C. J. Lada (1977). Various studies have been conducted to determine the timescales over which this process takes place. For example, Whitworth et al. (1994) states that a compressed layer around a HII formed by an O7 type star, evolving in a medium of 10^3 cm^{-1}, with a sound speed of 0.5 kms^{-1} in the layer, will become unstable after approximately 3 Myr. Whitworth et al. (1994) also states that in the O7 example about 7 fragments will form each with a mass of approximately 600 $M_{\odot}$.

The collect and collapse model favours the production of massive stars. This is due to the fact that providing the layer is not destroyed by dynamical instabilities, a large quantity of material accumulates within it over the course of the shells expansion, Deharveng, Zavagno, and Caplan (2005). When this layer collapses due to gravitational instabilities within it, it produces massive fragments spaced equally around the HII region, this can be seen at point 2 of Figure 1.11. These massive fragments then collapse in turn to begin the star formation process.

Deharveng, Zavagno, and Caplan (2005) developed a set of criteria in their paper for the selection of candidates for the collect and collapse process. The authors list predictions that must be verified if the collect and collapse process is at work around a star and mention how 'the presence of several fragments regularly spaced around the compressed layer is a strong argument in favour for the process as it allows the elimination of processes involving pre-existing clumps or clumps formed by turbulence'. However, none of the samples proposed by B. G. Elmegreen (1998) to illustrate the collect and collapse process are completely convincing as the morphologies of the region are too complex to verify if the pre-existing conditions are met. In order to prove the collect and collapse process is present the researchers need to find better candidates. To find better candidates the authors propose the following criteria:

1. A nearly spherical HII region around an exciting star or cluster.

2. A dust emission ring surrounding the ionised gas. The presence of this ring indicates that dense natural gas surrounds the HII region.

3. An MSX point source in the direction of the dust ring (we call a 'point source' any source listed in the MSX point source catalogue (Egan (1999) & Egan, Price, and Kraemer (2003))).

4. Red stars or clusters associated with the MSX point sources.

The researchers used the 2MASS survey to search for such objects (Deharveng, Zavagno, and Caplan (2005)). An example of a HII region that fulfills these conditions can be seen in Figure 1.12 which displays the HII region RCW40. The spherical overlay in the image shows the low ellipticity of the HII region and the contours overlayed over the top of the image, trace the full dust ring that surrounds the HII region. Deharveng, Zavagno, and Caplan (2005) also comment on the HII region, saying that MSX and IRAS sources are visible in the ring and when the HII region is observed at 1.2 mm indications of the collect and collapse process can be seen in several bright condensations along the ring.

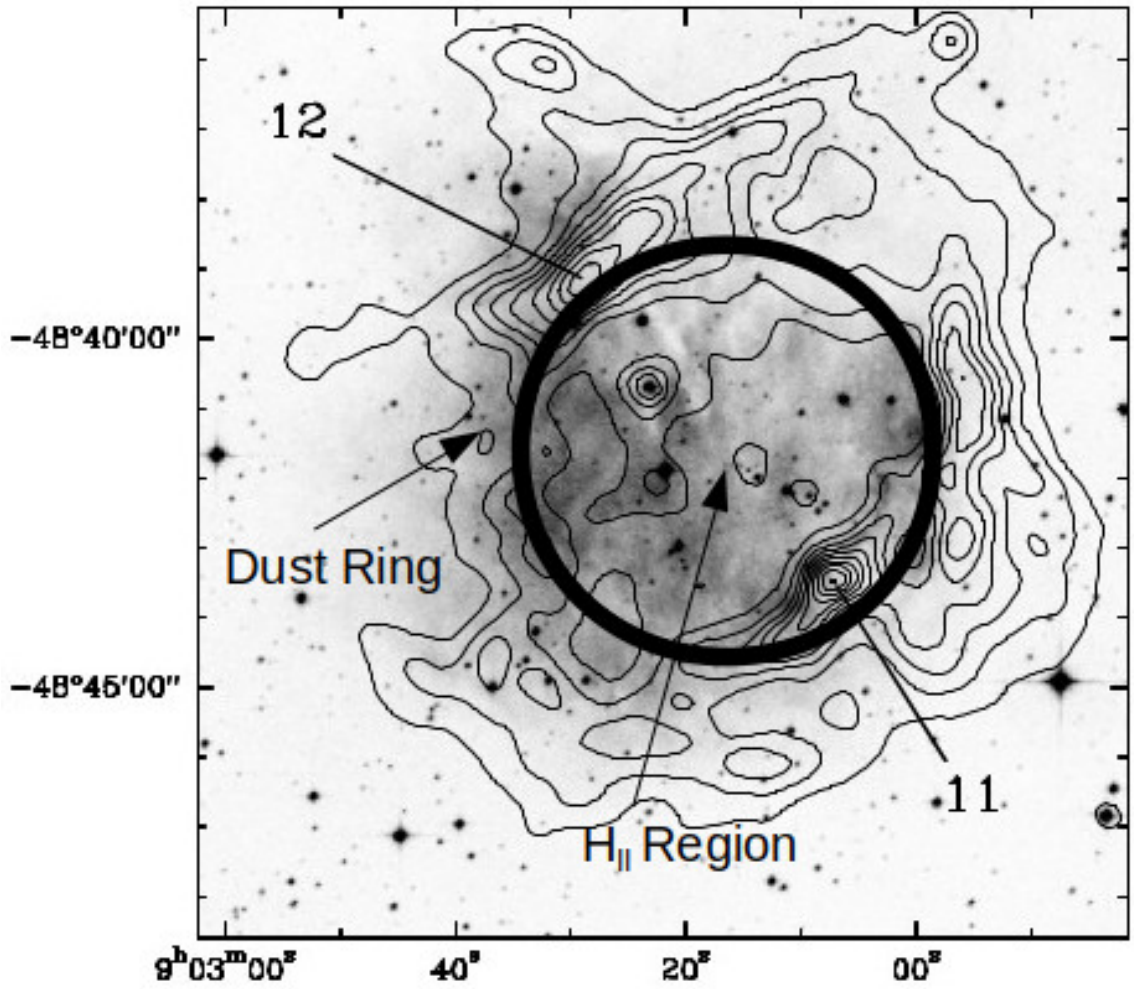

Figure 1.12: This Figure displays an annotated image from Deharveng, Zavagno, and Caplan (2005). It shows the HII region RCW 40 with MSX Band A contours superimposed on a DSS-2 red image. The HII region is presented as being an ideal candidate to study the collect and collapse process as it meets their proposed requirements is surrounded by a complete ring of dust emission.

Deharveng, Zavagno, and Caplan (2005) thusly lists two types of HII region as potential candidates for the collect and collapse process. The first type is a HII region surrounded by a nearly complete ring of dust emission. The HII regions listed in the 2005 publication are Sh104, RCW 40 , RCW 79, RCW 82 and RCW 120. See Figure 1.12 which displays RCW 40 as listed by Deharveng, Zavagno, and Caplan (2005). The other category of HII regions are of low brightness and surrounded by an incomplete dust emission source. These HII regions are source Z, Sh 219, Sh 241, and Sh 259. An example of these sources can be seen in Figure 1.13, where it can be seen that in comparison to Figure 1.12, not only is the HII region itself much fainter but the dust emission ring is

only partially complete. However, it is also worth noting that in accordance with the previously proposed criteria, the HII region Sh219 in Figure 1.13 is still spherical in nature. Note that the authors do not confirm that the collect and collapse process is present here and state that 'it will be interesting to determine if the collect and collapse process is at work in both types of HII regions and if the same kinds of stars are formed'.

Despite all the theoretical and computational advances in the field, the statistical impact of triggered star formation both as a whole and in the Milky Way is still unknown. However, dense clumps of material at the borders of HII regions such as BRC's provide excellent sites for investigation. The different physical parameters of these sites can be statistically compared with those of other sites that are not triggered. This is the focus of the work presented in this thesis, with the final goals to demonstrate a difference between triggered and spontaneous star formation and to estimate the percentage of Galactic star formation that occurs through a triggering mechanism. In Chapter 2 we present our methodology and selection criteria for triggered and non-triggered sources, in Chapter 3 we present our findings, Chapter 4 contains the discussion of the results, and we present our conclusions in Chapter 5.

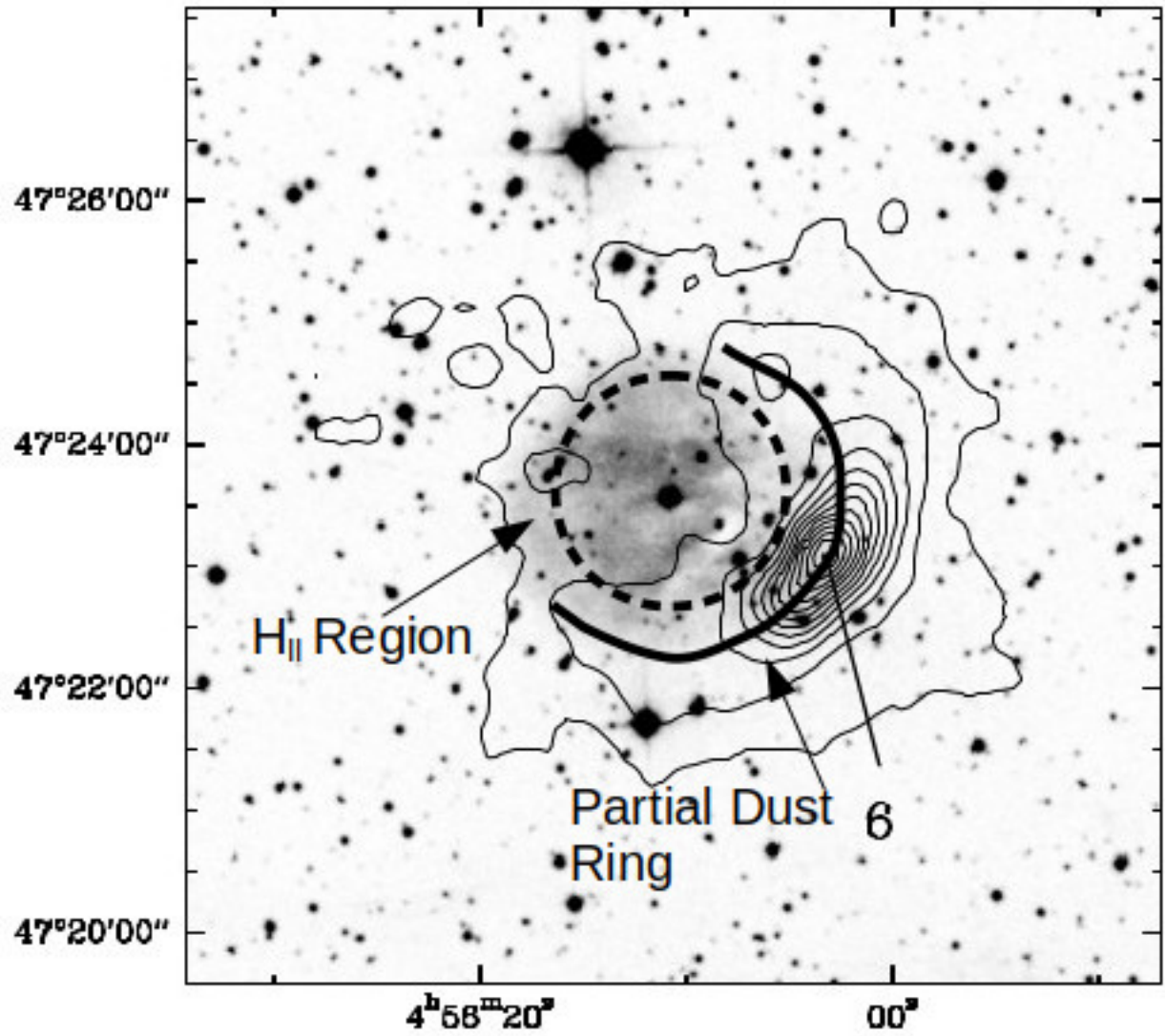

Figure 1.13: This Figure displays an annotated image from Deharveng, Zavagno, and Caplan (2005). It shows the HII region Sh 219 with MSX Band A contours superimposed on a DSS-2 red image. This HII is still considered a good candidate for the collect and collapse mechanism but does not meet the required standards to be an ideal candidate due to the incomplete dust ring surrounding it and it appearing much fainter in the survey than other HII regions such as the one shown in Figure 1.12

.

Chapter 2

Overview of Project and Methodology

2.1 Project Overview

Triggered star formation is still a subject for debate within the astrophysical community. There are several unanswered questions that still remain since the theorizing of triggered star formation back in the early 1980's. We will attempt to answer the following questions in the presentation of this thesis:

1. How does one distinguish between stars formed exclusively through triggering and stars that would form even if the triggering mechanism were not present?

2. Is there any difference between triggered star formation and spontaneous star formation?

3. What is the fraction of stars that form this way in the Galaxy?

The above questions will now be examined in detail.

Finding a difference between triggered and spontaneous star formation presents some obvious challenges. Once star formation has been triggered due to a particular mechanism, usually due to an environmental influence, there is no current simulation that exists that can test whether or not stars would form in the absence of a triggering mechanism.

Part of the method presented in this thesis for the analysis of different environments of star forming regions, includes a statistical comparison of the physical properties such as luminosity, temperature, radius and mass of such environments. If a statistically significant difference is found between one or more of the physical properties it could indicate a difference in whether or not stars would form via spontaneous formation or not in the absence of a triggering mechanism. If stars form anyway via spontaneous formation, then comparisons of physical properties could reveal insights into differences in star formation efficiency, star formation rates and/or the final physical properties of the created stars.

These differences in physical properties may also reveal fundamental differences between stars formed through a triggering mechanism and those formed through spontaneous star formation.

2.2 Background

As stated in the project overview, the broad aim of this project is to evaluate the impact of triggered star formation on a Galactic scale. Looking at the first question we present in the project overview: Would star formation still occur in triggered scenarios if the triggering mechanism was removed?, it becomes necessary for us to prioritise this question over the other 2 as, if there is no difference between stars formed through triggered mechanisms or spontaneous mechanisms and, stars that were formed through a triggering mechanism would have formed anyway through spontaneous formation, then the impact of triggered star formation in the Galaxy is greatly reduced.

Other studies have been carried out on the significance of triggered star formation. One such study by Thompson et al. (2012) was done to investigate a seeming overdensity of massive young stellar objects (MYSO's) around spitzer bubbles (HII regions identified with data from the spitzer space telescope). Conclusions listed in this paper included finding a statistically significant peak in MYSO's at a distance of 1 bubble radius and it being likely that a significant number of these MYSO's were likely to have been triggered. This publication does have its limitations however, for example the authors state that the

sample size is comparatively small, numbering only 322 bubbles, and whilst extrapolation is possible it would not be suitable to draw conclusions regarding Galactic star formation from it. Also, the common mid infra-red bands used to detect the bubbles may have led to a bias in the identification of the point sources at the bubble rims, Thompson et al. (2012).

A paper published by S. Kendrew et al. (2012) also speaks on the prevalence of triggered star formation on a Galactic level using both Thompson et al. (2012) as a base reference before using data from the Milky Way citizen science project to compile their own database. S. Kendrew et al. (2012) replicated the results of Thompson et al. (2012), also finding a statistical overdensity of MYSO's around HII regions found at 1 bubble radius. The selection process used by the Milky Way citizen science project resulted in an unbiased sample, however, S. Kendrew et al. (2012) state that they cannot conclusively prove or disprove the occurrence of triggering at these sites leaving the question of impactful triggering still open.

Other studies have been done on individual HII regions, such as Samal et al. (2014) and Liu et al. (2015), that have found evidence of triggering, but these are still listed as inconclusive. Dale, T. J. Haworth, and Bressert (2015) list many studies both of singular focus and those looking at the larger scale with similar results however state that the authors for these papers urge caution and do not present their results as conclusive evidence for triggered star formation.

2.3 Catalogues

ATLASGAL

The Apex Telescope Large Area Survey of the Galaxy (ATLASGAL) is a survey of the Galaxy conducted at 870 μm. The goal was to provide an accurate survey of the inner Galactic plane, mapping what amounted to several 100 deg^2 with uniform sensitivity. The survey consisted of $\sim$ 500 hours of observing time split between the Max Planck Institute, European Southern Observatory and the Universidad de Chile. The first data set

Parameter	#	$\bar{x}$	$\frac{\sigma}{\sqrt{(N)}}$	σ	$x_{\rm med}$	$x_{\rm min}$	$x_{\rm max}$
Temperature (K)	7861	19.52	0.07	5.80	18.60	7.90	56.10
MSF Temperature	1222	24.58	0.14	5.06	24.00	12.60	56.10
YSO Temperature	4053	20.93	0.08	5.25	20.10	8.60	53.00
Protostellar Temperature	1640	15.52	0.07	2.80	15.20	8.30	30.20
Quiescent Temperature	946	13.88	0.12	3.64	13.30	7.90	48.70
Radius (pc)	4836	0.71	0.01	0.62	0.52	0.01	7.73
MSF Radius	1017	1.00	0.02	0.77	0.78	0.01	7.73
YSO Radius	2552	0.70	0.01	0.59	0.52	0.02	4.86
Protostellar Radius	840	0.53	0.01	0.43	0.40	0.05	2.89
Quiescent Radius	427	0.47	0.02	0.37	0.38	0.03	2.25
Log[Luminosity ($L_\odot$)]	7614	2.95	0.01	1.03	2.89	−0.30	6.91
MSF	1191	4.01	0.03	0.93	4.03	−0.30	6.91
YSO	3922	3.12	0.01	0.84	3.10	0.43	6.24
Protostellar	1580	2.29	0.02	0.69	2.24	−0.30	4.62
Quiescent	921	1.99	0.02	0.72	1.93	0.00	4.83
Log[Clump Mass ($M_\odot$)]	7614	2.68	0.01	0.65	2.69	−1.00	5.04
MSF	1191	2.95	0.02	0.71	3.02	−1.00	5.04
YSO	3922	2.62	0.01	0.66	2.64	−0.40	4.72
Protostellar	1580	2.64	0.01	0.58	2.62	0.18	4.36
Quiescent	921	2.66	0.02	0.57	2.64	0.81	4.34
Log[$N(H_2)$ (cm^{-2})]	7861	22.33	0.00	0.29	22.30	21.58	24.02
MSF	1222	22.55	0.01	0.39	22.50	21.68	24.02
YSO	4053	22.25	0.00	0.26	22.22	21.58	23.54
Protostellar	1640	22.33	0.01	0.21	22.31	21.72	23.27
Quiescent	946	22.40	0.01	0.19	22.39	21.91	23.20
$L_{\rm bol}/M_{\rm clump}$ ratio ($L_\odot/M_\odot$)	7614	18.76	0.75	65.17	4.47	0.03	2519.50
MSF	1191	38.90	2.75	94.88	19.03	0.44	2519.50
YSO	3922	22.61	1.11	69.75	7.30	0.08	1944.37
Protostellar	1634	2.42	0.12	5.02	1.27	0.04	95.08
Quiescent	933	6.65	1.58	48.37	0.58	0.03	833.62
Log[Mass Surface Density ($M_\odot$ pc^{-2})]	4838	2.92	0.00	0.35	2.87	1.86	4.34
MSF	1019	2.80	0.01	0.26	2.78	1.92	4.05
YSO	2552	2.85	0.01	0.33	2.81	1.86	4.07
Protostellar	840	3.10	0.01	0.34	3.05	2.30	4.34
Quiescent	427	3.21	0.02	0.35	3.17	2.45	4.32
Scale height (z) (pc)	7123	−4.34	0.36	30.63	−5.50	−345.90	235.40

Figure 2.1: This table shows the physical properties for the ATLASGAL sample taken from Urquhart, König, et al. (2018). Column 2 shows the number of clumps in each subsample, columns 3-5 shows the mean, error on the mean and standard deviation and Columns 6-8 shows median, minimum and maximum values of the sample.

comprising of $\sim$ 11,000 individual sources, was available in 2007 and a paper published by Schuller et al. (2009) detailed how the data was going to be used and why it was necessary for such a survey to be carried out. Figure 2.1 shows a table of the physical properties of the ATLASGAL sample presented by Urquhart, König, et al. (2018), detailing the number of clumps per sub sample, the mean and the error on the mean, the standard deviation and the median, maximum and minimum values for the physical properties of the sample. The survey is complete across the inner Galaxy for clumps $>$ 1000 $M_\odot$, Urquhart, Csengeri, et al. (2014), and thus is a good representation of dense star forming clumps making it a good sample to evaluate triggered star formation due to its size and scope.

Glimpse/Mipsgal Survey

The Galactic Legacy Infra-red Mid-Plane Survey Extraordinaire (GLIMPSE) and its companion the Spitzer Multiband Imaging Photometer Galactic plane survey (MIPSGAL), referred to as GLIMPSE/MIPSGAL survey, are often combined into one survey. GLIMPSE being the primary survey, is a multiband infra-red survey taken using the Spitzer Space Telescope conducted at wavelengths of 3.6, 4.5, 5.8, 8 and 24 μm. The survey allowed deeper insights into star formation, the interstellar medium and the structure of the Milky Way. This is due to the dust and gas emission revealed when the Galaxy is viewed in the IR spectrum as opposed to visible light. A publication by Ed Churchwell et al. (2009) details the data collected, its meaning, how the authors believe it will help with our current understanding of the Galaxy and the use of GLIMPSE in the future.

The Milky Way Citizen Science Project

The Milky Way Citizen Science project (MWP) is a publicly available project that used public volunteers to classify a large sample of sources found by Spitzer Space Telescope. The primary sources found were HII regions (bubbles) and were identified by over 35,000 users on the MWP citizen science website. The survey uses false colour images from the GLIMPSE and MIPSGAL surveys. The colour composite images were made from the 4.5/8.0/24.0 μm images over the coordinate l $\leq 65°$, b $\leq 1.0°$. The images were then presented to the online users who would outline the sources with an ellipse drawing tool provided on the website to measure the thickness and diameter of the bubbles. The effective radius and thickness of the bubbles is given by the following equations derived by E. Churchwell et al. (2006):

$$R_{eff} = \frac{(R_{out}r_{out})^{0.5} + (R_{in}r_{in})^{0.5}}{2} \tag{2.1}$$

$$t_{eff} = (R_{out}r_{out})^{0.5} + (R_{in}r_{in})^{0.5} \tag{2.2}$$

Where $\mathrm{R_{in}}, \mathrm{R_{out}}$ are the inner and outer semimajor axes, and $\mathrm{r_{in}}, \mathrm{r_{out}}$ are the inner and outer semiminor axes respectively, the minimum $\mathrm{R_{eff}}$ possible from the above equations

is 0.27 arcminutes. The inner and outer diameters, eccentricities and position angles for the bubbles are all available in the MWP DR-1 catalogue and is publicly available on the Milky Way Project website.

The Data from the MWP is divided into two catalogues for large and small bubbles. The small bubbles were not drawn by the website tool but instead were outlined with a box and as such do not have the thicknesses or positional uncertainties listed in the large bubble catalogue. The total bubble count is 4434 which is split 3260 and 1174 for large and small bubbles respectively.

2.3.1 Sample Overview

In order to carry out a statistical comparison of star forming regions, we first classified 5410 ATLASGAL sources, from the original catalogue of $\sim$ 11,000, into 11 different sub-categories that are explained in detail below in Section 2.4, this was to create a sample of sources that we could analyze to draw our results from. These classifications will subdivide sources from those that are likely to have been triggered to those that are not.

ATLASGAL is complete across the inner Galaxy for clumps $>$ 1000 $M_{\odot}$. This is thought to be where the majority of Galactic star formation ($\sim$ 80%) takes place (Urquhart, Moore, et al. (2014)), and as such given our classification of $\sim$ 50% of ATLASGAL sources, selected at random, we can say that our data is thusly a good representation of massive clumps across the inner Galaxy.

However, since ATLASGAL does not cover the outer Galactic plane, we cannot say that it is in any way represented by our data. This means that all conclusions drawn from our results are only applicable to the population of star forming regions in the inner Galaxy, not the entire Galactic population.

Bias Potential of ATLASGAL

Two components of the ATLASGAL survey have the potential to cause bias in our results. The first of these comes from the fact that ATLASGAL is only complete for the most massive of clumps (clumps $>$ 1000 $M_{\odot}$), Urquhart, Csengeri, et al. (2014). This adds bias

to our results skewing them in favour of the more massive clumps meaning that they only provide representation of triggered star formation in these more massive clumps. This bias could potentially be removed in future work if the Hi-GAL survey was included and used to review and classify lower mass clumps however, this is beyond the scope of this project.

Secondly the ATLASGAL images were taken in the mid infra-red. Due to the nature of the sources we were attempting to classify and the large quantities of infra-red emission these sources were producing, we had to exclude many sources from our analysis due to uncertainties in the source type. Given the high emission of these excluded sources there was likely to be triggered star formation occurring at these excluded sources creating a bias against the triggered population. This is one of the reasons why we will set any estimation of the population of triggered star star formation as a lower limit.

Finally, if we had had more time for the project, we would have aimed to classify a greater percentage of sources than the $\sim$ 50% (5410 of $\sim$ 11,000) classified, so that our results provided an even better representation of the total sample.

2.4 Methodology

2.4.1 Classification

The first stage of the project required the classification of all of the individual sources making up the sample. This was done with a facility provided in the form of a website which can be seen in Figures 2.2 & 2.3. This made it possible to do fast classifications in a simple manner. We used the website to classify $\sim$ 5500 sources into the following classifications: Photon Dominated Region (PDR), Edge of Bubble, Infra-red Dark Cloud (IRDC), IRDC Filament, IRDC Complex, Bright Rimmed Cloud (BRC), Diffuse material, Source is HII region, Isolated, Complicated and None of the Above, this was done using the web page shown in Figure 2.3 where the given classification was selected from the drop down menu, once the information was submitted the classification was stored alongside the source in the database. Explanations of these and examples of them are detailed

below. The ATLASGAL and GLIMPSE surveys were ideal for this classification type as they both had some key features that made them critically useful in the identification process.

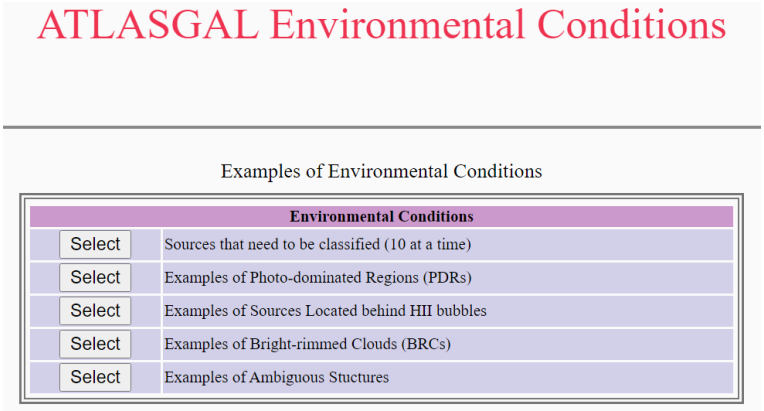

Figure 2.2: This is an image of the website that we used to classify the sources. We initially used the listed examples to assist us with classifying the sources before we built up enough confidence to classify the sources without them. There are additional notes beneath the function box outlining the basic functionality of the website and providing definitions of the classification categories that we define later in this section. The website can be found at the following URL: `https://atlasgal.mpifr-bonn.mpg.de/cgi-bin-private/ATLASGAL_MIR_ENVIRONMENTS_MW.cgi`

.

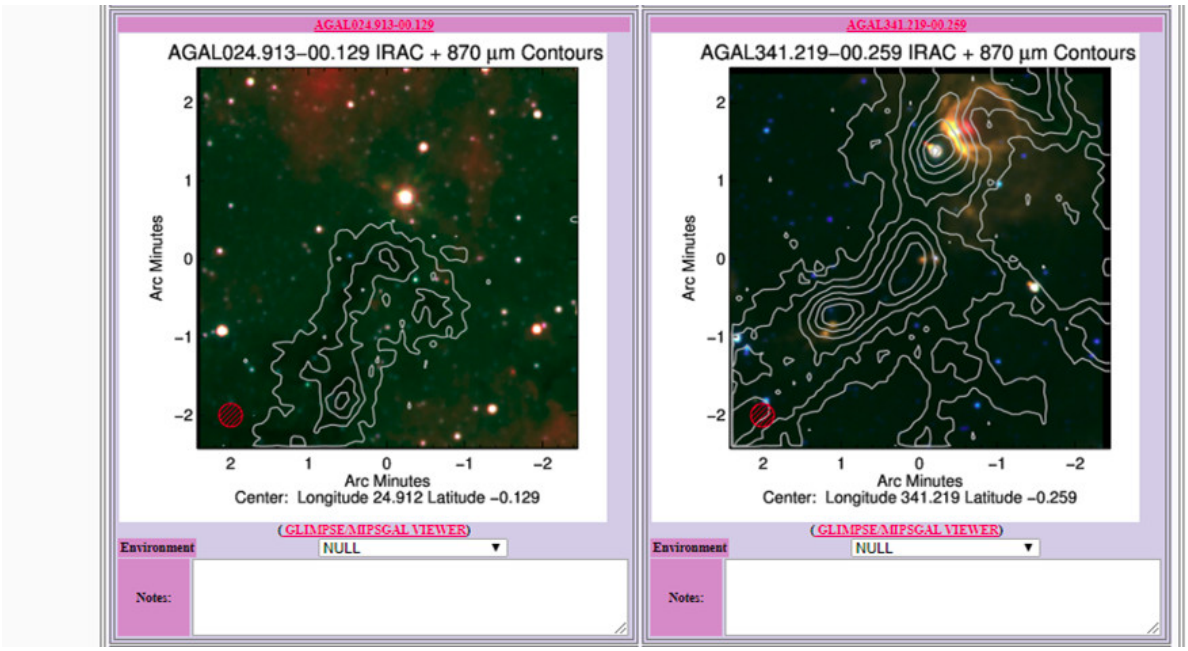

Figure 2.3: This image shows the website once the "Sources that need to be classified" option has been selected. This automatically loads in 10 sources that need to be classified. Once all sources are classified there is a submit button at the bottom of the web page. Any images that aren't classified are left as "Null" and are cycled back into the source library.

The 870 μm ATLASGAL images were overlaid with contours that provided crucial insights into different objects found in proximity of HII regions. The best method of working out if a source was a PDR, Edge of Bubble or BRC was to analyse the contours tracing the dense star forming gas that made up the focus of the image. This can be seen in the middle right panel of Figure 2.3 where the contours can be seen in tight concentric circles around what could be a star, protostar or YSO in the upper half of the image.

The 3 colour images provided by the GLIMPSE survey were also extremely useful in the classification process. PDR's are highlighted in the 8μm wavelengths used by GLIMPSE as are the IRDC's that can be seen, silhouetted dark against the bright background of the Galaxy. Meanwhile BRC's are outlined in both the 8 & 24 μm wavelengths, with the polycyclic aromatic hydrocarbon emission from YSO's at 5.8 μm standing out against the 24 μm particularly well.

2.4.2 Encountered Objects

The sources are classified into Photon Dominated Region (PDR), Edge of Bubble, Infrared Dark Cloud (IRDC), IRDC Filament, IRDC Complex, Bright Rimmed Cloud (BRC), Diffuse, Source is HII region, Isolated, Complicated and None of the Above. The main classifications that will be focused on for analysis are BRC, Edge of Bubble and Isolated. BRC and Edge of Bubble are the sources that we have deemed to be triggered and the Isolated sources are ones that are not triggered and are considered the control sample for the purpose of the project. The rest of the objects are considered contaminating objects that need to be classified to be removed from the sample.

2.4.3 PDR

Photon dominated regions are extremely bright regions found in proximity to HII regions. PDR's form at the boundaries of HII regions where the cold molecular gas outside the HII region meets the hot ionised gas inside the HII region. The UV radiation then ionises the molecular gas forming a bright, hot region that shows up very brightly in the infrared bands used by the GLIMPSE/MIPSGAL Survey (approximately 4-8μm) due to the

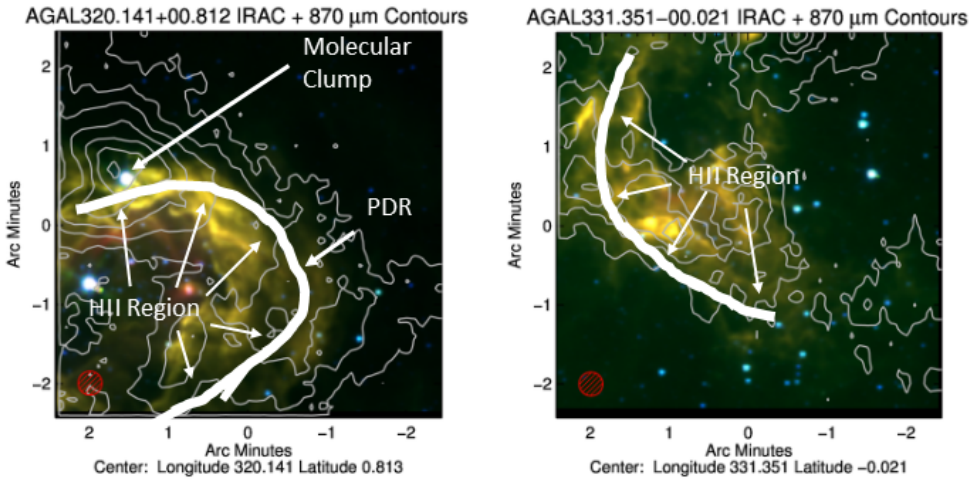

Figure 2.4: This figure displays two examples of sources that would be classified as "PDR", in the left image one can see an additional example of an "Edge of Bubble" type classification. The molecular clump embedded in the PDR has resisted the outward pressure from the HII region and made a dent in the rim of the HII region. If the molecular clump was the focus source of the image, the image would likely have been classified as "Edge of Bubble" due to the nature of the contours around the molecular clump. The contours along with the resisted material means that this particular area could be a candidate for triggered star formation as the resistance of the clump could cause pressure shocks to be driven into the clump possibly causing triggered star formation by way of radiative driven implosion. The right image just displays a HII region with a PDR region at its edge. As can be seen from the image there are no coherent contours displaying the presence of a molecular clump or other structure, meaning this HII region is unlikely to be undergoing star formation currently and the bright emission is just seen due to the extreme temperatures reached in the PDR.

excitement of complex molecules the regions such as polycyclic aromatic hydrocarbons (PAH's). This region is now a mixture of ionized, neutral and molecular material and is known as a PDR.

An example of how PDR's relate to triggered star formation is detailed in Urquhart, Morgan, and Thompson (2009), where it is reported how PDR's can form in relation to bright rimmed clouds during the radiative driven implosion triggering mechanism. PDR's form anywhere that UV photons ionize material. One example of how they form involves the radiative driven implosion mechanism occurring within a bright rimmed cloud. Either an ionisation flash can ionise enough of the cloud to turn it into material of a high enough temperature or just though the RDI process enough material can be ionised to form a PDR. This is a region that shows up in the GLIMPSE/MIPSGAL survey as extremely

bright. This is because whilst the material is sparse and not tightly clustered, due to the ionising radiation it is extremely hot and thus appears so bright in the survey. These regions are seen in the ATLASGAL and Glimpse surveys as very bright yellow or red regions around a central HII region. In the ATLASGAL images the contours overlaid on the image will be loose and spread out over the range of the PDR as opposed to other types of classification where they will be tightly concentrated.

Two different examples of PDR's can be seen in Figure 2.4 where the HII regions boundary is highlighted and the PDR's can be seen in the form of the bright yellow, hot gas surrounding the HII region. In the left-hand image of Figure 2.4 a molecular clump can be seen at the boundary of the HII region. That molecular clump could have created a BRC which in turn, as described above, could be responsible for the formation of the PDR at the HII regions boundary.

2.4.4 Edge of Bubble

"Edge of bubble" is the name for the classification that we are looking to compare to the "isolated" sources and the "BRC sources". These sources, when combined with the "BRC" sources, will make up our triggered sample. The majority of these sites are expected to be found in proximity to HII regions and are expected to be either undergoing some form of star formation process or already have stars formed at the source location. The process by which "Edge of Bubble" sources are classified involves visually identifying differences between the ATLASGAL contours of the "PDR" sources and "Edge of Bubble" sources. As seen in Figure 2.5 the contours around the central source are tightly and coherently bound around the source, signifying the presence of a clump like structure set behind the PDR, this is a good example of an "Edge of Bubble" source. If this is compared to the contours surrounding the sources in the ATLASGAL images in Figure 2.4 it can be seen that this figure does not possess the same coherency and instead of being concentrated around a single source, they are spread out over the shape of the PDR, this shows instead of being centered on a clump or clump like structure, they are spread out due to association with the warm dust of the PDR. The presence of tight and coherent contours surrounding

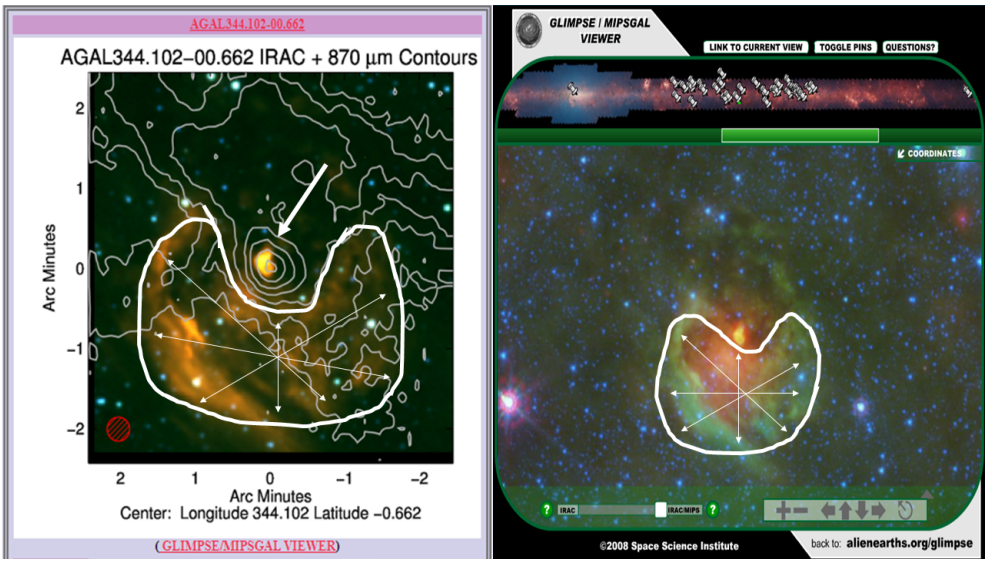

Figure 2.5: In this image one can see one example of a source that would be classified as "Edge of Bubble". In both the ATLASGAL and the Glimpse images an observer can clearly see the outline of the HII region where the molecular gas has been swept up by the expansion and where the dense molecular clump, outlined on the left by the contours and indicated by the thicker arrow, has resisted the expansion of the HII region. This allows the ionising radiation from the central massive star to potentially penetrate the clump. As detailed in the triggering mechanisms above this radiation can then cause the clump to fragment and collapse, potentially triggering star formation within it. If the process was younger and had not progressed to the stage that it is at now it would likely be classified instead, as a "bright rimmed cloud" which occurs when dense molecular clumps resist the expansion of the HII region but the remaining material surrounding them is still swept up resulting in a protrusion into the HII region.

the source was our main method of discerning whether or not a source was triggered. We did not deliberately select triggered sources that were specifically located at the edges of HII regions. The specific selection criteria for an "Edge of Bubble" source required only proximity to a HII region, we were more focused on the ATLASGAL contours overlaid on the source.

2.4.5 Infra-Red Dark Clouds

IRDC

Infra-red Dark Clouds are large regions of dense cold molecular gas that are seen 'silhouetted' against the background of the source images. An example of this can be seen in Figure 2.6, the size and simplicity of the IRDC located in 2.6 meant that it was classified

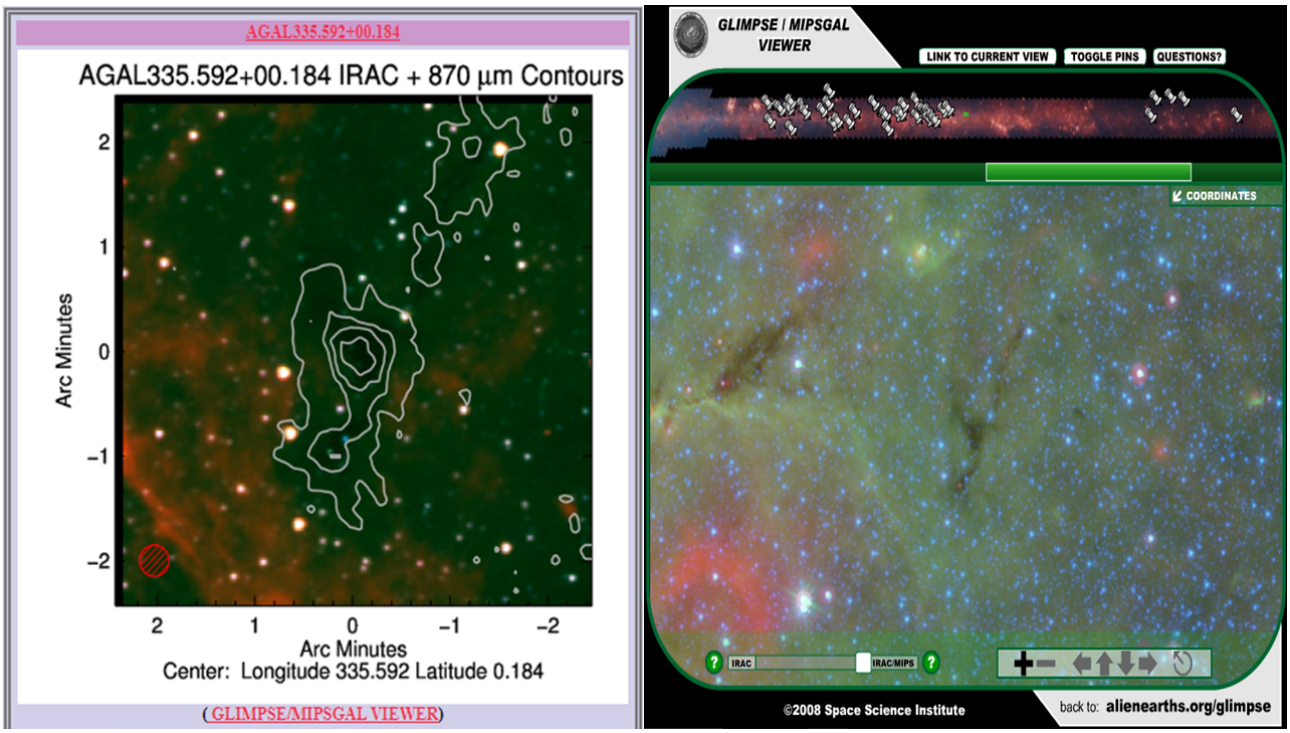

Figure 2.6: This image shows an example of a source that would be classified as an "IRDC". On the ATLASGAL image, less noticeable due to the colouration of the images but still observable is the dark areas where the IRDC can be located. It is also outlined by the inner contours of the image. Once the observer switches over to the glimpse viewer however, the IRDC becomes much more visually distinct when placed against the bright green background ionised gas and one can clearly see the dark cloud. The IRDC's size and relative simplicity means that it is classified as just an IRDC instead of a complex or filament cloud.

as an "IRDC" and not an "IRDC-Filament" or a Complex IRDC. IRDC's come in a huge variety of shapes and sizes leading to the next two classifications also being relevant. However, as discussed later in Section 3.1, despite the structure of the IRDC's varying quite dramatically, their physical properties are very similar, so from an analytical perspective it is more convenient to combine them into a single IRDC classification.

IRDC Filament

Infra-red dark cloud filaments are identified in the same way as IRDC's but vary in shape. A source will be classified as just an "IRDC" when it is smaller and/or has a more compact shape, such as appearing circular, such as the one seen in 2.6. If an IRDC is much longer and appears almost string like, then it would be classified as an "IRDC filament". One of the best examples of an IRDC filament is shown in Figure 2.7 below which displays

IRDC G1111-011 which has been named ‘The Snake’.

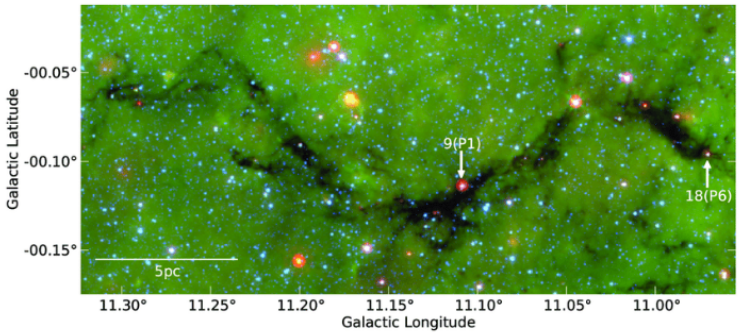

Figure 2.7: This figure displays the IRDC G1111-011 which is also known as ’The Snake’. It is a large IRDC that was discovered from NASA’s Spitzer images. This image can be found at the following URL: `https://www.researchgate.net/figure/A-Spitzer-composite-image-red-green-blue-24-8-45-m-of-the-Snake-nebula-The_fig1_259765201`.

IRDC Complex

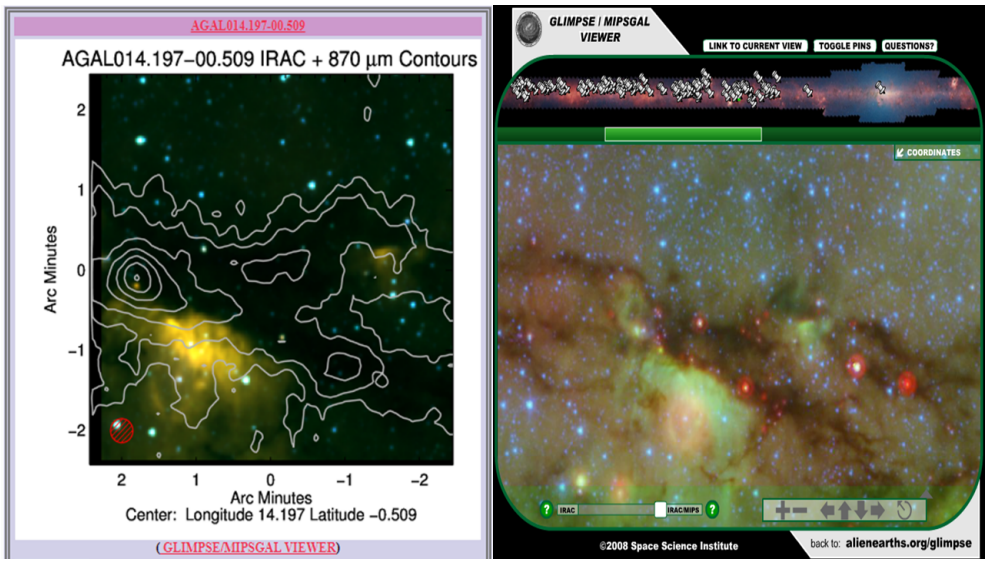

Figure 2.8: This figure shows an example of a source that would be classified as a complex IRDC. Complex IRDC’s are usually large and as such when viewed just on the Atlasgal catalogue do not appear in full and so need to be viewed in the glimpse viewer where an observer can zoom out of the image to view the entire cloud. An example of this can be seen in Figure 2.9 which displays the complex IRDC, seen only partially in this figure, as a full image.

Complex Infra-red Dark Clouds are again classified based on the same features as “IRDC’s” and “IRDC Filaments”, however, they are usually significantly larger than

Figure 2.9: This figure displays an example of the usefulness and versatility of the glimpse survey. In this image the user is able to zoom out from the image displayed on the right of Figure 2.8 to display the whole IRDC.

the two previous subcategories and have formed complex structures. Figures 2.8 & 2.9 show examples of complex IRDC's, with Figure 2.8 displaying the comparison between how a complex IRDC is seen in the ATLASGAL survey compared to it is displayed in the Glimpse survey. Figure 2.9 specifically shows the zoomed out Glimpse image of the complex IRDC displayed in Figure 2.8, showing the full cloud as opposed to the section displayed in Figure 2.8. In the upper right corner of Figure 2.9 it is also possible to see another smaller IRDC that would be classified as either an "IRDC" or "IRDC-Filament".

2.4.6 Bright Rimmed Clouds

As mentioned in Section 1.3, where we discussed the RDI mechanism, bright rimmed clouds occur when large amounts of ionising radiation are incident on a molecular cloud at the edge of a HII region. The high energy radiation erodes away the lower density molecular material which reveals the higher density cores that are present in the cloud.

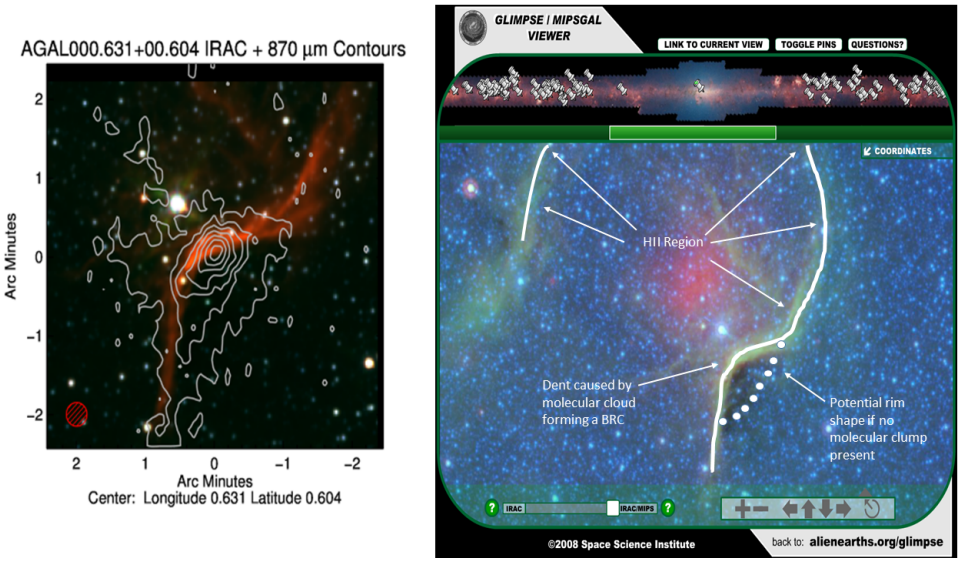

Figure 2.10: In this one can see an example of the Bright Rimmed Cloud classification type. Outlined in the glimpse image is the outer boundary of the HII region and a potential shape of the rim of the HII region if there were no molecular clump present to form a BRC. Note the dark red colour of the gas in the ATLASGAL image compared to the brighter yellow or orange colours that would be present if the source was classified as a "PDR". This classification type is also distinct from the "Edge of Bubble" type classification, as if the region were undergoing star formation one would expect to see a higher temperature present which would be noted by the gas in the glimpse viewer being an orange/yellow colour with the applied contours seen in the ATLASGAL image. The BRC may in the future evolve into an "Edge of Bubble" classification if the radiation pressure is high enough to compress the already ionised gas to a stage where it fragments, collapses and star formation begins.

These cores being of higher density are more difficult to erode and as such resist being ionised by the UV radiation. As the HII region continues to expand the partially eroded clump is left protruding into the HII region and is now what one would classify as a Bright Rimmed Cloud. An example of a "BRC" can be seen in Figure 2.10 where the cooler gas is indicated by the red colouration in the ATLASGAL image, and it can be clearly seen where the dense molecular clump has resisted the expansion of the HII region, and the ionised material has continued to expand on either side of the dense clump. There is also an approximation of what the HII region would look like if there was no BRC present represented by the dotted line.

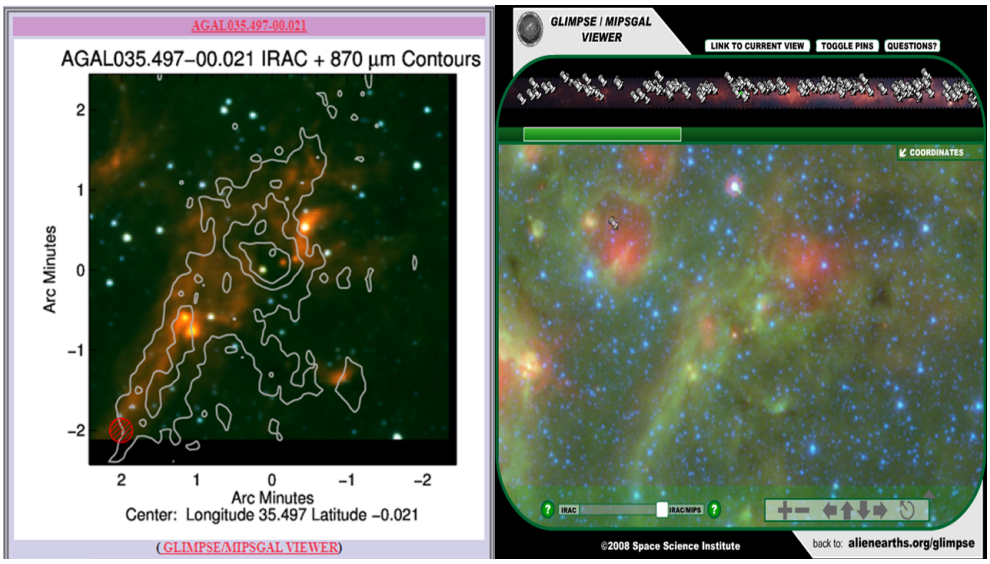

Figure 2.11: This figure shows an example of the diffuse material classification. Unlike the "isolated" sources there is generally some quantity of material present, or it is located near a site of interest as one can see the HII region located with the pin in the glimpse viewer on the left. However, this material is not currently undergoing any star formation and is unlikely to ever form stars. The diffuse material displayed could potentially contribute to star formation if it was accreted to a protostellar disk, if the nearby HII region forms a star but without knowing the distances between the sources this is little more than speculation.

2.4.7 Diffuse Material

Diffuse material sources are loose clumps of molecular material in space that are not currently undergoing star formation. They are seen in the Glimpse survey as large clumps of ionised gas sometimes located nearby to HII regions or other sites of interest. It is unlikely that this material will go on to form stars due to its density and lack of any nearby triggering mechanism. If the material is located close enough to a HII region or another type of star forming region it may be accreted by a protostar but without knowing the specific distance of the sources in the ATLASGAL and Glimpse surveys it is unlikely that this could be stated with any real confidence. An example of this can be seen in Figure 2.11 where in the ATLASGAL image the contours clearly are not focused on anything of any real importance and are just mapping the diffuse material. One can see that the gas in the Glimpse image on the right is not being affected by a source and is unlikely to end up forming stars or being affected by a HII region or another object of interest.

2.4.8 Source itself is a HII region

Sources in this category are themselves HII regions, they have not been classified as "PDR", "Edge of Bubble" or "BRC's" and this could be for a number of reasons such as being due to the distance of the HII region being so great, that it is impossible to classify it further as either a "PDR", "Edge of Bubble" or "BRC". It could also be that the massive star creating the HII region in question is the source of the image or some other reason that could be to do with the method of image capture on the spitzer satellite from which the Glimpse survey was built. This classification is not needed for a comparison of sources involving triggered star formation but needs to be classified and something may show up later that merits another look into these sources.

2.4.9 Isolated

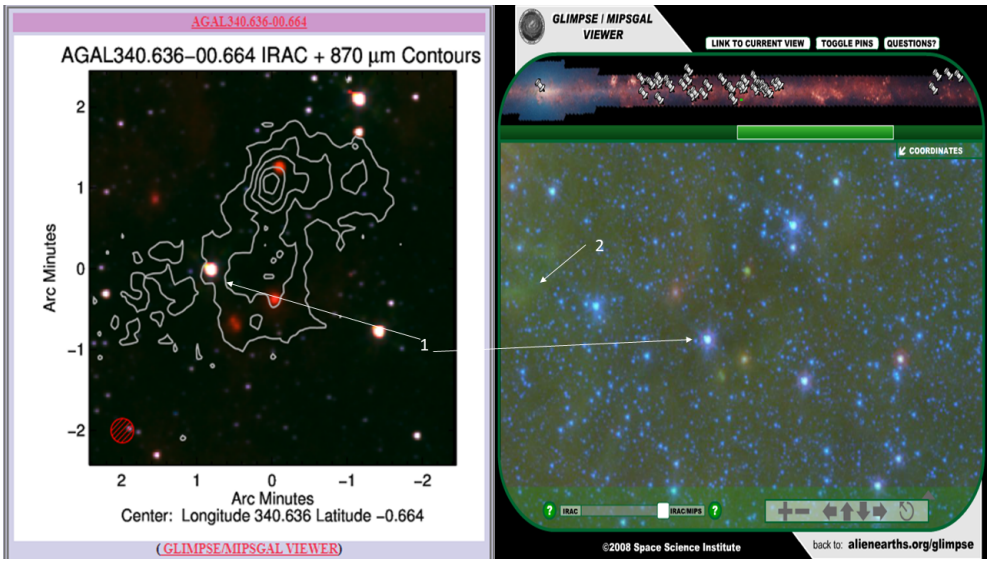

Figure 2.12: This figure shows an example of an "Isolated source". 1 is the reference star in the images used compare the source as there are no ways to locate the source in the glimpse images except by eye. This source would be classified as "isolated" as there are no processes currently occurring in the images nor is there any material that could become interesting later on. 2 initially appears as nearby diffuse material however, if one zooms out on the glimpse survey, they will see that it is in fact the outer boundary of a HII region.

This is the name for the control group for the project. For us to get a clear idea of how triggered star formation compares to spontaneous, we have to have a control group that we

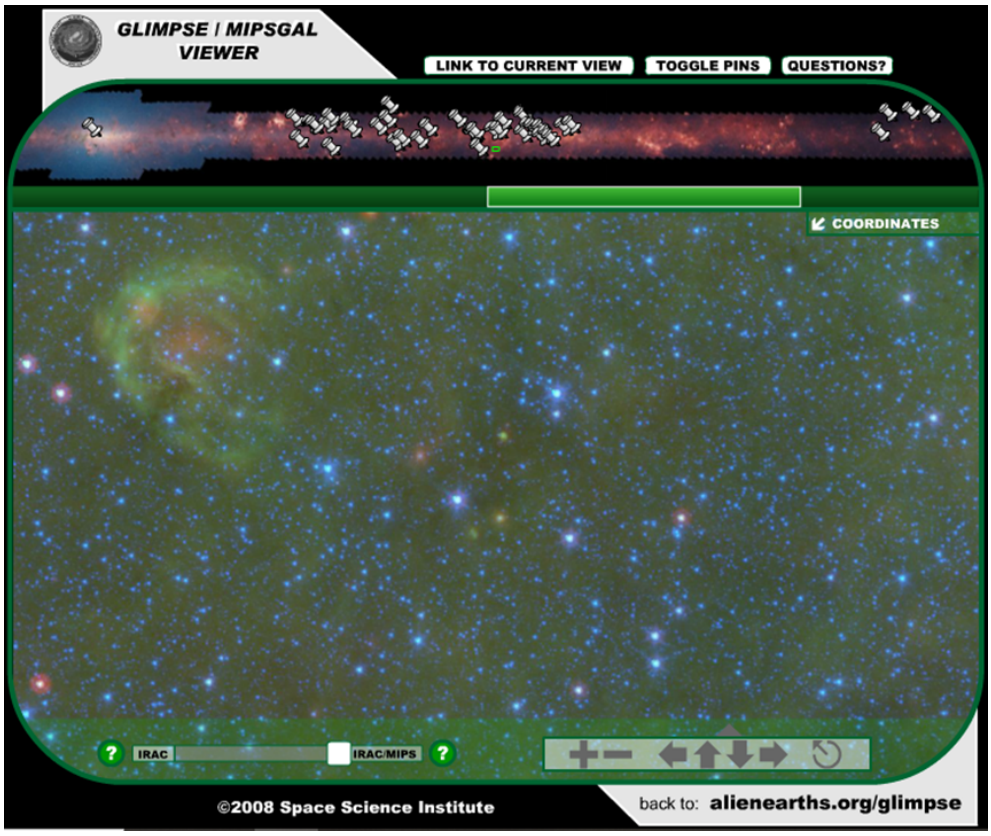

Figure 2.13: This figure shows the zoomed out glimpse image of Figure 2.12, where the full HII region can be seen in the upper left of the image. The source of the image however, as indicated has no process or element to it that could result in star formation and as such is classified as isolated.

compare the "Edge of Bubble" and "BRC" type classifications to. The classification type was originally named uninteresting for the purposes of classification however, the sources themselves being classified as this type are not necessarily uninteresting and isolated may be a better name for them as the sources have no potential triggering mechanism or the like near them. Figure 2.12 shows an example of an isolated source. As can be seen in the image there is no dense gas located at the source, nor is there any form of nebula or other potential star forming region. Given how isolated sources are often somewhat empty it is sometimes necessary to use the stars in the image to help locate the image source when switching back and forth between ATLASGAL and Glimpse surveys, an example of how these reference stars are used can be seen in Figure 2.12 as indicated by the arrows originating from the number 1. The arrow coming from number 2 corresponds to some dense gas in the corner of the image, which when zoomed out as seen in Figure 2.13 was actually part of the rim of a HII region.

2.4.10 Complicated

Figure 2.14: This figure shows an example of a complicated type classification. There are no identifiable structures or properties due to the inability to determine any, because of the extreme luminosity of the region.

The complicated classifications are regions of intense star formation that due to their high luminosities are almost impossible to be accurately classified. When the GLIMPSE survey is loaded the areas just appear as extremely bright images that are not discernible at either end of the infra-red scale. Certain examples of these types of classifications are the W43 (Westerhout 43) star formation region and the Galactic centre to name two. Other sources exist but it would be meaningless and timely to name them all. Figure 2.14 is an example of such a source and is an image of a source that is close to the Galactic centre in the Glimpse survey, showing the extremely bright region that does not fit any other type of classification.

2.4.11 None of the above

None of the above type classifications are for sources that have well defined, recognisable structures and/or properties but do not fit the description that would lead to them being classified as one of the other labels. There have only been a few sources that we have had to classify as "None of the Above", these are sources that appear to be located inside the rim of a HII region but do not posses the other characteristics to be labelled as "Bright Rimmed Cloud". If a significant enough number of these sources appear during the classification process it may be worth revisiting these sources after the main goals of project have been completed to see if they warrant further study.

2.4.12 Coding and Statistical Analysis

Once the sources were classified into their relevant categories, they were loaded into a database using MySQL software. Once the data was loaded into the database it was simple to manipulate it to extract the relevant parts for visualisation in MySQL workbench or to extract via python so that we could begin to statistically analyse it by visualising it in histograms and cumulative distribution functions (CDF's) made using the physical parameters of the data such as mass, temperature, radius, luminosity and luminosity/mass ratio which is explained in detail below.

The "BRC" and "Edge of bubble" classification types will make up the triggered sample and the "Isolated" classification will make up the non-triggered sample. Any difference in the physical parameters between these categories should indicate differences between star formation processes occurring in these environments. A difference in the star forming processes is what this project is hoping to find as that would help with the project objectives. Specifically, the 1st and 2nd objectives put forward in Section 2.1.

This project's source catalogue was compiled using data from the ATLASGAL survey, which as mentioned previously is complete across the inner Galaxy. This means that the number of classifications that are identified to be triggered will provide a good representation of triggered star formation occurring in the inner Galaxy. This will help in answering the third objective put forward in Section 2.1.

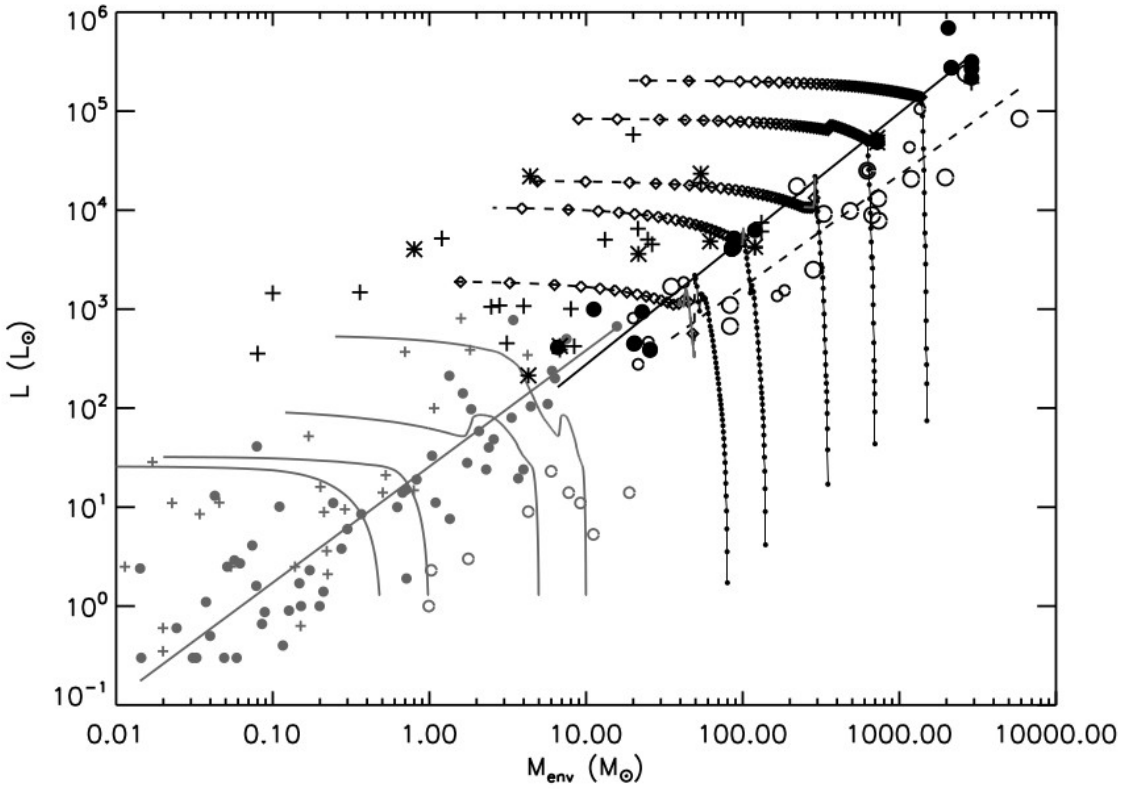

Figure 2.15: This figure displays a graph of the bolometric luminosity of low and high mass protostars plotted against the mass of their surrounding envelopes. The grey curves are those of low mass young stellar objects and were originally plotted by Saraceno et al. (1996). The black curves were plotted by Molinari et al. (2008) and it is from this publication that this figure is taken.

Luminosity/Mass Ratio

One of the more important physical parameters involved in this project is the differences between the luminosity to mass ratios of the difference classifications. The relationship between the mass of a protostars envelope and its bolometric luminosity was first mentioned by G. P. Kuiper (1938) where it was used to determine the mass of stars, specifically binary pairs. Saraceno et al. (1996) and Molinari et al. (2008) later use relationship between mass and luminosity to work out evolutionary stages of low and high mass star formation respectively.

This is possible based on the nature of star formation. For the sake of simplicity, we will use the example of an accreting low mass protostar, although Molinari et al. (2008) state that an up scaled model of inside out collapse allows a comparison to be extended to high mass star formation. As the protostar accretes material and begins to generate polar

outflows the overall mass of the envelope decreases as the outflows begin to disperse it. This can be seen in Figure 2.15 where the curves shift to the left slightly. Once accretion begins the luminosity starts to increase rapidly. This causes the plotted protostar to move almost vertically on the plotted L/M graph as can be seen in Figure 2.15. The protostars generated outflows will begin to have a much more noticeable effect on the mass, once the protostar reaches the main sequence and ceases its accretion. This causes the shift to the left on Figure 2.15.

Maximum expected values for the L/M ratio of star forming regions are ~ 100, around 5 orders of magnitude larger than the values of non-star forming clumps. This means that the luminosity mass ratio is not only a good tracer for star formation but also the evolutionary stage that it is progressing at.

2.5 Summary

To summarise, the 3 aims of this project are:

1. How does one distinguish between stars formed exclusively through triggering and stars that would form even if the triggering mechanism were not present?

2. Is there any difference between triggered star formation and spontaneous star formation?

3. What is the fraction of stars that form this way in the Galaxy?

The total number of sources classified 5410. It is with these sources that we shall be using python and MySQL to statistically analyze and try to find differences or abnormalities in the physical parameters of the different classification types. The primary way we shall be doing this is by making CDF's of the different physical parameters and plotting the different classifications against each other and then applying a KS test to plots to check for differences between them.

Any differences found should reveal insights regarding the star formation taking place at the different sites which will help in answering the aims of the project. We shall

also be making plots of the classifications deemed contaminants to check if there are any unforeseen abnormalities in the data.

Chapter 3

Results

3.1 Classification Overview

Classifications	Source Counts	Sample Percentage (%)	L/M Ratio	Temperature (K)
BRC	104	1.92	29.8	22.8
Complicated	188	3.47	109.5	27.1
Diffuse Material	200	3.70	8.2	20.1
Edge of Bubble	449	8.30	47.1	24.1
IRDC	895	16.54	4.4	15.3
IRDC Complex	159	2.90	4.4	14.7
IRDC Filament	282	5.21	3.8	15.1
None of the Above	39	0.72	35.8	21.8
PDR	441	8.15	55.9	25.6
Source itself is HII region	243	4.49	33.2	24.4
Isolated	2410	44.55	9.3	18.4
All	5410	100	-	-

Table 3.1: This table shows the basic overview of the classification process. You can see the number of sources that were sorted into all of the separate classifications as well as the percentage of the sample they make up, along with the average L/M ratio of the classifications and average temperature.

Table 3.1 shows an overview of the classifications performed. This shows that the Isolated classifications makes up almost half of the whole sample (44%). The triggered classification makes up just over 10% of the whole sample, before non-star forming sources are excluded. These two classifications will be the main focus of the analysis in the project. These amounts are more clearly seen in Figure 3.1, where one can easily see the grouped

categories of sources that make up our sample.

The IRDC classifications make up 24.70% of the whole sample and appear to be quite similar in terms of their physical properties. This can be clearly seen in Table 3.1, where their respective L/M ratios are separated by 0.6 and their respective temperatures also by 0.6 K. The IRDC classifications appear to identify structures with similar physical properties and so the separation into subcategories for these classifications is not particularly useful. We therefore combine them into a single IRDC class. This reduces the number of classifications that need to be focused on, simplifying the analysis, hence why there is only a single IRDC section seen in Figure 3.1.

The other classifications that are identified are essentially contaminants for the project and include 'Diffuse Material' and 'None of the Above', these classifications will be excluded from the project as it is unlikely star formation will occur at these sources. Furthermore, we also exclude 'PDR', 'Complicated' and 'Source itself is HII region' as whilst these sources are found in proximity to HII regions there is too much interference to reliably determine whether or not there is star formation occurring at the site, and whether or not, that star formation is likely to have been triggered.

The other classification categories as well, whilst still merit further study in their own right, are of no significance to the aims of the project and as such will also be excluded and not used in any subsequent analysis.

The 3 classifications that will be focused on for the remainder of this chapter are "edge of bubble", "bright rimmed cloud" and "isolated". The analysis concerning these classifications will help us to answer the aims of the project stated in Section 2.1.

3.2 Comparison of Statistical and Physical Properties

Physical Properties	BRC	Edge of Bubble	Isolated
Count	104	449	2410
Average Temperature (K)	22.77	24.07	18.36
Temperature Error (K)	2.77	2.97	1.80
Standard Deviation of the Temperature	4.22	4.60	4.69
Standard error of the Mean of the Temperature	0.41	0.22	0.1
Log[Average Luminosity ($L_\odot$)]	4.35	4.70	3.81
Log[Standard Deviation of the Luminosity]	4.88	5.14	4.43
Log[Standard error of the Mean of the Luminosity]	3.87	3.81	2.74
Log[Average L/M Ratio]	1.47	1.67	0.97
Log[Standard Deviation of the L/M Ratio]	1.83	1.91	1.44
Log[Standard error of the Mean of the L/M Ratio]	0.82	0.59	-0.24
Log[Average Mass ($M_\odot$)]	2.95	2.98	2.96
Log[Standard Deviation of the Mass]	3.12	3.20	3.41
Log[Standard error of the Mean of the Mass]	2.11	1.87	1.50
Average Radius ($R_\odot$)	0.47	0.41	0.44
Standard Deviation of the Radius	0.39	0.31	0.33
Standard error of the Mean of the Radius	0.04	0.01	0.01

Table 3.2: This table shows the main physical parameters of the triggered (Edge of bubble and BRC) and isolated (non-triggered) classifications that will be presented for analysis in this section.

Looking first at the differences in temperature, luminosity and the luminosity to mass ratio, visible in Table 3.2 and Figures 3.2, 3.3 and 3.4, there is a clear difference between the samples that are identified to have been triggered and those that form in isolated environments. This allows us to initially show the number of triggered sources in the sample. This comes as a lower limit for the sample as it is possible there are sources missed or purposefully excluded in the classification process. It can be seen from Table 3.3 and in Figure 3.1 that the isolated sources make up $\sim$44% of the sample and the triggered sources make up $\sim$10% of the sample. As this sample provides a reasonable representation of star formation taking place in the inner Galaxy and, once the sources that are identified as not contributing to star formation are excluded (Complicated, Diffuse Material, PDR and Source itself is HII region) we can say that this sample represents a lower limit in that $\sim$12.75% of star formation occurring in the inner Galaxy is likely to

have been triggered.

This figure of ∼12.75% could be translated into $M_{\odot}$/yr for a more precise measure of exactly how much stellar material is being formed by a triggered process however, due to the statistical nature of this project it is not possible to go from the measurements we have to a position where we could calculate this figure.

Instead we assume that the proportion of stars contributed by triggered sites to star formation is similar to the percentage of triggered sites found during this project. It is possible that we could use estimates of average galactic star formation rate of between 1 - 3 $M_{\odot}$/yr to predict a number however, this is unlikely to be little more than speculation.

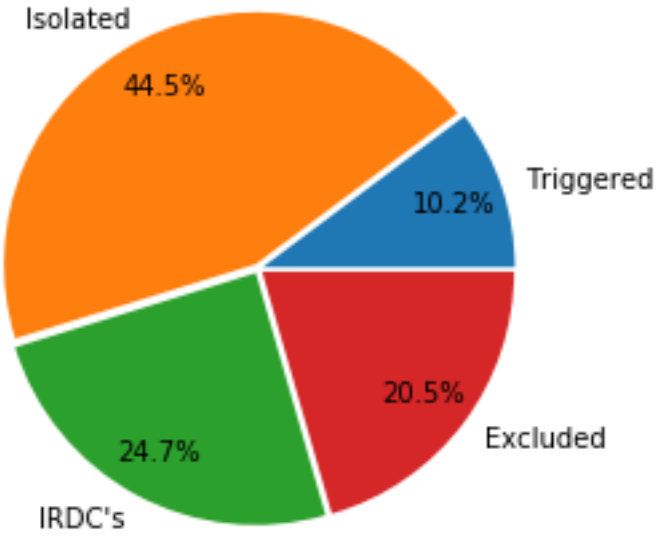

Figure 3.1: This figure displays a pie chart showing the respective sizes of the classified sources along with their respective percentages compared to the whole sample. Note the lower value of triggered sources, this is because we have not yet removed the excluded sources from the sample.

The value of ∼12.75% of Galactic star formation occurring through triggering can be compared to publications that have made an estimate based on their own samples. Thompson et al. (2012) present an upper and lower limit of 30% and 14% respectively for their sample of YSO's at the boundaries of HII regions found by the Spitzer Space Telescope. However, these figures assume that all of the YSO's found at the borders of HII regions are triggered with none forming through other means, such as supernova triggering or cloud-cloud collision; if these other triggering sources were to be included

the percentage would increase our estimated value.

Classification	Source Counts	Sample Percentage (%)
Triggered	553	10.22
Isolated	2410	44.55
IRDC	1336	24.70
Excluded	1111	20.54

Table 3.3: This table shows the source counts and respective percentage of the sample that the classifications make up, grouped together into larger categories that will be used during the analysis.

In Table 3.2 you can see the physical parameters of the main 3 sub classifications. This is our first look at a quantitative assessment of similarities or differences between the triggered and isolated classifications. Focusing on the temperature, there is a difference between the triggered and isolated classifications.

The triggered sample have a higher temperature on average than those that are not triggered. This is mirrored in the luminosity and luminosity to mass ratio of the classifications where, the triggered classifications have a higher average value than the isolated classification.

The scale of this difference is yet to be seen as based on the standard deviation of the parameters there is some overlap present between the classifications, but the significance of this difference will be seen later when we KS test the CDF's of the parameters. Upon KS testing the physical parameters we should be able to discern how different or similar they are, when looking between the triggered and non-triggered categories as, it initially appears that the average masses and radii of the two categories are similar whilst the average temperatures and luminosities are different.

The following figures are the cumulative distribution functions of Mass, Radius, Temperature, Luminosity and Luminosity to Mass Ratio for the triggered classifications (Edge of Bubble and BRC) and isolated classification.

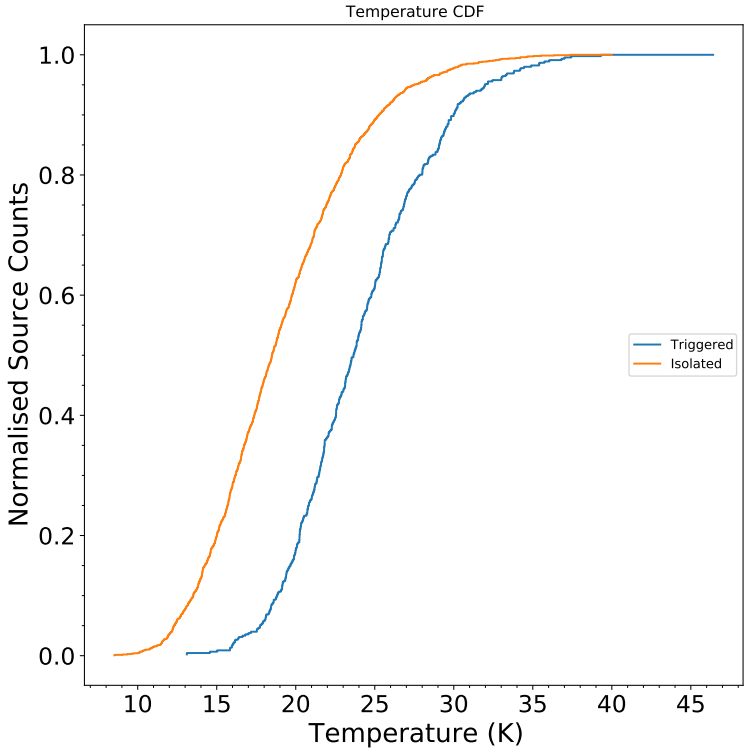

Figure 3.2: This figure shows the cumulative distribution function of the temperature for the triggered classification and the isolated classification.

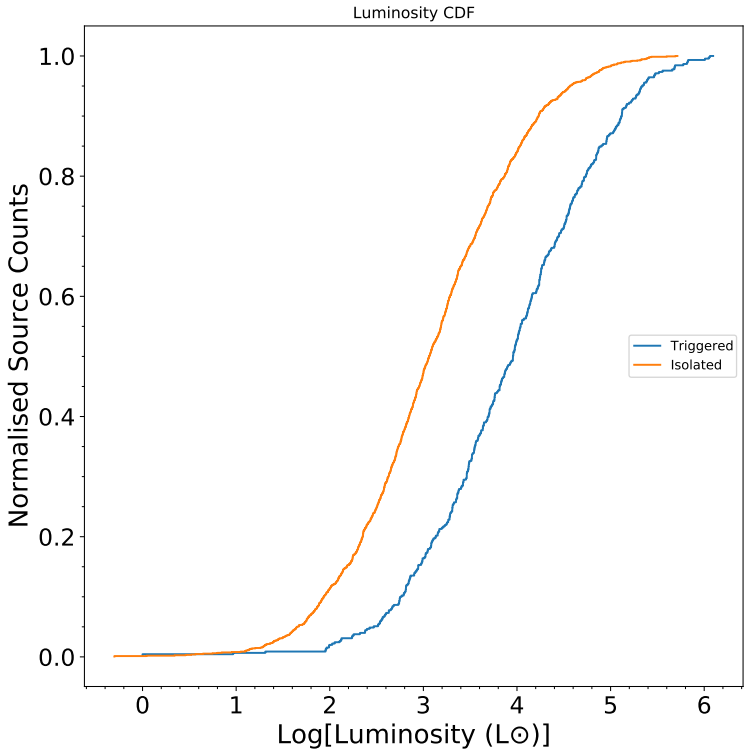

Figure 3.3: This figure shows the cumulative distribution function of the luminosity for the triggered classification and the isolated classification.

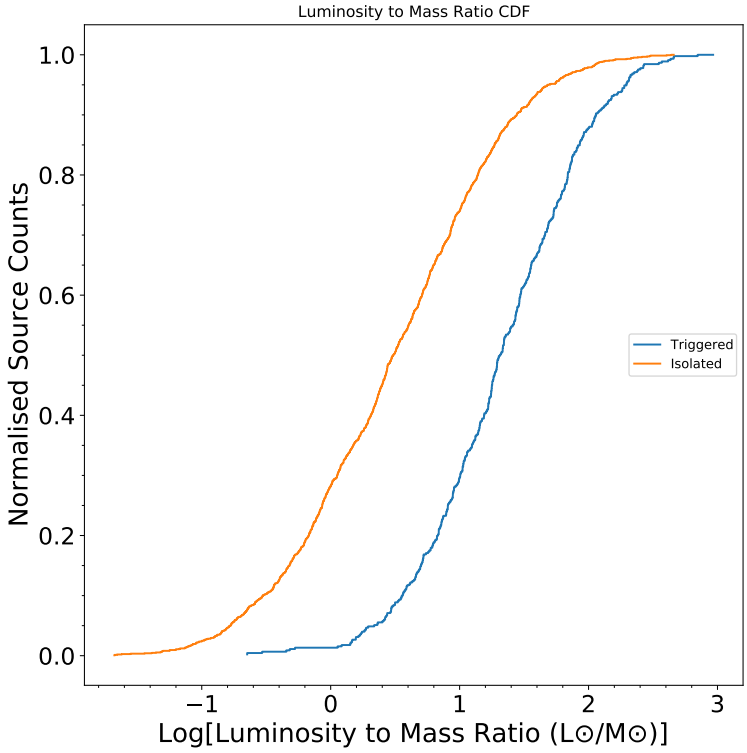

Figure 3.4: This figure shows the cumulative distribution function of the luminosity to mass ratio for the triggered classification and the isolated classification.

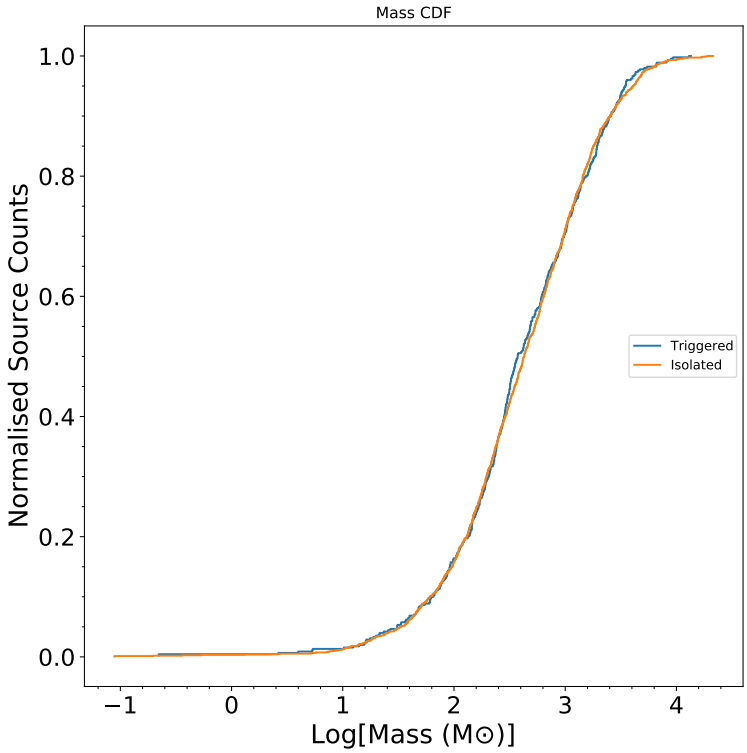

Figure 3.5: This figure shows the cumulative distribution function of the mass for the triggered classification and the isolated classification.

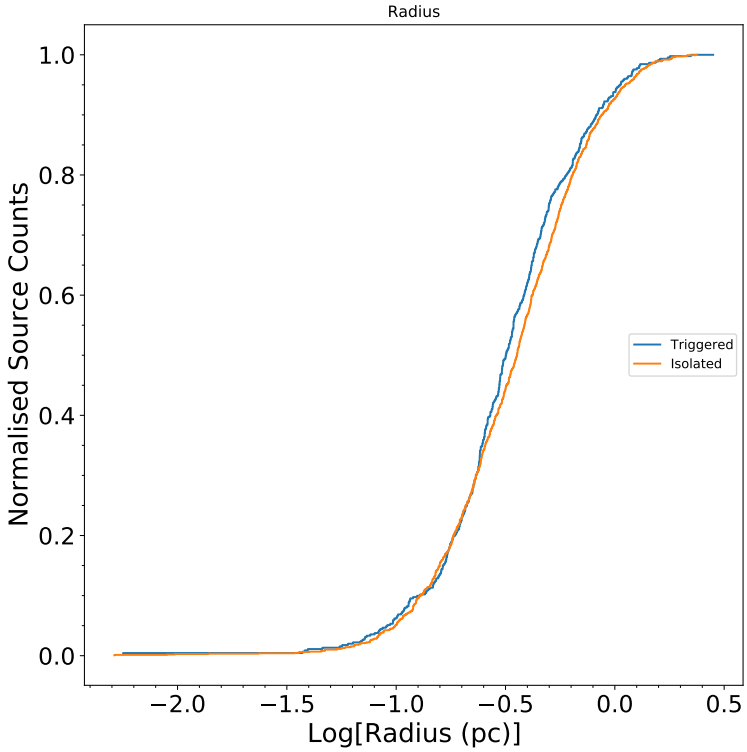

Figure 3.6: This figure shows the cumulative distribution function of the radius for the triggered classification and the isolated classification.

The data is presented in the form of cumulative distribution functions as these more clearly show differences in the distributions of the different physical parameters than if compared through more conventional histograms. The similarities or differences seen when looking at the physical parameters between classifications are more easily seen than in Table 3.2 where the gap between the curves on the CDF's represent the numerical difference in the physical parameters. Figures 3.5 & 3.6 show the overlap between the mass and radius of the triggered and isolated classifications, which is also seen in Table 3.2. The differences in temperature and luminosity can also be seen in Figures 3.2, 3.3 & 3.4 where the differences in the luminosity mass ratio have to be based on the differences in luminosity as according to Figure 3.5 the classifications all have very similar mass ranges.

We now test the significance of the difference between the curves seen on the CDF's above by subjecting them to Kolmogorov-Smirnov tests. This is a statistical test that will evaluate the real difference between the curves based on the outputted p -value. For

there to be a significant difference between the curves the p -value needs to be ≤ 0.0013.

	Temperature	Luminosity	L/M Ratio	Radius	Mass
Edge of Bubble vs BRC	0.00892	0.0423	$4.90\text{x}10^{-7}$	0.947	0.527
Edge of Bubble vs Isolated	$1.55\text{x}10^{-15}$	$1.67\text{x}10^{-15}$	$1.55\text{x}10^{-15}$	0.863	0.00230
BRC vs Isolated	$1.78\text{x}10^{-15}$	$3.80\text{x}10^{-7}$	$1.11\text{x}10^{-15}$	0.849	0.689.

Table 3.4: This table shows the p -values for the KS test results for comparing the physical parameters of the triggered and isolated classifications. For there to be a real significance between the curves of the CDF's the p -value needs to be less than 0.0013

The results from these KS tests confirm the other results that have been obtained so far. The p -values between the triggered sample and isolated sample show that there is a significant difference between the temperature, luminosity and luminosity to mass ratio with all three parameters being higher for the triggered sample compared to the isolated sample. The p -values for the radius and mass of the samples allows us to assume that there are no significant differences between the initial properties of the clumps. The differences seen between temperature, luminosity and L/M ration likely arise from environmental differences between the triggered and isolated sources.

This is consistent with the current theories of triggered star formation as the collect and collapse process and RDI are both thought to enhance star formation at the rim of HII regions.

A higher luminosity to mass ratio could be an indicator of a higher star formation efficiency. This could be due to increased accretion rate, where the triggering process causes the protostar to accrete mass at a faster rate than if it formed though spontaneous means brought about by the proximity of the sources to their parental HII region. The triggering mechanisms discussed in Section 1.3 both involved the compression of the accretion envelope due to the ionising feedback from the HII region. The increase in luminosity can also be seen in the differences between the temperature and luminosity of the triggered and isolated samples. However, this is still only speculation at this stage, all we can say for certain is the increased Luminosity to Mass ratio, with the clumps being of similar Mass and Radius, is an indicator of more star formation taking place at these locations.

Another possibility for the increased luminosity and temperature seen, could be due to contamination from nearby sources or a sources proximity to contaminating environments

within its own parental HII region. This could be an issue if the source is located in close proximity to certain objects such as an especially active PDR that is so bright its radiation emitted contaminates the source that is being focused on. This would come down to a factor of observational bias, the results will be closely examined in Section 3.4.3 to check for this effect.

3.3 Correlation of Triggered Sources with Bubbles

The principle of this section is rooted in HII regions themselves. As massive stars form HII regions they expand into their surrounding natal clump and sweep up material. This results in dense clumps of material being distributed around the rim of the HII region Deharveng, Zavagno, and Caplan (2005). These clumps should show up in surveys so it should be expected that we find a high density of sources occurring at the boundaries of HII regions, Thompson et al. (2012).

This process involved calculating the distances of triggered sources to their host bubble and then comparing that to the bubble radius. This was done using the listed positions from our data set for the sources and the bubble catalogue obtained from the Milky Way citizen science project of which the first data release can be seen in Simpson et al. (2012), for possible nearby HII regions. The source distance was calculated in terms of effective bubble radius, which allowed all sources beyond a limit of 5 bubble radii to be excluded. After this, the source count was divided by the surface area of the bubbles to get the source per unit area of the bubbles, this was necessary to be able to directly compare these findings to other publications such as Thompson et al. (2012) and S. Kendrew et al. (2012), listed in the following paragraphs. This was done first with all classified sources before then being carried out with just the triggered and isolated sources. The expectation was to find a peak in source counts of triggered sources at a distance of 1 bubble radius as this has been found in previously done studies, two of which are detailed below, as well as fitting with theorettical models of triggered star formation at HII regions.

Thompson et al. (2012) compare the positions of 846 young stellar objects (YSO's) from the RMS YSO catalogue to the radial distance of Spitzer bubbles. The authors

determined the distances in units of bubble radii as opposed to arcminutes to account for the range of sizes of the different bubbles and plotted the sources counts per unit area of the bubbles to account for the increased size of the annuli at larger bubble radii. The resulting histogram produced, displayed a large peak in source counts at a distance of 1 bubble radius showing that there is an effective overdensity of sources found at the rim of bubbles.

A concern was that due to the elliptical nature of the bubbles, in calculating the distances of the YSO's from the centre of their host bubbles incorrectly due to the differences found between the mean bubble radius and true bubble radius, there would occur a broadening of the observed peak in surface density. However, after the position angles of the elliptical fits of the bubbles were made available, a sample was tested and no significant difference was found between using the true bubble radius or mean bubble radius.

S. Kendrew et al. (2012) also perform a correlation analysis on the radial distance of RMS YSO's from their host bubble. They ran into some difficulties though due to the size of the Milky Way project bubble data base. When Thompson et al. (2012) performed the analysis they used a catalogue of ~ 322 bubbles and ~ 846 YSO's. In using the full MWP data set the number of bubbles jumped to 4434, S. Kendrew et al. (2012). This brought into question whether it would be possible to see an overdensity given a bubble to YSO ratio of 5 to 1. There were also worries about the positional uncertainties of some of the smaller bubbles as based on the technology used to identify them, some of the smaller bubbles identified had larger positional uncertainties than their diameters.

S. Kendrew et al. (2012) found that their results were consistent with those of Thompson et al. (2012), finding that YSO surface density is greatest towards thinner bubbles. They also found an increased correlation between YSO's and bubbles at smaller separations when compared to Thompson et al. (2012) but attributed this to the higher level of completeness of the MWP sample.

S. Kendrew et al. (2012) matched the MWP sample with the RMS catalog showing strong central correlation between the diffuse RMS HII regions and the MWP bubbles. They also noted that the compact and ultra-compact HII regions (CHII regions & UCHII

regions) listed in the RMS catalog may actually represent BRC's.

S. Kendrew et al. (2012) conclude in a similar way to Thompson et al. (2012) stating that whilst there is an observed overdensity of MYSO's at the borders of HII regions (22 +/- 2% between 0.8 - 1.6 radii) and that the majority of YSO's (67 +/- 3 %) lie within 2 bubble radii of their host bubble, this is not conclusive proof of triggering mechanisms enhancing star formation although, they do note that the largest bubbles are good candidates for the collect and collapse process to be observed and that it is likely their survey excludes stars triggered by the RDI method.

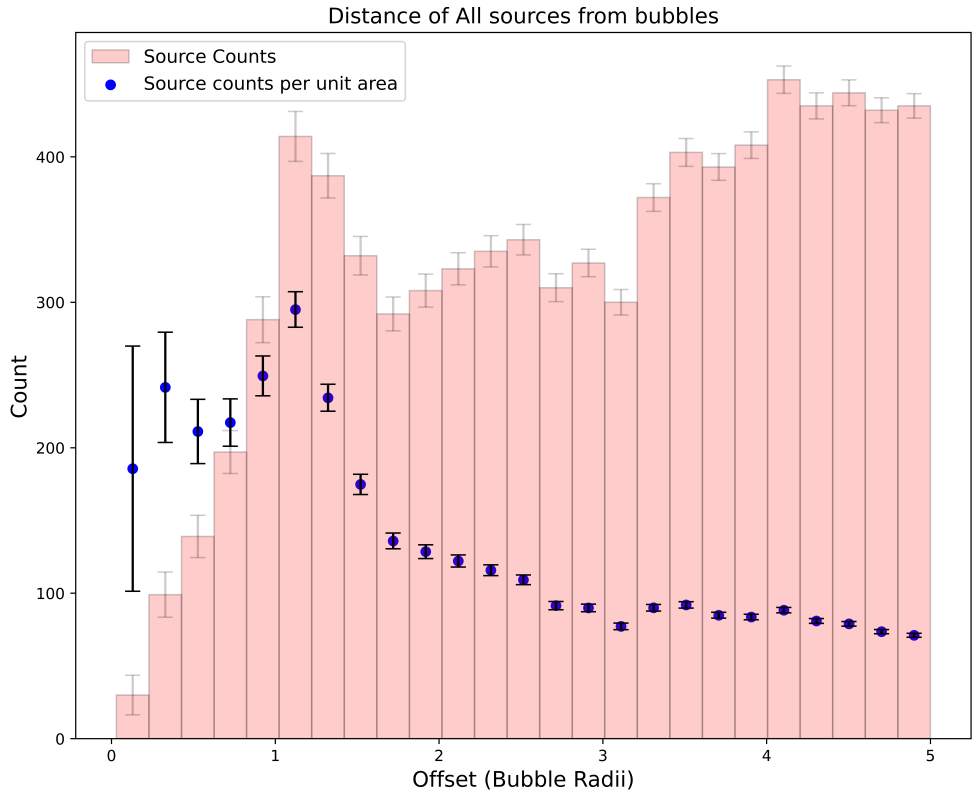

Figure 3.7: This figure shows a histogram of the source counts and source counts per unit area for the entire data set. The pale red histogram represents the source counts. The blue scatter points represent the source counts per unit area and are directly comparable to the results found in Thompson et al. (2012) and S. Kendrew et al. (2012).

The peak seen in Figure 3.7 and more clearly shown to be as a result of triggered sources in Figure 3.8 is a clear representation of an overdensity of triggered sources being located at a distance of one bubble radius from their host HII region. This result is in good agreement, both with previous models and previous publications. When comparing our results directly with Thompson et al. (2012) and S. Kendrew et al. (2012) there are

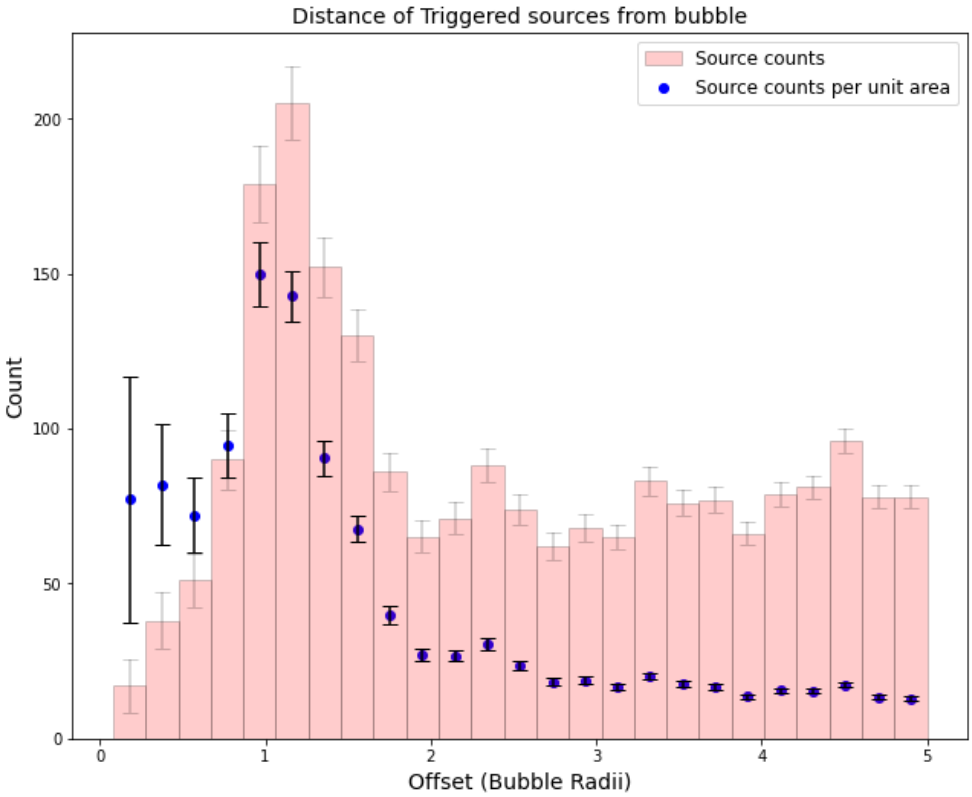

Figure 3.8: In this figure you can see the histograms for the triggered sample of the data set. The pale red histogram represents the source counts and the blue scatter points represent the source counts per unit area.

some differences worth noting between the data sets.

When these studies performed their correlation analysis, they managed to match a maximum of 227 YSO's with bubbles with a maximum source count of $\sim$ 2000 sources. Our data set is larger with 5410 total sources available for comparison and 997 sources lying within 2 bubble radii. As said previously this larger data set provides a better representation of star formation on a Galactic level and thus allows stronger conclusions to be drawn from the data. This is combined with the fact that we have physical properties of the sources to be able to directly compare the different environment whereas Thompson et al. (2012) and S. Kendrew et al. (2012) do not.

As pointed out in S. Kendrew et al. (2012) the larger MWP bubbles provide good observational sites for the collect and collapse process. As the HII region forms the ionisation front that it creates begins to sweep the molecular material that surrounds it radially outwards. This is the start of the collect and collapse process, as this material is eventually split into equally sized clumps of material that surround the rim of the bubble. As a result of this, all bubbles where the collect and collapse mechanism is present should measure an overdensity of sources at their boundaries as the HII region expands collecting progressively more material as time goes on. This material is then compressed by the ionisation front and, if kept from fragmenting from internal gravitational instabilities will collapse to form massive stars.

Finally, in Figure 3.9 the relatively constant number of source counts per unit area as a function of distance from host bubble shows that there is little to no correlation between isolated sources and HII regions, demonstrating that the peak seen in Figure 3.7 is almost exclusively due to the triggered sources. This difference between Figures 3.8 & 3.9 also helps to show that there is likely to be little to no contamination between our triggered and isolated sources.

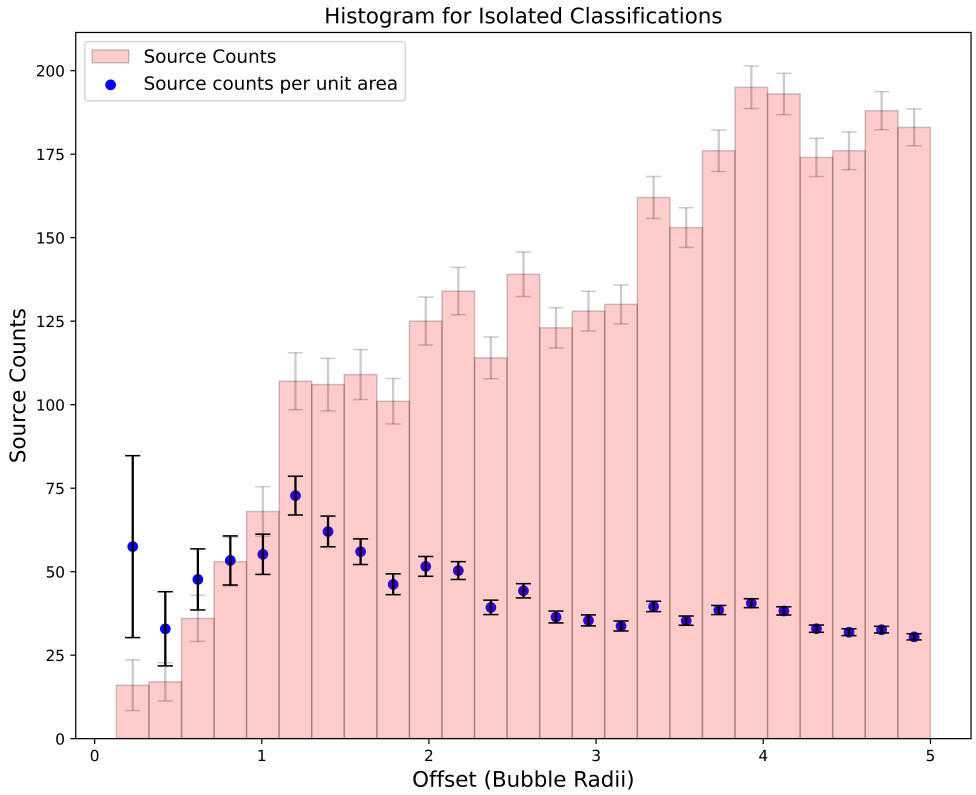

Figure 3.9: This figure depicts the histogram for the source counts and source counts per unit area of the isolated classification as a function of distance from the host bubble.

3.4 Bias in results

3.4.1 Distance, Mass and Size

As mentioned in Chapter 2, ATLASGAL is an unbiased survey, in terms of coverage and sensitivity. ATLASGAL is listed as being complete across the inner Galaxy, covering $\sim$ 80% of regions of active star formation, (Urquhart, Moore, et al. (2014)), for clumps with masses $>$ 1000 $M_{\odot}$. However, ATLASGAL is a flux limited survey and as such, there is bias for more massive clumps at larger distances. ATLASGAL being less complete for lower mass clumps (Urquhart, Csengeri, et al. (2014)), has the potential to skew our results in favour of higher mass clumps with increasing distance. This is down to the identifiable structures such as PDR's being harder to resolve at larger distances as the source becomes smaller, this would make our results only applicable to higher mass clumps undergoing star formation. This bias effect was mitigated when we compared the detection count

against source mass to check if there was any pattern or correlation between mass rates and detection rates for a distance controlled sample (2 kpc $\leq$ d $\leq$ 5 kpc) but, found no noticeable correlations between the data. In order to remove this bias entirely we would need to use additional data from other survey's that are more complete for lower mass clumps, such as Hi-Gal. However, this is beyond the scope of this project.

Additional bias could be found in more distant sources appearing point like and being harder to resolve, thus leading to classification ambiguities leading to said sources being excluded from the sample. This bias possibility is explored in greater detail in the following section.

3.4.2 Classification Ambiguities

Another potential for bias arises when we consider that the star forming regions we are looking at produce extremely bright emission in the infra-red. As the composite images, used in the classification, are also composed using light of infra-red wavelengths, if a source is too bright in the infra-red, it can lead to uncertainties as to how the source should be classified based on a visual inspection. This led to a number of sources that could have potentially been undergoing triggered star formation being excluded from the sample and means that the triggered statistics are likely a lower limit.

Many of the excluded sources could potentially be triggered, and if these were included in our triggered sample it could raise our triggered population up to $\sim 15\%$. This increase would serve to bring our lower limit more in line with lower limit estimates made by other publications such as Thompson et al. (2012).

Classification	Average Distance (kpc)
BRC	5.48
Complicated	3.60
Diffuse Material	5.31
Edge of Bubble	5.64
IRDC	3.88
IRDC Complex	2.84
IRDC Filament	3.42
Needs Discussion	3.60
None of the above	4.77
PDR	5.48
Source itself is HII region	6.39
Isolated	5.77
All	5.14

Table 3.5: This table displays the average distance of the sources in the individual project classifications.

The distance at which certain sources are found at could result in further bias from classification ambiguities. This can happen in two ways. The first of which involves near, bright sources being too ambiguous to classify accurately as described in the previous paragraph and thus being excluded from the sample.

The other way this is possible, as mentioned in Section 3.4.1, is if a source is at a far distance. When a source is sufficiently far away, it can be difficult to resolve the individual components in the image as the further away the source is located, the more point like it appears under visual inspection, meaning that clumps associated with bubbles at larger distances might be more difficult to classify.

Linking back to the potential bias of ATLASGAL caused by exclusion of potentially triggered sources deemed too ambiguous or complicated to be accurately classified, it is worth noting that the "Complicated" type sources, as seen in Table 3.5, are $\sim$ 2 kpc closer than other identified star forming regions in the sample. Another potential issue of a source being miss-classified could be when it appears sufficiently far away that the source appears as a HII region instead of a triggered region. This would lead to a potential "Edge of Bubble" or "BRC" being miss classified as a "Source itself is HII region", potential evidence of this can be seen in Table 3.5 where the average distance of a "Source itself is HII region" is $\sim$ 1 kpc more distant than the triggered classifications.

This bias potential helps to confirm our decision to describe our percentage of star formation occurring in the inner Galaxy as a lower limit as, if valid sources are being excluded due to ambiguity during the classification process then our triggered sample would in reality have a higher population count than that which was found using our classification method.

3.4.3 Source Contamination

One of our main results involves the difference in Temperature, Luminosity and Luminosity to Mass Ratio between the triggered and isolated samples. Potential observational bias in the samples could mean that the cause behind these differences is down to nothing more than proximity to a hot, bright source that would adversely affect our results.

A way to check for this is to closely examine all of the sources deemed triggered and create a subsample of more isolated sources that we can be sure are not affected by any possible contaminants. We will then subject this subsample to the same processes that led to the main results being found and see if they still provide the same conclusions.

We used a slightly modified version of the website that was originally used to classify the sources. This website can be seen in Figures 2.2 & 2.3 in Section 2.4. Doing this bias check also allowed us to double check our sample, removing any sources that were incorrectly classified when the project was initially started and we were unfamiliar with the classification process. The sources were classified as PDR-Loud, PDR-Quiet and Exclude. The numbers of these classifications can be seen in Table 3.6.

Classification	Source Counts
PDR-Quiet	256
PDR-Loud	131
Exclude	59

Table 3.6: This table displays the number of each type of source classification for the observational bias check.

The PDR-Quiet sources are the sources that will be used for the bias check. These sources were selected based on a visual inspection of ATLASGAL and GLIMPSE images, and we ensured that there was a clear separation between the PDR and the source clump,

so that we could be sure that the properties of the clump were affected as little as possible by the HII region. The PDR-Loud sources will not be used in the check but still included as part of the original sample, and consist of images still identified to be triggered but where we were unable to spot a clear difference between the clump and PDR, meaning that we were unable to confidently state that the clump properties were unaffected by the HII region. Finally the Exclude sources will be removed from the original sample.

Using the PDR-Quiet "Edge of Bubble" candidates as one data set and the original "Isolated" classification we generated CDF's for Temperature, Luminosity and L/M Ratio to see if there were any statistically significant differences between the two samples. Figures 3.10 & 3.11 and 3.12 show these results and contain the same difference between the triggered and non-triggered curves as our original results. The results of KS testing the produced curves seen in Figures 3.10 & 3.11 and 3.12 show that there were no significant differences between the bias check sample and the main data set. This provides additional confidence that our results are robust.

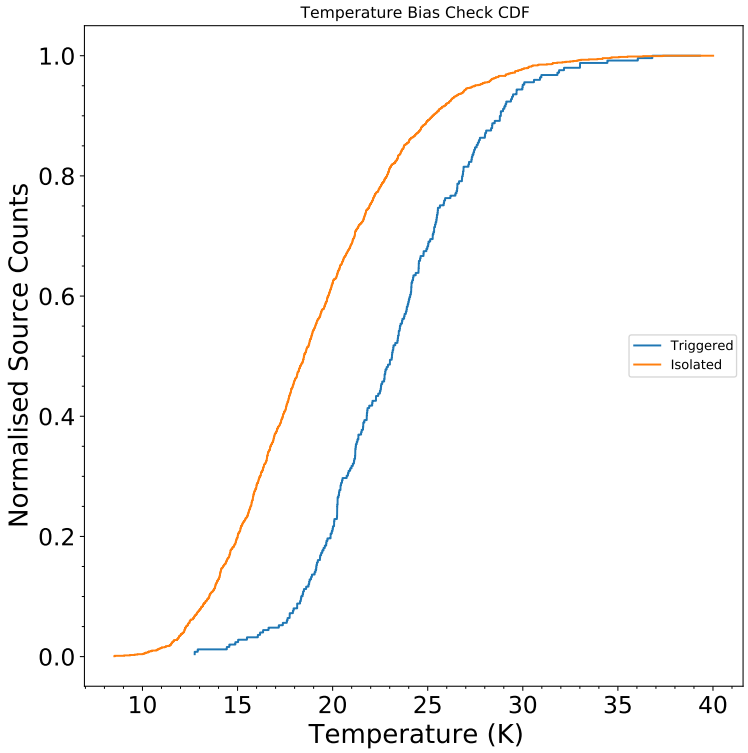

Figure 3.10: This figure shows the bias test where we test the refined Triggered sample against the original Isolated sample for the Temperature parameter to see if it provides the same results as the original samples.

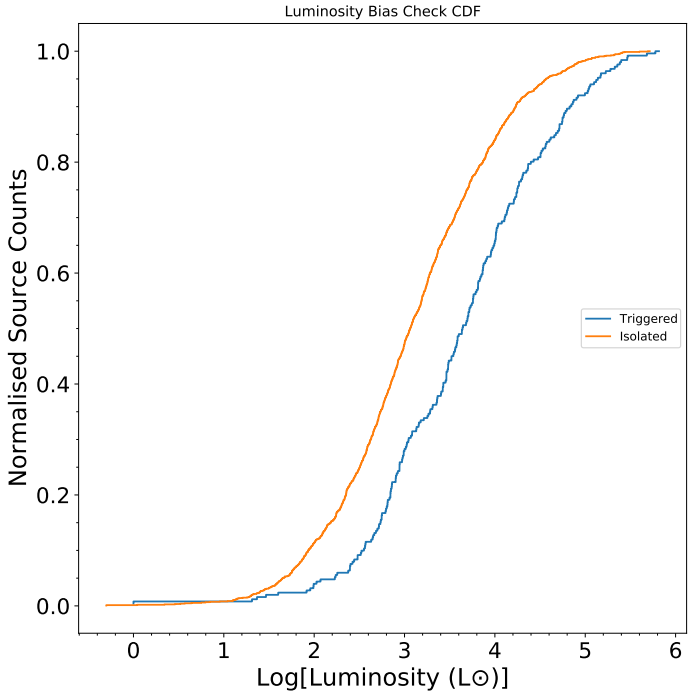

Figure 3.11: This figure shows the bias test where we test the refined Triggered sample against the original Isolated sample for the Luminosity parameter to see if it provides the same results as the original samples.

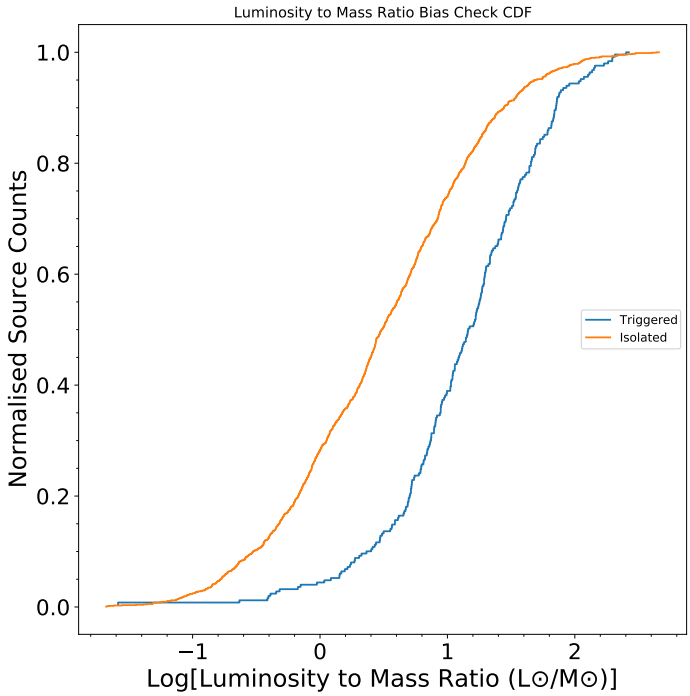

Figure 3.12: This figure shows the bias test where we test the refined Triggered sample against the original Isolated sample for the Luminosity to Mass Ratio parameter to see if it provides the same results as the original samples.

3.5 Physics behind results

3.5.1 Differences in physical parameters

Differences arising from a triggering mechanism

Both the collect and collapse method and radiative driven implosion, as discussed in Chapter 1, favour the production of more massive stars when compared to stars forming in the absence of a triggering mechanism. The collect and collapse mechanism, for example, sweeps up vast quantities of material over millions of years forming massive fragments at the edge of the HII region which are compressed by the pressure from the ionisation front and eventually collapse to form massive stars.

The radiative driven implosion mechanism is more aggressive than the slower gathering of molecular material in the collect and collapse process. As the clump is surrounded on all sides by ionising radiation, it is compressed by it. This compression can cause the clump to collapse, also collapsing preexisting clumps, leading to star formation.

Both of these triggering mechanisms are thought to lead to increased star formation efficiency, which given that they both are thought to favour the production of massive stars, would lead to a greater number of massive stars being formed than star formation occurring in the absence of a triggering mechanism. As massive stars form with higher temperatures and luminosity's than stars of lower mass, an increased number of high mass stars could account for the differences in physical parameters seen in Section 3.2

Differences arising from environmental effects

As the majority of our triggered population is found within a reasonable proximity to a HII region, the differences in temperature and luminosity, and by extension the L/M ratio could simply be down to the surrounding cloud being warmed by stellar radiation from the massive star powering the HII region.

In this scenario, the difference in temperature, luminosity and L/M ration seen in Figures 3.2, 3.3 & 3.4 would not be a result of the source being triggered but would instead be a result of the source being circumstantially close to a HII region. The energy

radiating off of the nearby HII region would warm the surrounding molecular gas which contributes to the overall luminosity seen. This could thusly result in a higher luminosity than would be observed otherwise which in turn would adversely affect the temperature and L/M ratio.

Are differences triggered or environmental?

As seen above, it is indeed possible that the increase in temperature/luminosity could be driven by a proximity to the nearby HII region as well as being due to a triggering mechanism however, it remains difficult to prove what the dominant effect behind the differences are. We attempted to check this in Section 3.4.3 where we created a subsample of triggered sources that we selected based on an observed lack of contamination from any nearby sources.

When we compared this smaller subsample, of more isolated sources, to the non-triggered sample, we still found differences between temperature, luminosity and L/M ratio with the KS-Tests for the cumulative distribution functions all yielding a real difference between the data. This demonstrates that our sources are free of any obvious contamination from nearby sources however, a subtle warming effect could still be present even in this subsample.

This remains an extremely difficult difference to evaluate. With the differences in results seen, potentially occurring from triggered, environmental or both effects. Data of a higher resolution where the differences could be easily distinguished between is needed to help with this issue.

3.5.2 Over density of triggered sources at HII region boundary

Looking at the triggering mechanisms discussed in Chapter 1 and the results of other publications, such as Thompson et al. (2012) and S. Kendrew et al. (2012) that we have examined in further detail in the discussion, it is not surprising that we found a peak of triggered sources at 1 bubble radius. As the ionisation front at the boundary of the HII region expands radially into the surrounding environment it sweeps up molecular material

forming it into clumps. Having been gathered by the ionisation front these clumps travel with it and as a result are theoretically located at the boundary of a HII region.

The radiative driven implosion mechanism can have a similar effect and also possibly accounts for the sources at a distance of ≤ 1 bubble radii seen in Figure 3.8. This is due to the nature of the mechanism where the clump is compressed by the ionisation front, increasing its density, meaning that the front usually sweeps past it. If the source is seen at the right moment in time, it would appear to be at the HII regions edge however, as the ionisation front continues to expand outwards the clump would be left behind, and now proceeds to undergo the star forming process inside the HII region, accounting for the sources seen inside the HII regions boundary.

3.6 Results Summary

Here we present a brief summary of the results obtained so far. The first of these is a detected overdensity of triggered sources at the boundaries of HII regions. This result is in good agreement with previous publications, such as Thompson et al. (2012) and S. Kendrew et al. (2012). The overdensity is most noticeable in Figure 3.8 where a clear peak around 1 bubble radius can be seen.

The second of these results is where we found comparative difference or similarities in physical properties of the environments. We discovered statistically significant differences between the temperature, luminosity and luminosity to mass ratio when comparing the triggered and isolated samples. Whilst finding the radius and masses of the samples to be comparably similar. This similarity between the radius, mass and by extension density indicates similar initial conditions of the clouds. This means that there is likely to be environmental differences occurring between the samples to cause the difference found in temperature, luminosity and luminosity to mass ratio.

The third result is that we set a lower limit of triggered star formation as a percentage of star formation occurring in the inner Galaxy. Based on our findings during the classification process we find that $\sim$12% of star formation taking place in the inner Galaxy appears to be occurring due to a triggering mechanism. We also state that this is likely to

be a lower limit due to other forms of triggering, such as supernova triggering and cloud-cloud collisions, not being included in this project as well as potentially valid triggered sources being excluded from the sample as a result of classification ambiguity caused by bias in our results.

Chapter 4

Discussion

4.1 Collect and Collapse Summary

HII regions are powered by massive OB type stars at their centres. These stars release large quantities of energy into the ISM in the form of radiation and stellar winds. This energy generates high pressures, which when combined with ionisation front generated by the radiation, causes the HII region to expand. Due to the location of the HII region and processes involved in forming massive stars, the HII region will expand into its own molecular clump that it formed in. Because of the extreme pressure and temperature differences between the environment of the HII region and the environment of the molecular clump, the surrounding molecular material will be swept up by the expansion of the HII region forming a dense layer around its border.

This layer will continue to build as the HII region continues to expand into the surrounding material, eventually becoming an inhomogeneous shell of material surrounding the HII region that collects in massive clumps evenly spaced around the rim. This shell continues to build over millions of years as the HII region expands eventually becoming so dense that parts of it will fragment and undergo gravitational collapse. These regions collapse to form massive clumps that are equally spaced around the HII region. These clumps then go on to form massive stars. This is the collect and collapse process and effectively results in massive clumps containing star formation activity being evenly spaced around the borders of HII regions, Deharveng, Zavagno, and Caplan (2005).

4.2 Comparison to Theoretical Models

The mechanisms of triggered star formation that are associated with HII regions, specifically RDI (Sandford, Whitaker, and R. I. Klein (1982)), and the Collect and Collapse method (B. G. Elmegreen and C. J. Lada (1977)), involve ionising radiation from the HII region sweeping up and compressing the surrounding material, which subsequently collapses to form a new generation of stars. This would mean that the majority of star formation activity would occur at the rim of the HII region. This is in good agreement with our results where we have found a peak in source counts at a distance of 1 bubble radii, which is also consistent with results reported by Thompson et al. (2012) and S. Kendrew et al. (2012) & Sarah Kendrew et al. (2016), who also report finding a peak in YSO source counts at HII region boundaries when using the RMS source catalogue.

Work reported by Palmeirim et al. (2017) also found that YSO candidates from the 2016 WISE catalogue showed a clear over density of sources towards the inner part of the bubbles. The peak in our data is consistent with these other results from past publications. Furthermore, as the sample we are using is larger than the previous samples, with it being around twice as large as the RMS catalogue used in S. Kendrew et al. (2012), and free of possible contamination from observational bias it strengthens these previous findings.

Furthermore, these other studies find that a high clump formation efficiency (CFE), and fractions of clumps that are associated with bubbles in their early stages of expansion, makes it likely that feedback from the parental HII region has accelerated the star formation process in these local environments. Lastly it was noted by Palmeirim et al. (2017) that more evolved sources such as class II YSO candidates were found to be concentrated towards the centre of the bubble whilst younger sources such as Hi-GAL and protostellar clumps were found at the rim of the bubble. This is consistent with the idea of sequential star formation which involves the oldest stars located in the centre of the bubble and ever younger protostellar objects being found at increasing distances from the centre of the HII region.

4.3 Investigating the differences in physical properties

In this thesis we have had access to the physical properties of the clumps, something that was not available in Thompson et al. (2012) and S. Kendrew et al. (2012) & Sarah Kendrew et al. (2016). This allows us to take their conclusions a step further with the analysis of certain physical properties such as temperature, luminosity, L/M ratio, radius and mass. Zhang et al. (2020) reports on the physical properties of star forming sites including HII regions and we shall be comparing several of our results of the physical parameters reported in this publication.

Zhang et al. (2020) state that several of their measured physical parameters suffer from a distance bias and that, Baldeschi et al. (2017) found that certain derived physical properties such as, temperature, the contribution of inter-core emission in the clumps and the fractions of starless clumps to protostellar or all clumps could change with distance. The L/M Ratio of the clumps, T_{dust} and N_{H_2} however, were found to be free of a distance bias when tested by Zhang et al. (2020) and thus will be suitable for comparison in this section.

4.3.1 Luminosity

The difference in luminosity found between triggered and isolated sources is in good agreement with past results. Dobashi et al. (2001) looked at a sample of 499 clouds and found 243 had protostar candidates selected from the IRAS point source catalogue. Their results showed that protostars close to HII regions were on average more luminous than protostars not associated with HII regions by roughly an order of magnitude.

Urquhart, Morgan, and Thompson (2009) found that their triggered sample were systematically more luminous and had higher surface temperatures and column densities than the spontaneous sample. Despite a skewed spontaneous result from UCHII regions being miss classified as BRC's and star clusters, it was still found that the average luminosity of the triggered sample was at least an order of magnitude above that of the

non-triggered sample.

Nobuyuki Yamaguchi et al. (1999), Reiko Yamaguchi et al. (1999), N. Yamaguchi et al. (1999) & R. Yamaguchi, Akira, and Yasuo (1999) found that IRAS sources in proximity to HII regions had an average luminosity of 780 $L_{\odot}$. Roughly an order of magnitude above the average luminosity of clouds far from HII regions which was found to be 63 $L_{\odot}$.

A higher luminosity is usually indicative of a higher mass star/protostar. This result is in good agreement with stars formed through the collect and collapse process as the process tends to favour the creation of massive fragments that then collapse to form stars.

Our data follows a similar trend to these past studies, with the luminosity of our triggered sample being roughly 3/4 of an order of magnitude higher than the isolated sample with values averaging $3.3\text{x}10^4$ $L_{\odot}$ and $6.5\text{x}10^3$ $L_{\odot}$. This is roughly a quarter of an order of magnitude less than what other studies have found, finding their triggered and isolated samples differing on average by a full order of magnitude. However, these other studies utilised IRAS sources, which when compared to the ATLASGAL sources that we used, are brighter and more luminous to begin with. Furthermore, we have purposely excluded ambiguous sources near bright objects or regions of intense star forming activity, which would be likely to have higher than average luminosity themselves, potentially lowering the average luminosity of our triggered sample.

4.3.2 Enhanced Star Formation

When looking at the measured values of the L/M ratio for the triggered and isolated samples we found the triggered sample to have a higher value than that of the isolated sample with them measuring 37.15 $L_{\odot}/M_{\odot}$ and 9.33 $L_{\odot}/M_{\odot}$ respectively. As the Luminosity to Mass Ratio can be a direct tracer of star formation and its evolutionary stage, this difference likely points to enhanced star formation in the triggered sample as a result of a higher star formation efficiency.

This increased L/M ratio is in agreement with Sugitani et al. (1989) who, when comparing 3 selected bright rimmed globules to 4 isolated dark globules found systematically higher L/M ratios for the bright rimmed globules, when compared with the dark globules

leading them to conclude that RDI may also lead to a higher star formation efficiency.

Zhang et al. (2020) applied a KS-Test to the L/M ratio parameter of their sample of unbiased High Mass Starless Clumps (HMSC's) that were associated or not associated with HII regions and found significant differences between HMSC's near HII regions with S-type stars (cool massive stars with strong zirconium oxide bands present in their spectra) , O-type stars and HMSC's not associated with HII regions, with S-type measuring the highest and not associated having the lowest L/M ratio.

The difference in star formation could be a result of a higher star formation rate/efficiency. This would mean that the triggering processes occurring at the edges of HII regions accelerates the star formation process as also found by Palmeirim et al. (2017).

This could result in higher mass stars being formed, which is found to be in agreement with several other publications. Thompson et al. (2012) mention how the collect and collapse method tends to form more massive stars rather than low or intermediate mass stars and Dobashi et al. (2001) and Morgan et al. (2008) found that RDI may also favour the formation of higher mass stars or small clusters of intermediate mass stars.

We are, however, unable to show a difference in the Initial Mass Function (IMF) of the different environments. This is due to our data not being extendable to test this, although given the universality of the IMF in all but the most extreme of Galactic environments, combined with results from Thompson et al. (2012), who say they do not find a difference in the IMF between triggered and non-triggered sources, it is unlikely that the triggering mechanisms discussed here are having a significant impact on the IMF.

4.4 Evidence for Triggering

Whether or not we can say that these sources have been triggered remains a problem in triggered star formation. The peak of sources at 1 bubble radius fits triggered star formation models, such as the collect and collapse model and radiative driven implosion, as it follows the theory of the surrounding molecular gas being swept up by the ionisation front that is the HII regions outer boundary.

Furthermore, the differences found in the physical properties of the star forming envi-

ronments are consistent with current predictions. This is due to the collect and collapse model being thought to favour massive star formation, due to massive fragments building up at the boundary of the HII region over time. Furthermore, the mechanism of radiative driven implosion is thought to enhance star formation efficiency, again, at the boundary of the parental HII region.

The differences in luminosity and luminosity to mass ratio provide evidence to show that if the stars had formed in the absence of a HII region their luminosities would likely be less. However, this difference only separates stars forming in proximity to HII regions and those that are not.

The difficulty lies in separating stars formed through triggering at HII regions and stars that were already undergoing the process of forming when they were swept up by the HII region.

This is arguably why neither Thompson et al. (2012), S. Kendrew et al. (2012) nor Sarah Kendrew et al. (2016) state conclusive proof of triggered star formation at any of the observed sites and instead conclude that certain sites are good candidates for triggered star formation or that it is likely triggered star formation is taking place at certain locations. Palmeirim et al. (2017) state that, it is likely star formation was triggered by a combination of RDI and the C&C process, when comparing clump fragmentation time scales to the dynamical age of the parental HII region.

Dale, T. J. Haworth, and Bressert (2015) report that objects found at the boundaries of HII regions may have already been forming stars before the ionisation front of the HII region impacted the clump. Furthermore, when using lagrangian hydrodynamic simulations to check differences between triggered and non-triggered populations at boundaries of HII regions they found that often the two populations became spatially mixed making distinction between them difficult.

However, whilst it is difficult, when observing HII regions, to identify areas of star formation that are definitely triggered when compared to other areas in similar environments. We have collected sufficient evidence to demonstrate that star formation found on the edges of HII regions is significantly different than star formation occurring in other en-

vironments, this is likely due to the impact of the HII region on the surrounding molecular gas, which points towards triggering.

4.5 Prevalence of triggering

As mentioned previously in this thesis, the size of the ATLASGAL catalog used for analysis in this project enables us to draw statistical conclusions regarding star formation taking place in the inner Galaxy. The sample of sources that we identified to be triggered consists of approximately $\sim 12\%$ of the total sample, after non-star forming sources are excluded.

Therefore, we can set a lower limit, estimating that $\sim 12\%$ of star formation that is taking place in the inner Galaxy is triggered via the processes discussed in Section 1.3. This is likely to be a lower limit estimate as other publications have also made estimates with Thompson et al. (2012) estimating between 14-30% and Deharveng, Schuller, et al. (2010) reporting an estimate of triggered star formation making up more than 25% Galactic star formation.

The methods of triggered star formation considered here only include stars formed in proximity to a HII region and thusly omits other mechanisms of triggering that are present in the Galaxy. These mechanisms include but are not limited to cloud-cloud collision and triggering via a super nova. This is recognised by Thompson et al. (2012), S. Kendrew et al. (2012) and Deharveng, Schuller, et al. (2010) with these publications stating that any estimates of triggered star formation put forward are likely to be lower limits, both due to the individual completeness levels of their samples, as well as stating that their samples do not include these other triggering mechanisms.

Furthermore, if the sources excluded from this thesis due to ambiguity could be analysed in more detail. It is likely that many of the "complicated" sources would be suitable candidates for triggered sources which would increase our lower limit further, making it similar to that posed by Thompson et al. (2012).

Chapter 5

Conclusion

5.1 Project Summary

In this project we have used the ATLASGAL catalogue combined with complimentary mid-IR images from the Glimpse/Mipsgal survey to identify a large sample of triggered star formation candidates. By visual analysis, with help from the Glimpse/Mipsgal images, we categorised the ATLASGAL sources into 11 different source types, these being: "PDR", "Edge of Bubble", "IRDC", "IRDC-Filament", "IRDC-Complex", "BRC", "Diffuse material", "Source itself is HII region", "Isolated", "Complicated" and "None of the above".

These categories were modified slightly as the project continued with it becoming more appropriate to rename the "Uninteresting" category to "Isolated" to better suit the type of sources within it, as well as grouping together the IRDC categories when results showed that the properties were statistically similar to each other. The "Edge of Bubble" and "BRC" categories were grouped together to define our "Triggered" sample and they would be tested against the "Isolated" sources, which would be used as our control group (non-triggered). We also used the data released from the Milky Way Citizen Science Project detailed by Simpson et al. (2012) to generate a separate catalogue of infra-red bubbles in the Galaxy for the purpose of replicating past results found by Thompson et al. (2012) and S. Kendrew et al. (2012).

We compared the 5 physical parameters of these groups: Temperature, Luminosity,

Luminosity to Mass Ratio, Radius and Mass. We looked for differences in these parameters between the "Triggered" and "Isolated" sample. We then used the listed positions of the sources from the ATLASGAL catalogue and listed positions of the Galactic IR bubble to calculate the distances between the triggered sample and their host bubbles in order to look for over-densities in sample population at a certain distance from their host bubble, mirroring the work of Thompson et al. (2012) and S. Kendrew et al. (2012).

5.2 Results

The results obtained during the completion of this thesis are as follows:

1. We have shown a statistically significant overdensity of sources occurring at the edges of their host bubbles. This overdensity peaked at 1 bubble radius, placing it approximately at the interface between the HII region and the molecular gas. This echoes the result found in previous publications such as Thompson et al. (2012) and S. Kendrew et al. (2012).

2. We have found statistically significant differences in key physical parameters such as luminosity and luminosity to mass ratio between our samples of triggered and isolated sources indicating a higher level of star formation at triggered sites. We also found similarities in the mass and radius parameters between our triggered and isolated samples indicating similar initial cloud conditions.

3. As our source catalogue is large enough to provide a statistical comparison to star formation in the inner Galaxy. We set a lower limit of triggered star formation in the inner Galaxy occurring at, or in proximity to a HII region of $\sim 12\%$. This triggering process is likely to involve the collect and collapse mechanism or the radiative driven implosion mechanism. This is lower than other published studies, but we are only considering two possible triggering mechanisms and have excluded many potentially ambiguous sources that also may well involve a triggering process.

5.3 Aims

When this thesis was started, we had the following aims that we were going to investigate:

1. How does one distinguish between stars formed exclusively through triggering and stars that would form even if the triggering mechanism were not present?

2. Is there any difference between triggered star formation and spontaneous star formation?

3. What is the fraction of stars that form this way in the Galaxy?

With regards to our first aim, we think that more work is required to be able to conclusively differentiate whether a triggering mechanism affects stars that were already in the process of forming. As discussed in Section 4.4 the best way to go about this would be to come up with a reliable enough model to investigate via a simulation and then looks for observational evidence involving the outcomes described in Dale, T. J. Haworth, and Bressert (2015). From an observational standpoint without prior knowledge of stars forming before an ionization boundary interferes with the formation. There still is not a reliable method of determining which stars were already in the process of forming and which stars were exclusively formed through a triggering process.

Our work involving the differences in physical parameters however, helps us provide an answer to the second aim. It seems likely that triggered star formation in proximity to an HII region can raise the star formation efficiency of a forming clump as seen from a higher luminosity to mass ratio.

Finally, we set a lower limit of triggered star formation occurring in the inner Galaxy at $\sim 12\%$. This is a lower limit than other publications but we were expecting this as we were exclusively looking at triggered star formation mechanisms occurring at or in proximity to HII regions. We also acknowledge that we are only including triggering caused by HII regions and do not include other forms of triggering in our calculations. Other methods include triggering through super nova remnants and cloud-cloud collisions. In fact, work reported by Fukui et al. (2020) states that Galactic star formation triggered by cloud-cloud collisions alone could be as high as 12%, which would increase our lower limit to $\sim 20\%$

putting it more in line with other published studies. Furthermore, we have excluded potentially valid sources due to ambiguities during the classification process which would further lower our sample rates.

5.4 Future Work

The question of triggered star formation is still not fully answered. We still have no way to differentiate between stars formed exclusively through a triggering mechanism and stars that were already in the process of forming when impacted by an ionisation boundary layer. Based on our analysis of other studies, it seems likely that the way that this problem will be solved in the future will be through the application of numerical simulations however, it is possible that a model will require observational evidence to confirm.

Furthermore, as stated in Section 3.4, due to the incompleteness of ATLASGAL when looking at sources < 1000 $M_{\odot}$ with increasing distance, our results are only properly applicable to the most massive clumps forming stars. This could be removed using another study such as Hi-GAL that has a higher level of completion for lower mass clumps. This would help to generalise our results for star formation in the inner Galaxy on a more general scale removing the skew of our results towards more massive regions. Another issue with the data involved differentiating between the differences in physical properties between triggered and non-triggered sources. This remains an issue when looking at triggered star formation, with the resolution of the data making it difficult to distinguish between differences caused by a triggering mechanism and differences caused by environmental factors. More work is needed with data of a higher resolution, where it is easier or even definitively possible to differentiate between the differences.

Lastly, whilst our sample provides a statistical representation of star formation occurring in the inner Galaxy, if it were to be extended with more sources, it could eventually provide a physical representation, which would allow much stronger claims to be drawn from it. Another benefit of a vastly bigger sample size is the potential of applying a machine learning algorithm to the classification process. This would enable the sources

to be classified significantly faster than on previous occasions and possibly increase the accuracy of the classifications as well, which in turn would strengthen the conclusions drawn from the data set. A way to improve the reliability of the statistical representation of the sample would involve classifying and analysing the remaining 4000 or so sources in our catalogue. As these sources would also have to be classified manually, we did not have time to do this but completing the catalogues classification would likely provide an improvement on the statistical reliability of the results whilst also increasing the number of regions in the Galaxy classified by $\sim 40\%$, giving a much more complete sample of the inner Galaxy.

However, given that we only have snapshots of these star formation regions it is unlikely that a conclusive difference between trigger stars and preforming stars will ever be found beyond a statistical approach utilising the difference in clump properties. A potential method could be to look at the molecular gas for kinematic signs of triggering (for example, shocks) using high resolution telescopes such as ALMA however, the limited sample size that this method would be applicable to combined with the long periods of observing time that would be needed brings into question the feasibility of conducting an experiment in such a manner.

Bibliography

Baldeschi, Adriano et al. (Dec. 2017). "Discussing the distance bias in the estimation of Hi-GAL compact source physical properties - II. Evolutionary status and star formation rate". In: 472(2), pp. 1778–1791. DOI: 10.1093/mnras/stx2128.

Bastian, N. and S. P. Goodwin (June 2006). "Evidence for the strong effect of gas removal on the internal dynamics of young stellar clusters". In: 369(1), pp. L9–L13. DOI: 10.1111/j.1745-3933.2006.00162.x. arXiv: astro-ph/0602465 [astro-ph].

Bate, Matthew R. (Feb. 2009). "The importance of radiative feedback for the stellar initial mass function". In: 392(4), pp. 1363–1380. DOI: 10.1111/j.1365-2966.2008.14165.x. arXiv: 0811.1035 [astro-ph].

Bate, Matthew R. (Feb. 2012). "Stellar, brown dwarf and multiple star properties from a radiation hydrodynamical simulation of star cluster formation". In: 419(4), pp. 3115–3146. DOI: 10.1111/j.1365-2966.2011.19955.x. arXiv: 1110.1092 [astro-ph.SR].

Bertoldi, Frank (Nov. 1989). "The Photoevaporation of Interstellar Clouds. I. Radiation-driven Implosion". In: 346, p. 735. DOI: 10.1086/168055.

Bonnell, I. A. (June 2008). "Competitive Accretion and the Formation of Massive Stars". In: *Pathways Through an Eclectic Universe*. Ed. by J. H. Knapen, T. J. Mahoney, and A. Vazdekis. Vol. 390. Astronomical Society of the Pacific Conference Series, p. 26.

Bonnell, Ian A. and Matthew R. Bate (July 2006). "Star formation through gravitational collapse and competitive accretion". In: 370(1), pp. 488–494. DOI: 10.1111/j.1365-2966.2006.10495.x. arXiv: astro-ph/0604615 [astro-ph].

Bonnell, Ian A., Matthew R. Bate, and Hans Zinnecker (July 1998). "On the formation of massive stars". In: 298(1), pp. 93–102. DOI: 10.1046/j.1365-8711.1998.01590.x. arXiv: astro-ph/9802332 [astro-ph].

Bradley W. Carroll, Dale A. Ostlie (2007). *An Introduction to Modern Astrophysics. Second Edition*. Pearson, Addison Wesley.

Burton, W. B. (Jan. 1977). "Remarks on the overall distribution of hydrogen in the galactic disk." In: *NASA Conference Publication*. Vol. 2. NASA Conference Publication, pp. 163–188.

Cesaroni, R. et al. (Jan. 2007). "Disks Around Young O-B (Proto)Stars: Observations and Theory". In: *Protostars and Planets V*. Ed. by Bo Reipurth, David Jewitt, and Klaus Keil, p. 197. arXiv: astro-ph/0603093 [astro-ph].

Chu, Y. H., J. P. Cassinelli, and M. G. Wolfire (Aug. 1984). "Properties of R 136a as derived from its optical light distribution." In: 283, pp. 560–565. DOI: 10.1086/162340.

Churchwell, E. et al. (Oct. 2006). "The Bubbling Galactic Disk". In: 649(2), pp. 759–778. DOI: 10.1086/507015.

Churchwell, Ed et al. (Mar. 2009). "The Spitzer/GLIMPSE Surveys: A New View of the Milky Way". In: 121(877), p. 213. DOI: 10.1086/597811.

Commerçon, Benoıt, Patrick Hennebelle, and Thomas Henning (Nov. 2011). "Collapse of Massive Magnetized Dense Cores Using Radiation Magnetohydrodynamics: Early Fragmentation Inhibition". In: 742(1), L9, p. L9. DOI: 10.1088/2041-8205/742/1/L9. arXiv: 1110.2955 [astro-ph.SR].

Crowther, Paul A. et al. (Feb. 2016). "The R136 star cluster dissected with Hubble Space Telescope/STIS. I. Far-ultraviolet spectroscopic census and the origin of Heii 1640 in young star clusters". In: *Monthly Notices of the Royal Astronomical Society* 458(1), pp. 624–659. ISSN: 0035-8711. DOI: 10.1093/mnras/stw273. eprint: https://academic.oup.com/mnras/article-pdf/458/1/624/8181162/stw273.pdf. URL: https://doi.org/10.1093/mnras/stw273.

Dale, J. E., T. J. Haworth, and E. Bressert (June 2015). "The dangers of being trigger-happy". In: 450(2), pp. 1199–1211. DOI: 10.1093/mnras/stv396. arXiv: 1502.05865 [astro-ph.GA].

Deharveng, L., F. Schuller, et al. (Nov. 2010). "A gallery of bubbles. The nature of the bubbles observed by Spitzer and what ATLASGAL tells us about the surrounding neutral material". In: 523, A6, A6. DOI: 10.1051/0004-6361/201014422. arXiv: 1008.0926 [astro-ph.GA].

Deharveng, L., A. Zavagno, and J. Caplan (Apr. 2005). "Triggered massive-star formation on the borders of Galactic H II regions. I. A search for "collect and collapse" candidates". In: 433(2), pp. 565–577. DOI: 10.1051/0004-6361:20041946. arXiv: astro-ph/0412602 [astro-ph].

Dewangan, L. K. et al. (Aug. 2020). "Probing the Physical Conditions and Star Formation Processes in the Galactic H II Region S305". In: 898(2), 172, p. 172. DOI: 10.3847/1538-4357/ab9c27. arXiv: 2006.03244 [astro-ph.GA].

Dobashi, Kazuhito et al. (Feb. 2001). "The Most Luminous Protostars in Molecular Clouds: A Hint to Understand the Stellar Initial Mass Function". In: 53(1), pp. 85–92. DOI: 10.1093/pasj/53.1.85.

Egan, M. P. (Dec. 1999). "Object Identification Using MSX-based Infrared Colors". In: *American Astronomical Society Meeting Abstracts*. Vol. 195. American Astronomical Society Meeting Abstracts, p. 88.12.

Egan, M. P., S. D. Price, and K. E. Kraemer (Dec. 2003). "The Midcourse Space Experiment Point Source Catalog Version 2.3". In: *American Astronomical Society Meeting Abstracts*. Vol. 203. American Astronomical Society Meeting Abstracts, p. 57.08.

Elmegreen, B. G. (Jan. 1998). "Observations and Theory of Dynamical Triggers for Star Formation". In: *Origins*. Ed. by Charles E. Woodward, J. Michael Shull, and Jr. Thronson Harley A. Vol. 148. Astronomical Society of the Pacific Conference Series, p. 150. arXiv: astro-ph/9712352 [astro-ph].

Elmegreen, B. G. and C. J. Lada (June 1977). "Sequential formation of subgroups in OB associations." In: 214, pp. 725–741. DOI: 10.1086/155302.

Elmegreen, Bruce G. and John Scalo (Sept. 2004). "Interstellar Turbulence I: Observations and Processes". In: 42(1), pp. 211–273. DOI: 10.1146/annurev.astro.41.011802.094859. arXiv: astro-ph/0404451 [astro-ph].

Franco, Jose, Guillermo Tenorio-Tagle, and Peter Bodenheimer (Jan. 1990). "On the Formation and Expansion of H II Regions". In: 349, p. 126. DOI: 10.1086/168300.

Fuente, A. (July 2001). "Outflow Dynamics, Accretion and Chemical Abundances in YSOs". In: *The Promise of the Herschel Space Observatory*. Ed. by G. L. Pilbratt et al. Vol. 460. ESA Special Publication, p. 177.

Fukui, Yasuo et al. (Dec. 2020). "Cloud–cloud collisions and triggered star formation". In: *Publications of the Astronomical Society of Japan* 73(Supplement$_1$), S1–S34. ISSN: 2053-051X. DOI: 10.1093/pasj/psaa103. URL: http://dx.doi.org/10.1093/pasj/psaa103.

Glover, Simon C. O. and Mordecai-Mark Mac Low (Apr. 2007). "Simulating the Formation of Molecular Clouds. II. Rapid Formation from Turbulent Initial Conditions". In: 659(2), pp. 1317–1337. DOI: 10.1086/512227. arXiv: astro-ph/0605121 [astro-ph].

Gordon, M. A. and W. B. Burton (Sept. 1976). "Carbon monoxide in the Galaxy. I. The radial distribution of CO, H_2, and nucleons." In: 208, pp. 346–353. DOI: 10.1086/154613.

Haworth, Thomas J., Tim J. Harries, and David M. Acreman (Oct. 2012). "Testing diagnostics of triggered star formation". In: 426(1), pp. 203–217. DOI: 10.1111/j.1365-2966.2012.21838.x. arXiv: 1205.6993 [astro-ph.SR].

Hayashi, C. (Jan. 1961). "Stellar evolution in early phases of gravitational contraction." In: 13, pp. 450–452.

Hennebelle, P. et al. (Apr. 2011). "Collapse, outflows and fragmentation of massive, turbulent and magnetized prestellar barotropic cores". In: 528, A72, A72. DOI: 10.1051/0004-6361/201016052. arXiv: 1101.1574 [astro-ph.GA].

Johnstone, Doug, James Di Francesco, and Helen Kirk (Aug. 2004). "An Extinction Threshold for Protostellar Cores in Ophiuchus". In: 611(1), pp. L45–L48. DOI: 10.1086/423737. arXiv: astro-ph/0406640 [astro-ph].

Johnstone, Doug, Christine D. Wilson, et al. (Dec. 2000). "Large-Area Mapping at 850 Microns. II. Analysis of the Clump Distribution in the ρ Ophiuchi Molecular Cloud". In: 545(1), pp. 327–339. DOI: 10.1086/317790.

Kahn, F. D. (Dec. 1974). "Cocoons around early-type stars." In: 37, pp. 149–162.

Kendrew, S. et al. (Aug. 2012). "The Milky Way Project: A Statistical Study of Massive Star Formation Associated with Infrared Bubbles". In: 755(1), 71, p. 71. DOI: 10.1088/0004-637X/755/1/71. arXiv: 1203.5486 [astro-ph.GA].

Kendrew, Sarah et al. (July 2016). "The Milky Way Project and ATLASGAL: The Distribution and Physical Properties of Cold Clumps Near Infrared Bubbles". In: 825(2), 142, p. 142. DOI: 10.3847/0004-637X/825/2/142. arXiv: 1602.06982 [astro-ph.GA].

Keto, Eric (Dec. 2002). "On the Evolution of Ultracompact H II Regions". In: 580(2), pp. 980–986. DOI: 10.1086/343794.

Keto, Eric (Sept. 2007). "The Formation of Massive Stars: Accretion, Disks, and the Development of Hypercompact H II Regions". In: 666(2), pp. 976–981. DOI: 10.1086/520320. arXiv: astro-ph/0603856 [astro-ph].

Krumholz, Mark R. (2015). "The Formation of Very Massive Stars". In: *Very Massive Stars in the Local Universe*. Ed. by Jorick S. Vink. Vol. 412. Astrophysics and Space Science Library, p. 43. DOI: 10.1007/978-3-319-09596-7_3.

Krumholz, Mark R., Andrew J. Cunningham, et al. (Apr. 2010). "Radiation Feedback, Fragmentation, and the Environmental Dependence of the Initial Mass Function". In: 713(2), pp. 1120–1133. DOI: 10.1088/0004-637X/713/2/1120. arXiv: 1001.0971 [astro-ph.GA].

Krumholz, Mark R., Richard I. Klein, and Christopher F. McKee (Feb. 2007). "Radiation-Hydrodynamic Simulations of Collapse and Fragmentation in Massive Protostellar Cores". In: 656(2), pp. 959–979. DOI: 10.1086/510664. arXiv: astro-ph/0609798 [astro-ph].

Krumholz, Mark R., Richard I. Klein, and Christopher F. McKee (Oct. 2011). "Radiation-hydrodynamic Simulations of the Formation of Orion-like Star Clusters. I. Implications

for the Origin of the Initial Mass Function". In: 740(2), 74, p. 74. DOI: 10.1088/0004-637X/740/2/74. arXiv: 1104.2038 [astro-ph.GA].

Kuiper, G. P. (Nov. 1938). "The Empirical Mass-Luminosity Relation." In: 88, p. 472. DOI: 10.1086/143999.

Kuiper, Rolf et al. (May 2011). "Three-dimensional Simulation of Massive Star Formation in the Disk Accretion Scenario". In: 732(1), 20, p. 20. DOI: 10.1088/0004-637X/732/1/20. arXiv: 1102.4090 [astro-ph.SR].

Lada, Charles J. and Elizabeth A. Lada (Jan. 2003). "Embedded Clusters in Molecular Clouds". In: 41, pp. 57–115. DOI: 10.1146/annurev.astro.41.011802.094844. arXiv: astro-ph/0301540 [astro-ph].

Lefloch, B. and B. Lazareff (Sept. 1994). "Cometary globules I. Formation, evolution and morphology." In: 289, pp. 559–578.

Liu, Hong-Li et al. (Jan. 2015). "A Feedback-driven Bubble G24.136+00.436: A Possible Site of Triggered Star Formation". In: 798(1), 30, p. 30. DOI: 10.1088/0004-637X/798/1/30. arXiv: 1411.1226 [astro-ph.SR].

Loren, R. B. (Oct. 1976). "Colliding clouds and star formation in NGC 1333." In: 209, pp. 466–488. DOI: 10.1086/154741.

McKee, Christopher F. and Eve C. Ostriker (Sept. 2007). "Theory of Star Formation". In: 45(1), pp. 565–687. DOI: 10.1146/annurev.astro.45.051806.110602. arXiv: 0707.3514 [astro-ph].

McKee, Christopher F. and Jonathan C. Tan (Mar. 2002). "Massive star formation in 100,000 years from turbulent and pressurized molecular clouds". In: 416(6876), pp. 59–61. DOI: 10.1038/416059a. arXiv: astro-ph/0203071 [astro-ph].

McKee, Christopher F. and Jonathan C. Tan (Mar. 2003). "The Formation of Massive Stars from Turbulent Cores". In: 585(2), pp. 850–871. DOI: 10.1086/346149. arXiv: astro-ph/0206037 [astro-ph].

Molinari, S. et al. (Apr. 2008). "The evolution of the spectral energy distribution in massive young stellar objects". In: 481(2), pp. 345–365. DOI: 10.1051/0004-6361:20078661.

Morgan, L. K. et al. (Jan. 2008). "A SCUBA survey of bright-rimmed clouds". In: 477(2), pp. 557–571. DOI: 10.1051/0004-6361:20078104. arXiv: 0711.0775 [astro-ph].

Motte, F., P. Andre, and R. Neri (Aug. 1998). "The initial conditions of star formation in the rho Ophiuchi main cloud: wide-field millimeter continuum mapping". In: 336, pp. 150–172.

Motte, Frédérique, Sylvain Bontemps, and Fabien Louvet (Sept. 2018). "High-Mass Star and Massive Cluster Formation in the Milky Way". In: 56, pp. 41–82. DOI: 10.1146/annurev-astro-091916-055235. arXiv: 1706.00118 [astro-ph.GA].

Myers, Andrew T. et al. (Apr. 2013). "The Fragmentation of Magnetized, Massive Star-forming Cores with Radiative Feedback". In: 766(2), 97, p. 97. DOI: 10.1088/0004-637X/766/2/97. arXiv: 1211.3467 [astro-ph.SR].

Offner, Stella S. R. et al. (Sept. 2009). "The Effects of Radiative Transfer on Low-Mass Star Formation". In: 703(1), pp. 131–149. DOI: 10.1088/0004-637X/703/1/131. arXiv: 0904.2004 [astro-ph.SR].

Palmeirim, P. et al. (Sept. 2017). "Spatial distribution of star formation related to ionized regions throughout the inner Galactic plane". In: 605, A35, A35. DOI: 10.1051/0004-6361/201629963. arXiv: 1705.09877 [astro-ph.GA].

Peters, Thomas et al. (Dec. 2010). "Limiting Accretion onto Massive Stars by Fragmentation-induced Starvation". In: 725(1), pp. 134–145. DOI: 10.1088/0004-637X/725/1/134. arXiv: 1005.3271 [astro-ph.GA].

Samal, M. R. et al. (June 2014). "The molecular complex associated with the Galactic H II region Sh2-90: a possible site of triggered star formation". In: 566, A122, A122. DOI: 10.1051/0004-6361/201321794. arXiv: 1403.7925 [astro-ph.SR].

Sandford M. T., II, R. W. Whitaker, and R. I. Klein (Sept. 1982). "Radiation-driven implosions in molecular clouds." In: 260, pp. 183–201. DOI: 10.1086/160245.

Saraceno, P. et al. (May 1996). "An evolutionary diagram for young stellar objects." In: 309, pp. 827–839.

Schuller, F. et al. (Sept. 2009). "ATLASGAL - The APEX telescope large area survey of the galaxy at 870 μm". In: 504(2), pp. 415–427. DOI: 10.1051/0004-6361/200811568. arXiv: 0903.1369 [astro-ph.GA].

Scoville, N. Z. and P. M. Solomon (Jan. 1974). "Radiative Transfer, Excitation, and Cooling of Molecular Emission Lines (co and Cs)". In: 187, p. L67. DOI: 10.1086/181398.

Simpson, R. J. et al. (Aug. 2012). "The Milky Way Project First Data Release: a bubblier Galactic disc". In: 424(4), pp. 2442–2460. DOI: 10.1111/j.1365-2966.2012.20770.x. arXiv: 1201.6357 [astro-ph.GA].

Spitzer, Lyman (1978). *Physical processes in the interstellar medium*. DOI: 10.1002/9783527617722.

Sugitani, K. et al. (July 1989). "Star Formation in Bright-rimmed Globules: Evidence for Radiation-driven Implosion". In: 342, p. L87. DOI: 10.1086/185491.

Svoboda, Brian E. et al. (May 2016). "The Bolocam Galactic Plane Survey. XIV. Physical Properties of Massive Starless and Star-forming Clumps". In: 822(2), 59, p. 59. DOI: 10.3847/0004-637X/822/2/59. arXiv: 1511.08810 [astro-ph.GA].

Thompson, M. A. et al. (Mar. 2012). "The statistics of triggered star formation: an over-density of massive young stellar objects around Spitzer bubbles". In: 421(1), pp. 408–418. DOI: 10.1111/j.1365-2966.2011.20315.x. arXiv: 1111.0972 [astro-ph.GA].

Tigé, J. et al. (June 2017). "The earliest phases of high-mass star formation, as seen in NGC 6334 by Herschel-HOBYS". In: 602, A77, A77. DOI: 10.1051/0004-6361/201628989. arXiv: 1703.09839 [astro-ph.GA].

Urquhart, J. S., T. Csengeri, et al. (Aug. 2014). "ATLASGAL - Complete compact source catalogue: 280¡ℓ¡ 60". In: 568, A41, A41. DOI: 10.1051/0004-6361/201424126. arXiv: 1406.5741 [astro-ph.GA].

Urquhart, J. S., C. König, et al. (Jan. 2018). "ATLASGAL - properties of a complete sample of Galactic clumps". In: 473(1), pp. 1059–1102. DOI: 10.1093/mnras/stx2258. arXiv: 1709.00392 [astro-ph.GA].

Urquhart, J. S., T. J. T. Moore, et al. (July 2014). "ATLASGAL – towards a complete sample of massive star forming clumps". In: *Monthly Notices of the Royal Astronomical Society* 443(2), pp. 1555–1586. ISSN: 0035-8711. DOI: 10.1093/mnras/stu1207. eprint: https://academic.oup.com/mnras/article-pdf/443/2/1555/13766461/stu1207.pdf. URL: https://doi.org/10.1093/mnras/stu1207.

Urquhart, J. S., L. K. Morgan, and M. A. Thompson (Apr. 2009). "Observational study of sites of triggered star formation. CO and mid-infrared observations". In: 497(3), pp. 789–804. DOI: 10.1051/0004-6361/200811149. arXiv: 0902.4751 [astro-ph.GA].

Whitworth, A. P. et al. (Oct. 1994). "Fragmentation of shocked interstellar gas layers." In: 290, pp. 421–427.

Wolfire, Mark G. and Joseph P. Cassinelli (Aug. 1987). "Conditions for the Formation of Massive Stars". In: 319, p. 850. DOI: 10.1086/165503.

Yamaguchi, N. et al. (Dec. 1999). "A Study of Dense Molecular Gas and Star Formation toward the Vela Molecular Ridge with NANTEN". In: *Star Formation 1999*. Ed. by T. Nakamoto, pp. 80–81.

Yamaguchi, Nobuyuki et al. (Dec. 1999). "A Study of Dense Molecular Gas and Star Formation toward the Vela Molecular Ridge with NANTEN". In: 51(6), pp. 775–790. DOI: 10.1093/pasj/51.6.775.

Yamaguchi, R., M. Akira, and F. Yasuo (Dec. 1999). "Molecular Clouds and Star Formation in the Southern HII Regions: Dynamical Effects of HII Regions on Star Formation". In: *Star Formation 1999*. Ed. by T. Nakamoto, pp. 383–384.

Yamaguchi, Reiko et al. (Dec. 1999). "Molecular Clouds and Star Formation in the Southern H II Regions". In: 51(6), pp. 791–818. DOI: 10.1093/pasj/51.6.791.

Zhang, S. et al. (May 2020). "H II regions and high-mass starless clump candidates. I. Catalogs and properties". In: 637, A40, A40. DOI: 10.1051/0004-6361/201936792. arXiv: 2003.11433 [astro-ph.GA].

Zinnecker, Hans and Harold W. Yorke (Sept. 2007). "Toward Understanding Massive Star Formation". In: 45(1), pp. 481–563. DOI: 10.1146/annurev.astro.44.051905.092549. arXiv: 0707.1279 [astro-ph].

Zuckerman, B. and P. Palmer (Jan. 1974). "Radio radiation from interstellar molecules." In: 12, pp. 279–313. DOI: 10.1146/annurev.aa.12.090174.001431.